Frequency and initiation mechanisms of submarine slides on the Fraser Delta front

by

Cooper D. Stacey
BSc, Saint Mary's University, 2011
BA, Saint Mary's University, 2005

A Thesis Submitted in Partial Fulfillment
of the Requirements for the Degree of

Master of Science

in the School of Earth and Ocean Sciences

Supervisory Committee

Frequency and initiation mechanisms of submarine slides on the Fraser Delta front

by

Cooper D. Stacey
BSc, Saint Mary's University, 2011
BA, Saint Mary's University, 2005

Supervisory Committee

Phil Hill, Geological Survey of Canada, Natural Resources Canada
Co-Supervisor

Vera Pospelova, School of Earth and Ocean Sciences, University of Victoria
Co-Supervisor

Gwyn Lintern, Geological Survey of Canada, Natural Resources Canada
Outside Member

Sophia Johannessen, Department of Fisheries and Oceans, University of Victoria
Outside Member

Abstract

Supervisory Committee

Phil Hill, Geological Survey of Canada, Natural Resources Canada
Co-Supervisor
Vera Pospelova, School of Earth and Ocean Sciences, University of Victoria
Co-Supervisor
Gwyn Lintern, Geological Survey of Canada, Natural Resources Canada
Outside Member
Sophia Johannessen, Department of Fisheries and Oceans, University of Victoria
Outside Member

The Fraser delta hosts a population of over 500,000 including the municipalities of Richmond and Delta and the Vancouver International Airport. The main arm of the Fraser River has been fixed in place by construction of a jetty focusing sediment deposition on the Sand Heads area. There is a history of submarine slide events at the delta crest which pose substantial risk to coastal infrastructure near the delta front. A submarine channel, characterized by prominent levee deposits, extends seaward from the Sand Heads area.

In this study, sand beds in cores from levee overspill deposits are dated using excess ^{210}Pb activity. They are interpreted as the downstream deposits of channelized turbidity currents generated by liquefied slide material. Sedimentation is characterized by sandy mud, interpreted to be deposited continuously by river plume suspension fall-out, and two distinct kinds of sand beds which represent two genetically different processes. The first type of sand bed (Facies 6) is thick, sharp based and clean, often showing classic Bouma turbidite elements including a massive sand base with laminated sands fining up to a mud top and is interpreted as the deposit from slides involving large volumes of material at the upper reaches of the tributary channels. The second type of sand bed (Facies 5) is characterized by muddy sand, has gradational contacts, and is interpreted as a low density deposit from either river generated turbidity currents or distal turbidites from smaller slide events. Facies 6 sand beds often occur as sets of 2 to 4 beds and individual bed sets have been dated to approximately the same ages of known large-scale slide events.

Facies 5 sand beds occur more frequently and generally occur after periods with high flow.

Sediment cores show three distinct phases of levee growth within the past 100 years approximately. A basal phase consists of very thick beds of medium sand that are interpreted to represent the early stage of channel-levee evolution when continuous overspill occurs during turbidity current events. The second stage is characterized by thick sets of frequent Facies 6 fine grained sand beds separated by less than one year of mud deposition. These sand beds are interpreted as representing a period of levee growth where channel relief is low and overspill events occur often. The third phase is characterized by thick mud intervals with less frequent fine sand beds. Phase 3 is interpreted to reflect a state when levee growth has increased channel relief to a height greater than that of the typical channelized turbidity current. In the third phase, sediment bypass is common and only larger density flows are capable of spilling onto the levees. Deposits interpreted to represent large slides have a return interval of 10 to 15 years during the past 40 years. Deposits of smaller events occur on average every four to five years. Event ages are compared to large spring floods from the Fraser River and seismic activity to determine any causal relationship. There is some relationship between ages of event beds and river flood years, but the largest sand beds do not correspond to unusually large flood years or seismic activity. It is concluded that there are likely a combination of factors which contribute to slope failure including over steepening and increased pore pressure.

Table of Contents

List of Tables

List of Figures

Acknowledgments

I owe my deepest gratitude to my supervisor, Phil Hill, whose passion for marine sedimentary processes inspired me to complete this thesis. He always had time for scientific discussion and his patience, good judgement and good input kept the ball rolling. I would also like to thank my internal supervisor, Vera Pospelova, for her guidance and constructive criticism. Her kindness towards her students is reassuring and her advice was always helpful.

I am indebted to committee members Gwyn Lintern (Geological Survey of Canada) and Sophie Johannessen (Department of Fisheries and Oceans) who both do fascinating work in the Strait of Georgia. I am glad that I was able to latch on and learn from their expertise in the field. Gwyn – I enjoyed the late night Tully lab discussions and hope to have many more in the future!

I would also like to thank the Geological Survey of Canada for my graduate funding and everyone at the Pacific Geoscience Centre. Many great conversations took place in the hallways, lunchrooms and research cruises about thesis and non-thesis related subjects from which I have learned so much. Special thanks go to Audrey Dallimore and Royal Roads University for the use of the MSCL at PGC and to Randy Enkin for spending countless hours helping out with physical property measurements in the lab. Thanks to Michael Riedel for helping with seismic processing. Sean Mullan has been an excellent office mate who always had meaningful input and helped me get my bearings when arriving on Vancouver Island.

The faculty and students in the University of Victoria School of Earth and Ocean Sciences have been very supportive and have provided an excellent environment for learning. Special thanks go out to Shahin Dashtgard and Korhan Ayranci at Simon Fraser University for the use of the x-radiograph.

Finally, I would like to thank my family who have always been supportive of my endeavours. We are spread all over the country, but seem to have managed a way to remain close. Thanks for all your love and support.

1 Introduction

1.1 Purpose of Study

The Fraser Delta hosts a population greater than 500,000 including the municipalities of Richmond and Delta and the Vancouver International Airport. Coastal infrastructure has been constructed to facilitate the growing shipping, transportation and fishing industries including the Roberts Bank Superport coal and container terminals, the Tsawwassen ferry terminal, and the Sand Heads Lighthouse. Any infrastructure built on coastal Holocene deltaic sediment is at risk of exposure to submarine slides and/or subsequent tsunamis. The Fraser Delta front is no exception and has a history of large slide events, prehistoric and recent, which pose a substantial risk to coastal infrastructure.

While a chronology of slope failure events has been inferred through the change in position of the delta crest from 1970 to 1985 (McKenna et al., 1992), little is known about the long term history of slides in the Main Submarine Channel. The presence of a channel prior to surveys from 1970 (McKenna et al., 1992) indicates that similar processes have been active for some time, presumably since the main arm of the Fraser River was fixed in place by jetty construction beginning in 1912. The observation of well developed levees on the banks of the Main Submarine Channel is further evidence that there is a history of slide events. With coastal infrastructure necessary for the local shipping and fishing industry within several hundred metres of the active head of the Main Submarine Channel, a better understanding of the frequency and initiation mechanisms of slope failures is required.

Slope failure events trigger far reaching density flows such as debris flows and turbidity currents that typically leave distinct deposits in the sediment record. The deposits of slope

failures can then be used to determine the frequency of historical failure events. This study analyzes delta front levee deposits which are inferred to be the deposits of slide events from the delta crest area, and attempts to synthesize a chronology of events over the past 100 years approximately.

1.2 Objectives

The primary objective of this thesis is to establish the frequency of slide events that occur on the Fraser Delta front, and to examine possible initiation mechanisms. This is achieved through detailed examination of sediment cores collected on the levee deposits from the Main Submarine Channel which extends from the Fraser River mouth. Sediment cores are dated using excess ^{210}Pb activity to determine a sedimentation rate and ages of sand beds are inferred based on their depth in the sediment record. The four main aims of this study are:

1. To use sand beds from levee deposits as an analogue for slide events at the delta crest and establish a chronology of events.
2. To determine if dated sand beds in the sediment record can be correlated to historical slide events.
3. To correlate the age of sand beds with dates of possible trigger mechanisms such as peak river flood years, dredge disposal, and seismic activity to determine if there are any causal relationships.
4. To determine sediment transport mechanisms and how slide activity affects sedimentation on the Fraser River delta front.

1.3 Regional Setting

The modern Fraser Delta is Holocene aged and extends west into the Strait of Georgia from the Coast and Cascade Mountains (Fig. 1.1). Beginning with deglaciation of the Fraser Lowland, the Fraser floodplain advanced westward through a partially submerged, glacially scoured trough, reaching the Strait of Georgia by 10,000 BP (Clague et al., 1983, Fig. 1.2). Delta sediments average 120 m in thickness (Matthews and Shepard, 1962) and are characterized primarily by interbedded sand, silty sand and sandy/clayey silt with local variations likely resulting from migrating channel positions and sea level fluctuation during the Holocene (Clague et al., 1983).

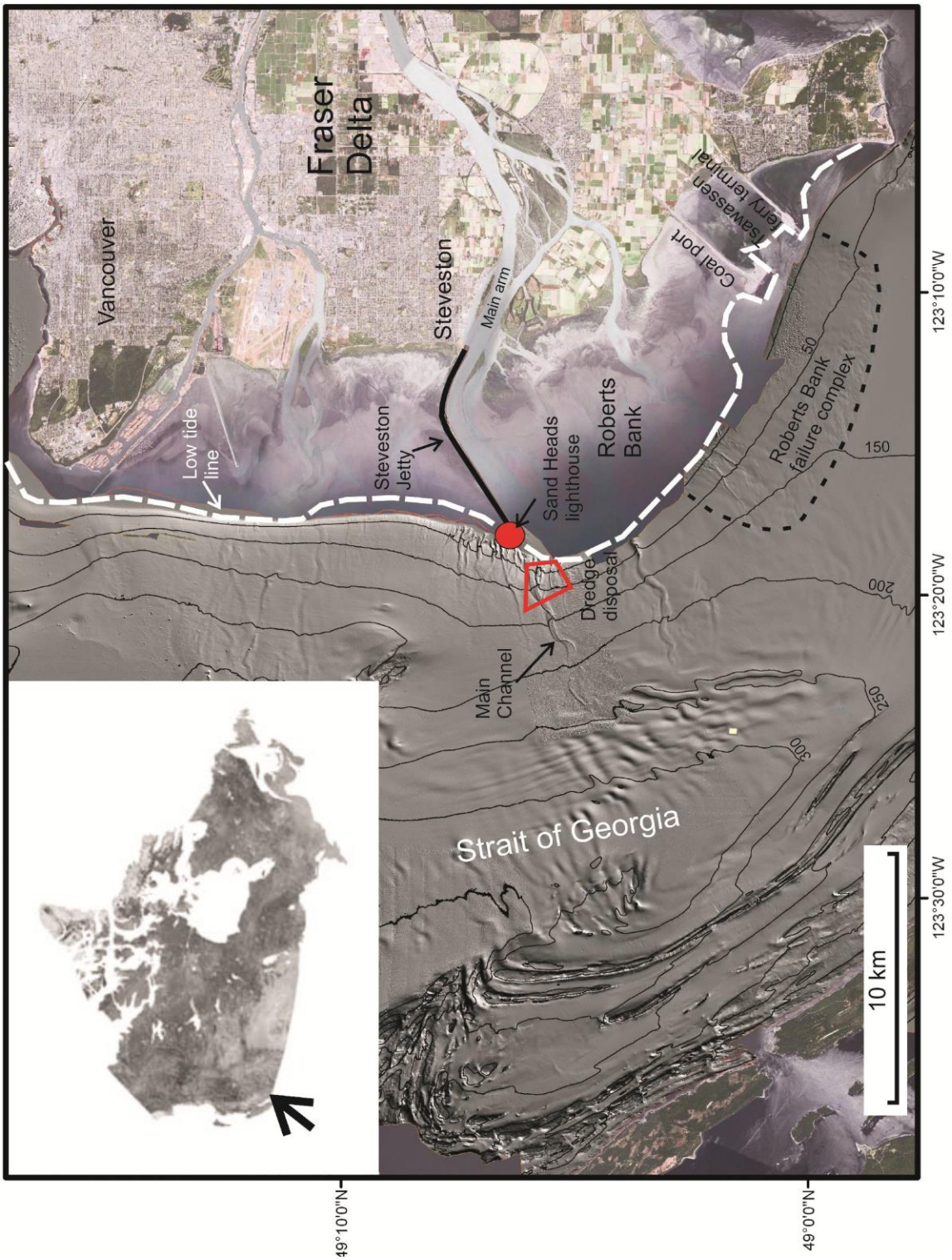

Fig. 1.1. Regional map of the Fraser Delta front showing the Fraser Main Submarine Channel which extends from the main arm of the Fraser River and the Roberts Bank failure complex on the delta front. Coastal infrastructure includes the Steveston jetty, Sand Heads lighthouse, Roberts Bank Coal Facility and the Tsawwassen ferry terminal. Bathymetric contours are in metres. Modified from Hill (2012).

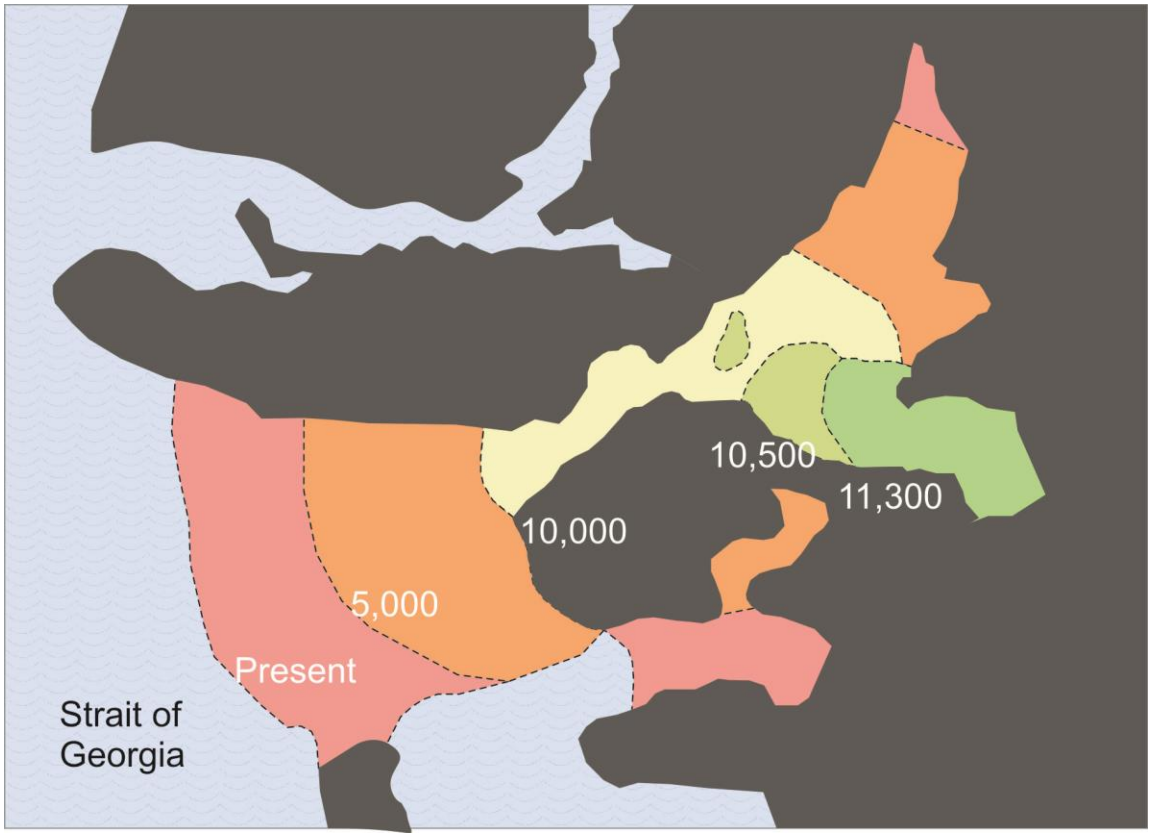

Fig 1.2. History of the Fraser Delta progradation. Colours represent growth since deglaciation. Modified from Clague et al. (1983).

Distributary channels of the Fraser River have left coarse deposits of medium to coarse sand, pebbles and gravel, and have scoured to depths of up to 22 metres below sea level (mbsl) (Matthews and Shepard, 1962). The seaward margin of the delta has experienced frequent shifts in channel position (Johnston, 1921, Fig. 1.3) up until the construction of a jetty in from 1912 to 1932. The delta front is characterized by a number of submarine channels, some currently active and others inactive which extend from the terminal positions of former river distributaries. Several large slide scars are also present, including the Robert's Bank failure complex, which covers an area of about 4000 km^2 and has a volume greater than 1,000,000,000 m^3 (Christian et al., 1997). Based on

stacked units, the failure complex is interpreted to have resulted from a sequence of slides (Christian et al., 1997).

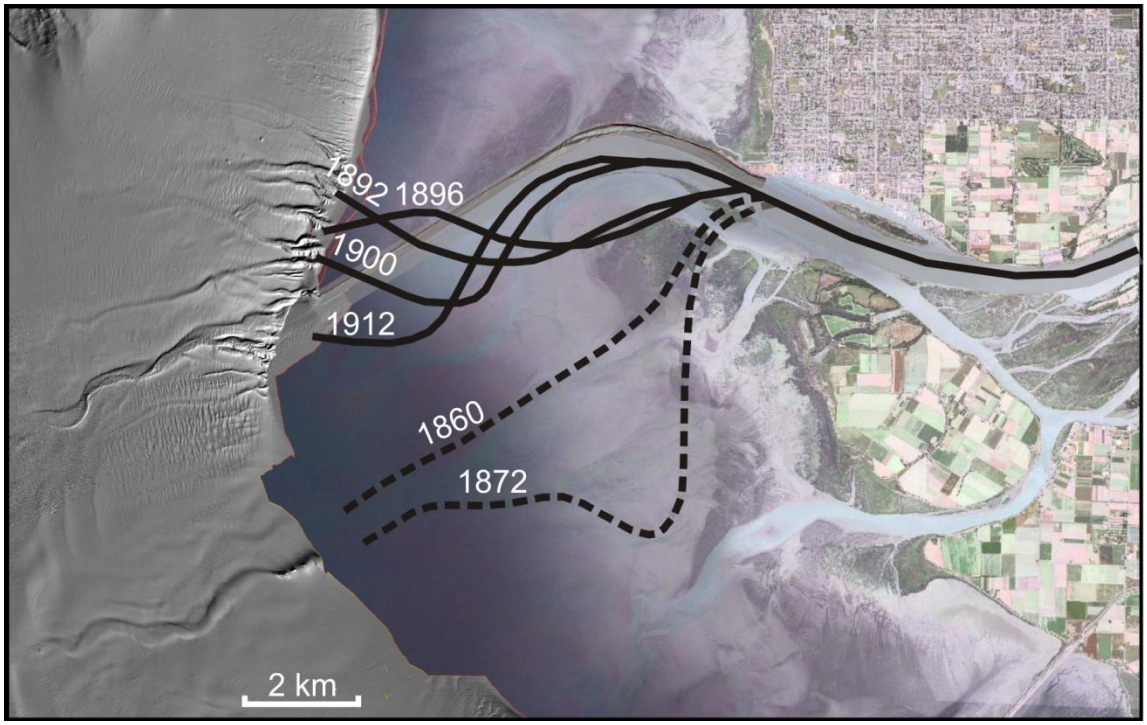

Fig. 1.3. Fraser River with 150 years of changing distributary channel positions. Modified from Johnston, 1921.

1.4 Sedimentation

The Fraser River currently collects sediment from a drainage basin of 234,000 km^2 of mountainous terrain and has a mean discharge of 3400 $m^3 s^{-1}$ (Matthews and Shepard, 1962). Sediment load measured 42 km upstream from the river mouth averages 6.4 x 10^6 tonnes yr^{-1} consisting of 35% sand, 50% silt and 15% clay (Hart et al., 1998). Discharge amounts are low in the fall and winter and peak during the spring freshet when snowmelt occurs.

Estuarine circulation in the lower Fraser River reaches as far upstream as 18 km when discharge is low (Ages and Woolard, 1976). Estuarine circulation and the position of the

salt wedge are controlled by river discharge and tidal height. A stratified salinity gradient occurs in the river mouth when the salt wedge intrudes into the estuary channel resulting in lower flow velocities. At low tide when the salt wedge is seaward of the distributary mouth bar flow velocities exceed 2 $m^3 s^{-1}$, allowing for entrainment of sandy bed material and higher suspended sediment concentrations (Kostaschuk et al., 1993).

A buoyant surface plume extends into the Strait of Georgia and is modified continuously by surface currents which are driven by tide and wind activity (Meule, 2005). Coarser sediment settles rapidly near the mouth of the river where accumulation rates have been determined to be between 10 and 14 cm y^{-1} from ^{137}Cs dating (Hart et al., 1998) and in excess of 1 m yr^{-1} based on repeat miltibeam surveys (Hill, 2012). Finer sediment remains in suspension and is carried away from the river mouth. There is a decrease in suspended sediment concentration with distance from the river mouth likely resulting from a decrease in plume velocity and associated turbulence and flocculation of fine sediment particles (Kostaschuk et al., 1993). Settling rates out of Canoe Passage, on Roberts Bank south of the Main Submarine Channel, were calculated to be 1.5 to 35 mm s^{-1} based on ADCP velocity measurements (Meule, 2005).

Tides in the Strait of Georgia are semi-diurnal with a mean range of 2.6 m and maximum range of 5.4 m. Measurements from Roberts Bank have shown that flood tides are substantially stronger than ebb tides, and have a mean velocity of 0.35 m s^{-1} and a maximum of 1.3 m s^{-1} to the north (Atkins et al., 1998). Both peak flood and ebb tides produce currents that are capable of resuspending fine sand off the seafloor, but net sediment transport is directed to the north due to higher bed shear velocities for longer durations on the flood tide (Hill et al., 2008). Seabed current velocities at positions as

deep as 90 m are capable of exceeding shear velocity critical values (Kostaschuk et al., 1995). Subaqueous dunes in water depths as much as 100 m on Roberts Bank have heights of 0.3 to 2.6 m and wavelengths of 26 to 55 m. These dunes are asymmetric with steeper faces on the northwest sides. This is taken as evidence of net northward transport by stronger flood tides (Carle and Hill, 2009).

1.5 Dredge Disposal

The main arm of the Fraser River is used extensively for shipping purposes. Dredging operations have been active since 1883 with average annual volumes of dredged material range from 1.64 x 10^6 m^3 between 1961 and 1974 to 4.70 x 10^6 m^3 between 1975 and 1991. Dredge spoils are taken to a designated disposal site in the Sand Heads area (Fig. 1.1) by barges with load capacities of 2,600 m^3 of sediment. Annual disposal amounts are as high as 1,128,669 m^3 (Hill, 2012). A study was performed in 2009 by Natural Resources Canada to observe the sediment dispersal patterns of the dredge spoil which found evidence that much of the discharged material was being deposited at the site of disposal (Lintern et al., 2009). Hill (2012) hypothesised that stacked, wedge-shaped, depositional units that infill the northern tributary may result from dredge disposal events as their incremental growth over repeat surveys is comparable to the volume of dredge disposal material. As well, deposition occurs in the closest position to the river mouth where barge disposal ships are permitted to deposit their loads.

1.6 Human Influence

The Fraser Delta has been confined by human development, resulting in a history of slope failures. The Fraser delta supports a population greater than 500,000 people and hosts a variety of industrial activities including a variety of port facilities. The installation of jetties has fixed the main arm of the Fraser River in place in order to maintain a safe shipping route to the Steveston area of Richmond, British Columbia. The result of the jetty installation is the continual rapid sediment deposition at the mouth of the main arm and the Sand Heads area.

1.7 Fraser Submarine Channel

Since the main arm of the Fraser River was fixed in place, sedimentation has been focused on the Sand Heads margin of the delta crest. An active channel has formed at the river mouth, which has three main sections (Kostaschuk et al., 1992): upslope tributary channels, mid-slope sinuous Main Submarine Channel and base-of-slope distributary channels. Tributary channels at the head of the channel are deeply incised and steep walled with widths exceeding 380 m and depths of 32 m. These tributaries coalesce to form the Main Submarine Channel. The Main Submarine Channel is sinuous with five distinct bends and decreases seaward in width and relief. Channel gradient decreases from 2° at the upper end to 0.7° at the lower end. Kostaschuk et al. (1992) identified elevated banks on both sides of the lower reaches of the channel and speculated that they might be depositional levees produced by overbank flows. At 205 mbsl the Main Submarine Channel becomes shallow and branches into a number of distributary

channels. The bed of the channels consists of fine to medium sand and the interchannel margins are characterized by silty clay (Evoy et al., 1994).

Channel morphology has been described in detail using multibeam bathymetry data from surveys between 1994 and 2006. Hill (2012) has summarized the morphology of the entire channel system and notes bathymetric changes including net sediment accumulation in most areas. The thickness of accumulation decreases with distance from the Fraser River mouth. Areas of high relief, such as the tributary channels, experienced the highest amounts of sediment accumulation with higher amounts of net accumulation in the northern tributary. Erosion has been noted where the southern tributary channel incises the delta-slope break and generally at headwalls within the tributary channels. New escarpment positions were inferred to be the result of slope failure activity involving volumes of sediment between 2×10^5 m^3 and 5×10^5 m^3.

Sediment transport and channel formation occur through gravity flows involving mass wasting of sandy material at the head of the Main Submarine Channel (Kostaschuk et al., 1992; Hart et al., 1992; Evoy et al., 1994). McKenna et al. (1992) describe five slide events identified based on comparison of successive bathymetric surveys between 1970 and 1985 at the mouth of the main arm. The first four events resulted in a retrogression of the position of the delta crest by amounts ranging between 40 and 90 m and a general steepening of headscarps. The fifth event in 1985 was the largest with the position of the delta crest retrogressing by 350 m. A minimum of 1×10^6 m^3 of sediment failed, which is estimated to be most of what had accumulated at the river mouth since 1977. This event

created a new gully which extended landward into the delta and came within 100 m of the Sand Heads Lighthouse (McKenna et al., 1992). McKenna et al. (1992) speculated that a future large failure may be imminent, posing serious risk to the Sand Heads Lighthouse. Sediments on the delta front are unconsolidated silty sands and are prone to liquefaction. Combined with morphological evidence and numerical modelling, post slide surveys reveal the absence of large blocks of failed material downslope from the source area. This supports the idea of liquefaction and subsequent transport via turbidity currents (McKenna et al., 1992; Chillarige et al., 1997). Liquefaction may be facilitated by a combination of factors including tidal conditions: low tides reduce sediment confining pressure and allow for expansion of interstitial gas, resulting in excess pore pressure (Chillarige et al., 1997).

Much of the coarse sediment from the Fraser River is channelized resulting in sediment bypassing of the upper slope (Evoy et al., 1997). Five sedimentary facies are recognized from sediment cores on the delta front (Evoy et al, 1994). Facies I and II are massive and finely-laminated silty clay/clayey silt interpreted to be deposited from suspended sediment sourced from the river plume. Facies III is plane parallel and laminated to lenticular bedded clayey silt with very fine grained sand interpreted as mixed suspension and traction deposition. Facies IV is very fine to medium grained sands with sharp erosive bases, little internal stratification, rare mud rip-up clasts and evidence of post depositional fluidization, and is interpreted as sediment bypass material via turbidity currents. Facies V is composed of chaotically bedded mud rip-up clasts, shell fragments

and resedimented organics in a sandy matrix interpreted as a debris flow (Evoy, 1997; Evoy et al, 1994).

1.8 Channelized Turbidity Currents and Levee Construction

Turbidity currents may be initiated by three different processes including slides, hyperpycnal flows from rivers and storm-generated flows near the shelf edge. Slide initiated turbidity currents occur when slide/slumped material liquefies. As fluid content and velocity increase, individual grains may become fully supported by fluid turbulence and the slide transforms into a turbidity current (Lowe, 1976). Hyperpycnal flows occur when sediment rich river discharge has a higher density than that of the water body into which it enters (Mulder and Alexander, 2001). Storm-induced turbidity currents occur when down-canyon flow is generated by heavy surf and wind, which acts to stir up sediment (Shepard and Marshall, 1973).

Channel inception occurs when successive turbidity currents with sufficiently high transportive energy scour a trough into the seabed (Irman and Parker, 1998; Conway et al., 2012). As successive turbidity currents occur, the trough experiences further erosion and becomes a conduit for subsequent flows eventually leading to sediment bypassing (Arnott, 2010). Channelized turbidity currents which overspill channel walls generate levee deposits (Primez et al., 1997; Skene et al., 2002) that act to increase channel relief further. With levee deposition and increased channel relief channel confinement occurs and overspill events become less frequent. This requires larger turbidity currents to overtop the levees. A general fining up sequence is observed in levee deposits reflecting channel confinement and levee growth (Straub and Mohrig, 2008).

Levee construction occurs by multiple forms of channel overspill. Flow stripping occurs when the upper fine grained portion of the flow is separated from the lower flow at channel bends (Piper and Noramark, 1993). Channel run-up occurs when a fast moving flow reaches a channel bend and is forced up the channel wall due to its own inertial force (Hay, 1987). Continuous overspill may result on straight channel segments, from flows with height in excess of channel relief (Arnott, 2010). Once the flow escapes the channel, rapid expansion and collapse occurs resulting in higher rates of deposition proximal to the channel and rapidly decreasing rates of deposition with distance from the channel axis (Arnott, 2010). This style of deposition results in sand beds which thin with distance from the channel axis. Levee deposits are characterized by multiple thinning sand beds which result in a tapered architecture. Sand-rich levee deposits tend to concentrate at outer bends of channels (Arnott, 2010).

Sedimentary facies within levee deposits consist of sand facies and clay and mud rich facies. Sand beds represent overspill events, and may exhibit sedimentary structures that preserve the depositional flow regime. Clay or mud rich facies represent normal hemipelagic sedimentation (Kane et al., 2007). Sedimentary structures include those produced by traction currents such as parallel lamination and ripple-cross lamination, and may be accompanied by other elements of the Bouma sequence such as sharp-based massive sand fining up to a clay or a mud top (Bouma, 1962; Kane et al., 2007). Sand beds can be laterally correlated on levee deposits, but tend to thin and pinch out with distance from the channel axis (Hickson and Lowe, 2002; Kane et al., 2007).

2 Methods

2.1 Introduction

In order to investigate the frequency of submarine slides in the Sand Heads area of the Fraser Delta, the Geological Survey of Canada performed a survey with the assistance of the Canadian Coast Guard and the Canadian Hydrographic Service in a mission numbered 2011004 PGC. New multibeam bathymetry data and 20 new sediment cores were collected in August 2011. Older data including repeat multibeam bathymetry surveys from 2006, 2007, 2008, and 2010, backscatter data from 1994, and Huntec data from 1992 were used in combination with the new data. Multibeam bathymetry and backscatter data were used to determine where areas of active sedimentation were occurring. Huntec records were used to reveal ideal levee architecture. Sediment cores were collected after multibeam and Huntec analysis. Core placement was done to sample areas of frequent channel overspill events to capture as complete a sediment record as possible, and the maximum number of sand beds. The acquisition of 20 new piston cores provided important sedimentological information: visual and textural analysis was facilitated by gamma-ray density, magnetic susceptibility, high resolution photography and x-radiography in order to identify sand beds. Cores were dated using ^{210}Pb analysis.

2.2 Multibeam Data

Repeat multibeam surveys of the Fraser Delta Main Submarine Channel dating back as far as 1994 and the new survey performed in 2011, were analyzed to delineate morphological changes in the study area (Table 2.1). Difference maps based on different gridded datasets using ArcGIS reveal the net accumulation or loss of sediment, and

indicate where deposition or erosion/slides have occurred. These difference maps are used to calculate local sediment accumulation rates and are useful in the determination of which areas of the delta front are most active. Errors in precision of difference maps are approximately ± 0.4 m (Hill, 2012).

Table 2.1. Multibeam datasets used in this thesis.

Survey year	Multibeam transducer	Horizontal Resolution (m)
2011	Kongsberg Simrad EM 710	2
2010	Kongsberg Simrad EM 710	5
2008	Kongsberg Simrad EM 3002	2
2007	Kongsberg Simrad EM 3002	2
2006	Kongsberg Simrad EM 3002	2
1994	Kongsberg Simrad EM 100	3

Multibeam backscatter maps show the distribution of different sediment grain sizes on the seabed. Areas of low backscatter intensity are interpreted as finer sediment while higher backscatter is interpreted as coarser deposits. Coarser deposits would be expected at the mouth of the river where there is a sudden loss of competency as the sediment load leaves the confined river channel and enters the Strait of Georgia. ArcGIS was used to analyze backscatter data.

2.3 Seismic Data

High resolution seismic reflection data collected by the GSC-Pacific from cruise 92006 were used to synthesize levee architecture. Data were collected in 1992 with a Huntec IKB Seistec system which consisted of a boomer source and a line-and cone receiver. Paper records were scanned using a Kyocera KM-5050 scanner and Corel Draw 14 was used to enhance the contrast of seismic images.

2.4 Sediment Cores

Sediment samples were collected with a Benthos piston corer onboard the CCGS Vector. All core barrels were 6.096 m (20 ft) long except cores 88 and 89 which were 12.192 m (40 ft). Core liners were cut into segments shorter than 157 cm in order to fit the track of the multi-sensor core logger (MSCL).

2.4.1 Core Locations

Twenty new piston core samples were collected from the north bank of the Main Submarine Channel just beyond the first bend in the channel. This is an area where levee overspill events are expected to be frequent (fig 2.1). Seismic images of this area show well defined levee structure (Hill, 2012). Coring sites are organized into four transects of five cores which are oriented roughly perpendicular to the channel axis. Transect 1 is most proximal to the river mouth and transect 4 is the most distal (Fig. 2.1). Transects were designed to follow the Huntec lines that best reveal ideal levee architecture. Coring transects range in water depth from approximately 120 to 150 mbsl and penetrated to depths of up to 10 metres below sea floor (mbsf). Spacing between transects ranges from 190 to 500 m. Individual transects start at or near the levee crest and cores are spaced roughly 100 m apart northward from the Main Submarine Channel. Individual core location information is summarized in Table 2.2.

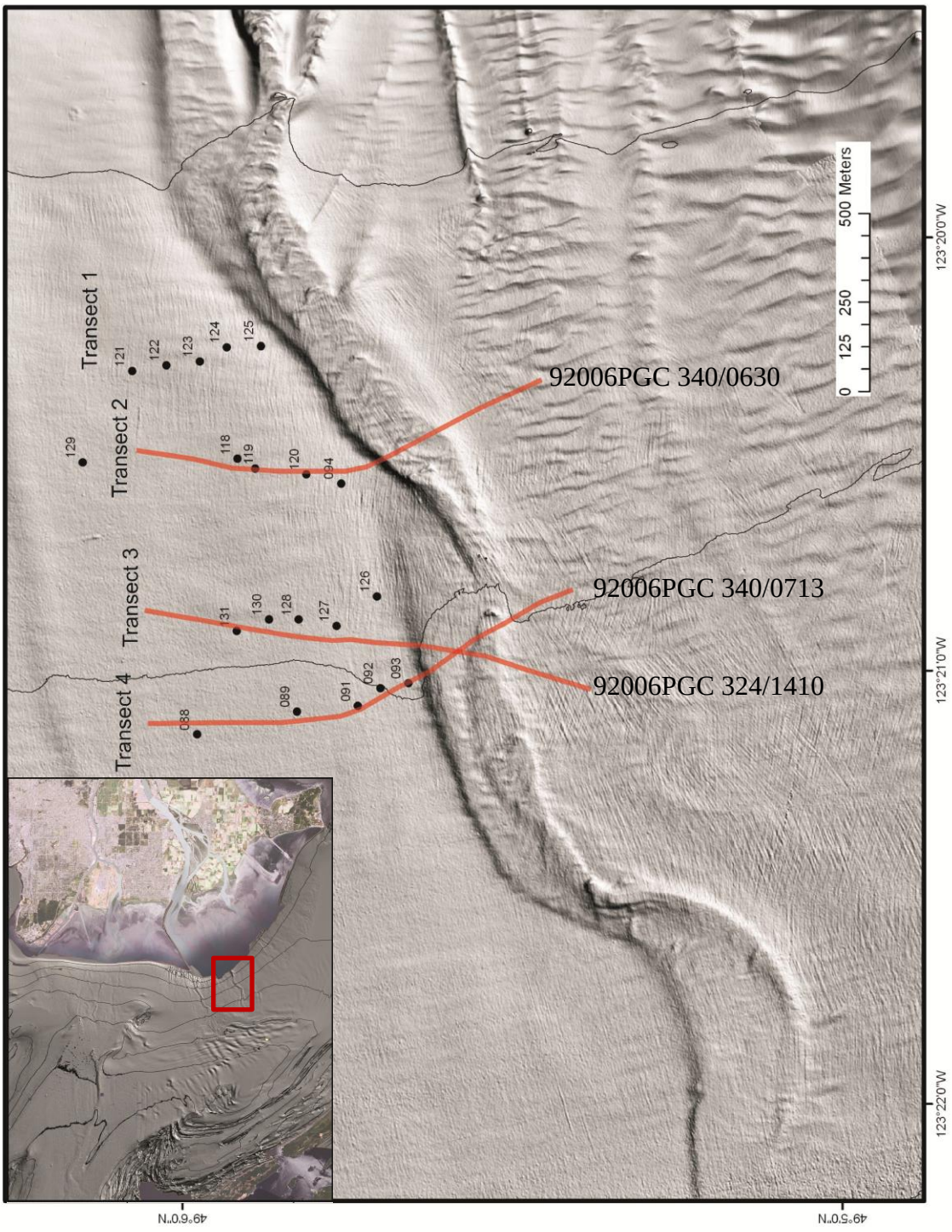

Fig. 2.1. Core locations and Huntec seismic lines. Locator map at top left outlines study area in red box.

Table 2.2. Information on core sites used in this thesis.

	Core	Latitude (°N)	Longitude (°W)	Core Length (cm)	Distance from river mouth/jetty (m)	Distance from levee crest (m)	Water depth (m)
Transect 1 (T1)	125	49.0981	-123.3376	533	2689	39.9	116.8
	124	49.0990	-123.3377	546	2662	110.6	119.6
	123	49.0997	-123.3382	495	2680	196.3	120.0
	122	49.1005	-123.3384	492	2666	266.6	121.6
	121	49.1014	-123.3386	518	2663	346.6	121.6
Transect 2	94	49.0961	-123.3429	505	3126	95.9	133.2
	120	49.0970	-123.3425	419	3068	141.8	131.6
	119	49.0983	-123.3423	412	3014	246.4	133.2
	118	49.0987	-123.3420	497	2970	277	131.6
Transect 3	126	49.0952	-123.3472	485	3458	26.8	142.5
	127	49.0962	-123.3484	480	3502	164.9	147.7
	128	49.0972	-123.3481	408	3451	258.6	148.0
	130	49.0979	-123.3481	508	3430	339.7	149.2
	131	49.0987	-123.3486	341	3438	437.2	148.4
Transect 4	93	49.0944	-123.3506	67	3721	16.3	150.0
	92	49.0951	-123.3508	104	3705	92.3	152.4
	91	49.0957	-123.3514	290	3731	169.5	155.2
	89	49.0972	-123.3517	775	3700	342	155.6
	88	49.0997	-123.3526	694	3699	625.7	154.8

2.4.2 Core Splitting and Description

All cores were brought to the GSC-Pacific core lab to be split and described. Cores were left upright in a storage fridge for three months before splitting. Cores were split in half lengthwise using a machine which pulls two small hooked blades along the length of the core liner. A thin metal wire was drawn down the length of the core to separate both halves of sediment and in most cases the core halves came apart unaided when the cut was rotated to a vertical position. Spatulas were used to help separate the halves which

did not separate on their own. Core surfaces were scraped with a small spatula in order to remove artefacts from the splitting process and enhance contacts between sedimentary units. Sedimentological descriptions were performed, including texture, sedimentary unit boundaries, bioturbation and the presence of organic debris.

2.4.3 Multi Sensor Core Logger

MSCLs at the Pacific Geoscience Centre (PGC) were used to get high resolution core photography, gamma ray density and magnetic susceptibility data from cores. Two Geotec MSCL machines were used, the MSCL-S collects gamma ray density and magnetic susceptibility from whole cores and the MSCL-XZ collects high resolution data from split cores including core photography and magnetic susceptibility.

2.4.3.1 Core Photography

High resolution photography was used to record a digital image of the fresh cut sediment surface. Images used in this thesis were taken after sediment at the split surface had reached a uniform level of oxidation – a step which was required as upon splitting the cores, fresh sediment was black while sediment adjacent to cracks were oxidized to a light brown colour and were very distracting. A Geotec line scanner was used which scans the split core under cross polarized light to minimize specular reflections from wet sediment surfaces. The scanner acquired data from 2,000 pixels across the field of view with a resolution of 50 µm. Photographs were processed with Corel Draw 14 to enhance brightness and contrast.

2.4.3.2 Physical Properties

Whole core gamma-ray density was logged with an Oakfield Instrument scintillation machine and a ^{137}Cs gamma source. Whole core magnetic susceptibility was logged with a Bartington MS-2 magnetic susceptibility meter with an 11 cm coil. High resolution magnetic susceptibility was logged on split cores in contact with the sediment surface using a Bartington MS-2E with a 3 mm spatial resolution.

Gamma-ray density indicates bulk density and is converted to g cm^{-3} using density calibration samples. Mud intervals have lower densities, while sand intervals are typically characterized by higher density. Magnetic susceptibility readings indicate the degree of magnetization of material in response to an applied magnetic field. The sediment load of the Fraser River originates from the Rocky Mountains, the Coast Mountains and the Cascade Mountains, some of which are volcanic and contain minerals which have high magnetic susceptibility values including magnetite. Sediment from the Fraser River is expected to have higher magnetic susceptibility values than ambient levels in the Strait of Georgia.

Muddy units with low density and low magnetic susceptibility are interbedded with sandy units of higher values which have been transported downslope from the mouth of the Fraser River. Peaks in density and magnetic susceptibility are expected to correlate as they both indicate the presence of sediment transported from the mouth of the river. Intervals where both measurements peak are considered to be anomalous and are excellent candidates for potential turbidite sands.

2.4.4 X-radiography

X-ray images were acquired using a Soyee SY-31-100P portable x-ray unit, a typical unit used by veterinarians. Images were taken on Kodak POC Carestream Directview Vita Computed Radiography (CR) System radiographic plates and processing system. The x-ray unit was mounted on a frame pointing vertically towards the floor and four core sections were scanned side-by-side at a time. Contrast enhancement was performed using Corel Draw 14.

X-ray images reveal a 2D greyscale representation of cores revealing internal sedimentary structures. Denser sediment such as sand and gravel appears lighter, contrasting with less dense material which appears dark. Internal structures which may be observed through this technique include fine sandy laminations, graded bedding, shell and other organic debris, cracks or voids in the sediment and bioturbation (i.e., infaunal burrows).

2.4.5 Core Quality

The quality of sediment cores was typically very good with well-preserved primary structures. Many of the cores, however, suffered from gas expansion resulting in frequent cracks and void gaps throughout the sediment record. When gaps were present the resulting physical property and x-ray data was compromised. During the three months of waiting to split the cores oxidation occurred around areas exposed to air including areas in contact with gas expansion cracks and the tops of core sections (sometimes penetrating >50 cm down from the top as water drained to the bottom of the section). A fresh cut sediment surface was black and would oxidize to a light brown colour within 24 hours.

In the case of x-ray images dry and cracked cores appear white and washed out with no traces of internal structure such as burrow traces or laminations. Physical property measurements, including density and magnetic susceptibility, show a signal which drops out instantly at intervals with cracks. For sediment accumulation rate calculations, cracks were removed mathematically.

Bioturbation was present at various levels throughout cores, sometimes extensive, sometimes minor, but present in all cores. The extent of bioturbation is best determined by visual inspection of x-ray images.

2.5 Sediment Accumulation Rate Model

2.5.1 Introduction

Jetty construction dates back to 1912-1932, and resulted in the confinement of the Fraser River main channel. In order to determine the sediment accumulation rate during this time interval, analysis of ^{210}Pb isotopes are ideal due to their short half life of 22.3 years. Models which use ^{210}Pb to date sediment rely on the decay of naturally occurring atmospheric ^{222}Rn into ^{210}Pb. This daughter isotope is referred to as unsupported ^{210}Pb. A separate source of ^{210}Pb comes from the decay of ^{226}Ra which occurs continuously in marine sediments. This decay supplies a consistent background level of ^{210}Pb. Surface sediment interacts with the atmosphere where the amount of ^{210}Pb activity is at a maximum level. ^{210}Pb decays to ^{210}Po as deposition on the sea floor and subsequent burial occurs. Unsupported ^{210}Pb will decay to amounts below a detectable limit within five half lives or roughly 100 years. After this time, the only detectable ^{210}Pb will be that which is constantly being produced by the decay of ^{226}Ra, providing a background level of ^{210}Pb. To determine the unsupported ^{210}Pb activity, the ^{226}Ra activity is subtracted

from the total ^{210}Pb activity. The amount of ^{210}Pb activity typically decreases with depth in an exponential fashion as younger sediment is deposited on top of older sediment (Robbins, 1977).

2.5.2 Excess ^{210}Pb Sediment Accumulation Rate Model

The sediment accumulation rate used in this study was established by determining the slope of ln(excess ^{210}Pb) with depth. The ^{210}Pb disintegration constant is divided into the slope and provides a sedimentation rate in cm yr $^{-1}$. Intervals and activities from ^{210}Pb analysis are shown in Appendix-A.

Calculations used to determine sediment accumulation rate (Robbins, 1977):

1. **Radioactive Decay Equation**
   $N=N_0e^{-\lambda t}$

   N=Activity or the number of radioactive nuclei.
   N_0=Original activity or number of radioactive nuclei in the sample when t=0
   λ=disintegration constant (^{210}Pb = 0.03114 yr $^{-1}$)
   t=time

2. **Excess ^{210}Pb activity**
   $N_{(Ex\ ^{210}Pb)} = N_{(total\ ^{210}Pb)} - N_{(total\ ^{226}Ra)}$

3. **Sediment velocity**
   $$ws = \frac{\lambda}{\text{Slope of } Ln(N_{(Ex\ ^{210}Pb)})}$$

4. **Age at depth (in the absence of mixing)**
   $t=d/ws$

   t=age
   d=depth
   ws=sediment velocity

This model relies on the following assumptions:

1. Constant input of ^{210}Pb from the atmosphere. Therefore the supply of initial unsupported ^{210}Pb will not change for different time intervals.
2. ^{226}Ra levels also do not change through time, due to an occurrence known as secular equilibrium where ^{226}Ra in sediments have the same level of radioactivity as the ^{238}U, its initial source.
3. Sedimentation rate or sediment input is constant through time.
4. No migration of ^{210}Pb within the sediment column (except from the top ~10 cm surface mixing layer).
5. No compaction has occurred within the interval of sediments being used for ^{210}Pb dating.

2.5.3 Estimation of Error and Uncertainties

2.5.3.1 Estimation of Error

Analytical error is calculated by using a propagation of error formula which includes ^{210}Pb and ^{226}Ra counting errors and errors in the exponential fits to the data (Johannessen et al., 2003).

2.5.3.2 Considerations When Dating With ^{210}Pb.

Mixing - Sediment mixing, especially from burrowing organisms, can result in material being found out of place in the primary sedimentary succession. Sediment deposited at a discrete time can be mixed downward and even upward after burial resulting in a smearing effect, producing erroneous ages (Johannessen and Macdonald, 2012). Downward mixing emplaces a younger signal into older material making the sedimentation rate appear higher than in reality. The Fraser Delta is known to be a

productive biological environment with a variety of burrowing organisms. In sediments near the Fraser Delta Main Submarine Channel the extent of biomixing is limited as frequent sand beds in the sediment record are difficult to penetrate for burrowing organisms, acting as barriers to communication between mud units. Ages collected near sand beds are likely to be true representations due to the relatively undisturbed nature of the interbedded muds.

Transported Sediment - Sediment reworking from bottom currents including density flows and tidal resuspension/traction may emplace older material with younger material. To avoid material which has been reworked by bottom currents, subsamples for ^{210}Pb analysis were not collected from intervals with sand mottles or laminations, but from intervals with as little sand as possible.

Compaction – With the process of burial, sediment at depth will experience a reduction in porosity as overburden weight increases. The distribution of ln(excess ^{210}Pb) activity in a sediment column should have a linear decay with depth in uncompacted sediment. In compacted sediment the distribution of excess ^{210}Pb activity would trend as a downward curving decay line with depth and would have a lower ^{210}Pb activity, appearing older than sediment at an equal depth in uncompacted sediment (Robbins, 1977). To account for this problem, porosity was measured for all ^{210}Pb subsamples (Appendix 2). It was found that no substantial variation in porosity occurred over the length of the cores which were analyzed.

Molecular Diffusion – Chemical mobility through pore water may occur, but is considered to be negligible in this study. In aquatic environments ^{210}Pb has an affinity for the particulate state and thus is considered to be relatively immobile (Robbins, 1977).

Human error – Facies misidentification can lead to substantial error in calculation of sedimentation rate. For example, a 10 cm thick sandy mud bed may have been deposited at the distal reaches of a turbudite event over a period of hours or days. If this deposit was not classified as a sand bed it would be considered to be part of the constant hemipelagic deposition and the interval will then represent one or more years of sedimentation. Furthermore, some sand units may have boundaries which are unclear (i.e. gradational) and any error in classification would also effect the calculation of sedimentation rate. Designation of sedimentary units was performed using physical properties and visual/textural analysis to minimize any misclassification.

2.5.3.3 Sources of Uncertainty

The following list outlines potential sources of uncertainty which could not be quantified, but may be significant in the establishment of a reliable sediment accumulation rate.

- Differentiating between slide-generated turbidites and hyperpycnite/resuspension events.
- Defining upper/lower boundaries of event beds at gradational boundaries.
- The assumption was made that the sediment accumulation rate is constant through time. In reality there is seasonal variation. One spring with high amounts of snow melt and precipitation could deliver as much river discharge and sediment as the entire year previous.
- If event beds are erosive, the amount of material removed or reworked beneath event beds is unknown.

2.5.4 ^{226}Ra Background Level

^{226}Ra activity was used to determine background levels in order to calculate the unsupported ^{210}Pb activity. Each core that was analyzed for ^{210}Pb also had three subsamples measured for ^{226}Ra activity: from the top, middle and bottom intervals. The three values from each core were averaged to establish a constant background activity that could be applied to ^{210}Pb activities from all intervals. This method was required because none of the subsamples analyzed have activities as low as the background level. This was determined before knowing the ^{226}Ra activities because the regression line of ^{210}Pb activities does not reach the point where it flattens out where the background level would be interpreted to occur.

2.5.5 Criteria for Identification of Sand Beds and Correlation.

Two separate methods were used for identifying sand beds and correlating adjacent cores. Density and magnetic susceptibility were used as a proxy for grain size where increasing values represent increasing grain size (St-Onge et al., 2008). In most cases peaks in density corresponded to peaks in magnetic susceptibility. Background values of density and magnetic susceptibility were inferred to represent ambient hemipelagic deposition and peaks were inferred to represent sand beds. Information such as normal and inverse grading, and cracks or voids in the sediment were also ascertained using this proxy. Correlations were performed along-transect by visual inspection and by matching corresponding peaks of density and magnetic susceptibility with similar characteristics between adjacent cores. The first attribute was depth of sand bed, assuming that there would be minimal variation in sedimentation rate between cores of the same transect which generally are the same distance from the river mouth. Visual signatures such as

sharp base, internal lamination and fining up structure were used to correlate sand beds from one core to another. Facies 6 sand beds with thick clean sand intervals of a lighter brown colour were used to make initial correlations as they stood out clearly from the predominantly muddy sediment. As facies 6 sand beds tend to occur in sets of two or more, sets of sand beds were matched at similar depths along transects.

From core transects 1 through 4, distance from the river mouth increases with each transect. Sedimentation rates generally decrease with distance from the river mouth from 10 cm yr^{-1} proximal to the river mouth to 1 cm yr^{-1} (Hart et al., 1998).

It was expected that with each transect there will be a corresponding drop in sediment accumulation rate. With a known sediment accumulation rate from ^{210}Pb activities, it becomes possible to correlate sand beds from transect to transect. Even without ^{210}Pb activities, sets of sand beds could be visually correlated from transect 1 to transect 2. Correlations from transect 2 to transect 3 or 4 were very difficult as no similar sets of sand beds were identified in sediment of corresponding age.

2.5.6 Criteria for ^{210}Pb Site Selection and Subsampling Procedure

2.5.6.1 Core Selection

Cores were selected for sediment accumulation rate analysis based on the ability to correlate sand beds to adjacent cores. Transect 1 has a number of sand beds which can be correlated across its length and to most cores in transect 2. Core 125 is closest to the levee crest in transect 1 and has the highest number of sand beds. An assumption was made that any turbidity current event in the sediment record would likely be represented here if anywhere in the suite of cores as it most proximal to both the river mouth and channel axis. Core 125 was selected due to its completeness of event beds. Core 123 was

also selected because many of the sand beds can be correlated from core 125 and it is useful to determine if the sedimentation rate changes with distance from the channel axis. There were no obvious correlations between transect 2 and 3. Initial correlations along transect 3 and 4 were made possible by linking facies 7 basal sand unit. Because this basal unit is not observed in transects 1 and 2 and under the general assumption that sedimentation rate declines with distance from the river mouth it was inferred that these cores represented older material deposited by a slower sediment accumulation rate. Subsamples from this area were collected with the intention of dating older material and linking the lower part of the stratigraphy to the upper part of the stratigraphy. The upper portion of the stratigraphy is seen in higher detail in transects 1 and 2. Cores 126 and 127 were selected from transect 3 as they had more sand beds in the top metre of the record that could possibly be correlated to the first two transects. These cores also have facies 7 basal sands which are the basis for correlation to other cores in transects 3 and 4.

2.5.6.2 Subsample Site Location

Sand intervals were assumed to represent event beds or otherwise potentially transported sediment. Consequently, subsamples were taken from mud intervals, which according to the model, represent relatively constant sedimentation. Sand intervals were mathematically removed to generate an "eventless" stratigraphy. Voids and major cracks were also removed in this calculation resulting in a "corrected depth". Once removed the assumption was made that uniform hemipelagic deposition occurred through time. The cumulative thickness of sand beds and voids was subtracted from the full length of the core and the remaining length was divided into 12 in an attempt to subsample at regular intervals. While subsample extraction was under way, some sample positions were

relocated to optimize the chances of subsampling material that had not been reworked. In some places, sand laminations or mottles were subsampled due to the lack of sand-free intervals from which to obtain a subsample. This is especially true for cores that were collected from the levee crests including cores 125 and 126 which have a high number of sand beds.

A different strategy was employed for subsampling core 126 after sand and void intervals were removed from the total length of the core. Core 126 becomes very sandy at depths greater than 2.8 m. Core 127 terminates at roughly the same depth. In order to achieve a similar density of subsamples with less sand influence (compared to core 127) twelve subsamples were taken above the sandy interval in core 126. Five more subsamples were taken from intervals between repetitive facies 6 sand beds from 280 to 400 cm to see if any reasonable ^{210}Pb activities could be detected.

2.5.6.3 Sediment Subsampling

A steel constant volume sampler (CVS) with a diameter of 2.22 cm and height of 2.605 cm was used to extract sediment from the cores. The CVS was lubricated with Pam cooking oil to minimize sediment compression when being inserted and was pressed into the split core. The CVS was not deep enough to reach the core liner which may have drawn down sediment from higher intervals during the initial coring process. Wet weight was recorded and all samples were placed on aluminum trays and dried overnight in an oven at a temperature of 50°C or until the dry weight was stable. Dry weight was recorded, then samples were ground up and homogenized using mortar and pestle. ^{210}Pb activities were measured through digestion/distillation-alpha spectroscopy at Flett

Research Ltd. Three of the subsamples from each core were also analysed for ^{226}Ra by a digestion ^{222}Rn Emanation-Alpha process.

3. Results

3.1 Delta Front Morphology

The main morphological features of the Main Submarine Channel are outlined in Fig. 3.1.

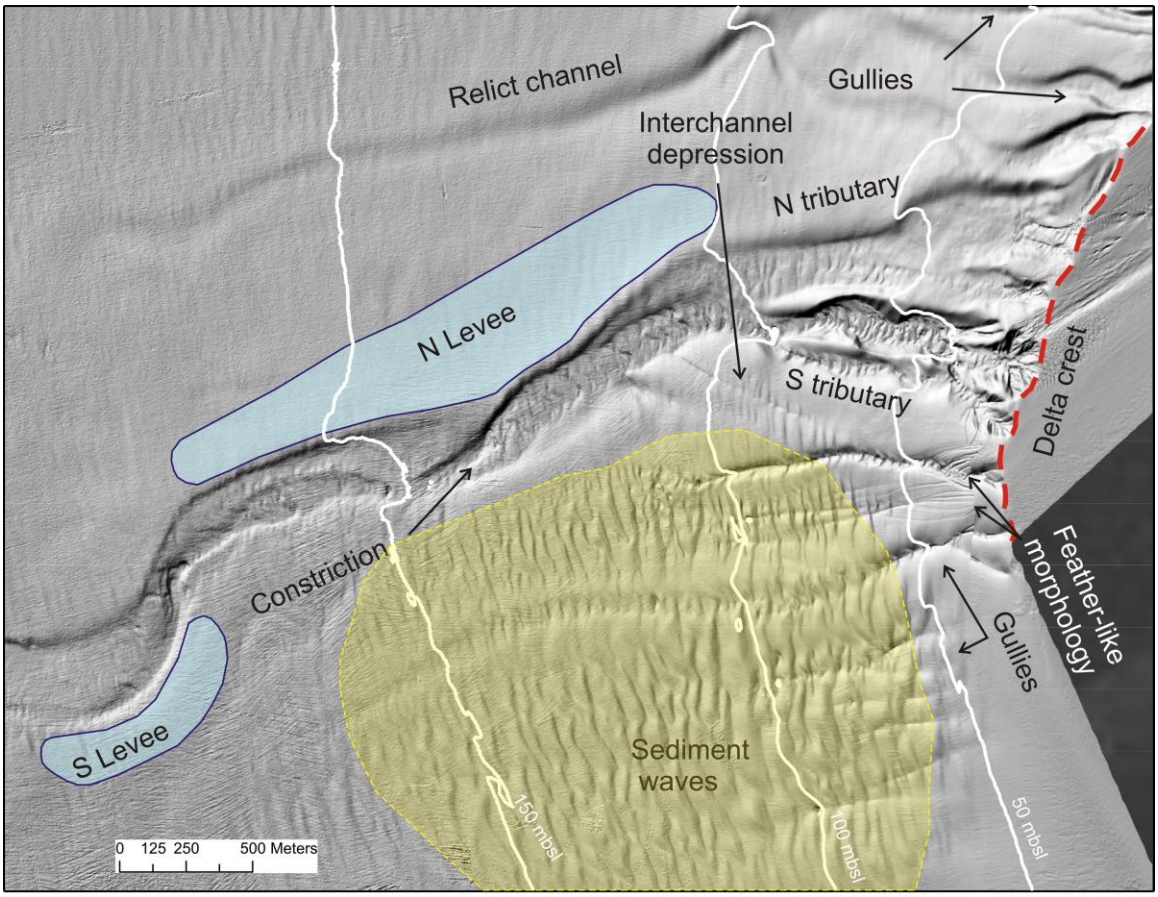

Fig. 3.1. Shaded relief image of multibeam bathymetry showing morphological features. Levees are outlined in blue, sediment waves in yellow and the delta crest is outlined in a dashed red line.

3.1.1 Delta Profile

The concave cross section profile of the non-channelized delta front gradually becomes less steep with distance from the delta crest (Fig. 3.2). Seaward of the crest, which is at 5 mbsl, in the non-channelized margin the average slope starts at 8.4°. Major slope breaks

occur at depths of 36 and 82 mbsl where slope decreases to 5.3° and 2.3° respectively. A minor slope break occurs at 174 mbsl decreasing to 1.3°.

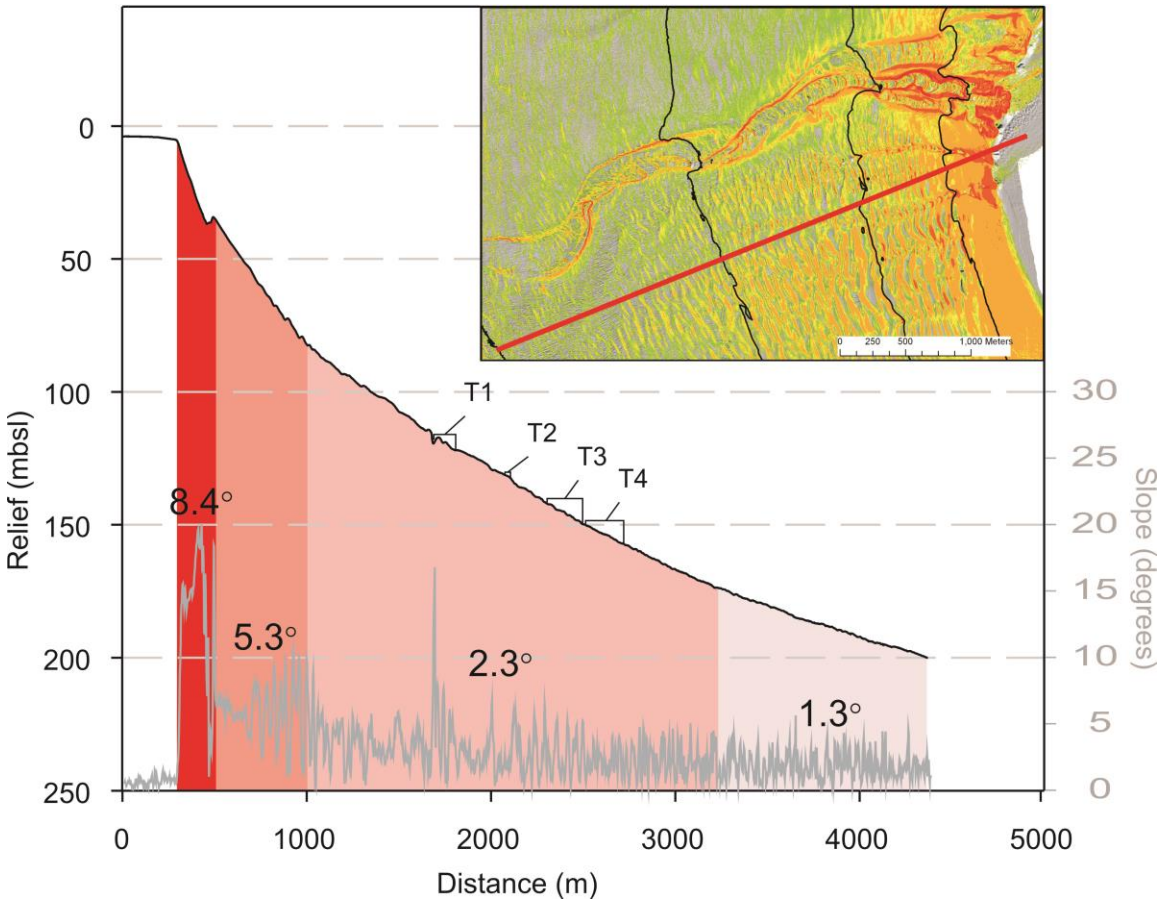

Fig. 3.2. Fraser Delta front non-channelized relief and slope. Profile is from red line in slope map (upper right). The delta front has a concave shape and becomes less steep with distance from the delta crest shown by the black relief curve. Slope curve is shown in grey. Slope breaks are indicated by a colour change in the red-to-pink fill under the relief curve. After the crest, there are two substantial slope breaks, at 36 and 82 mbsl. There is a minor break at 174 mbsl. Average slope shown above slope curve. Core transects 1 to 4 are marked as T1 to T4.

3.1.2 Tributary Channels

Consistent with Hill (2012) bathymetric difference maps from 2005-2006, the south tributary channel appears to experience high rates of sediment accumulation. New bathymetric difference maps from 2007-2006 and 2007-2008 reveal two primary sites of

net erosion in the south tributary (Fig. 3.3A). The most obvious is a 100 m wide scallop-shaped bedform just below the 50 mbsl contour. This feature is characterized by a net decrease in elevation of greater than 3 m between 2006 and 2007. From 2007-2011 the headwall of the bedform migrates upslope, while sediment accumulation fills its position from previous surveys. Similar but smaller crescentic bedforms migrate upslope during this time sequence. These bedforms are on the scale of 10s of meters and experience net loss of sediment between 1 and 3 m. The difference map between 2006 and 2011 shows a longer range net accumulation of greater than 3 m over most of the channel bed of the southern tributary and shows no signs of these crescentic bedforms.

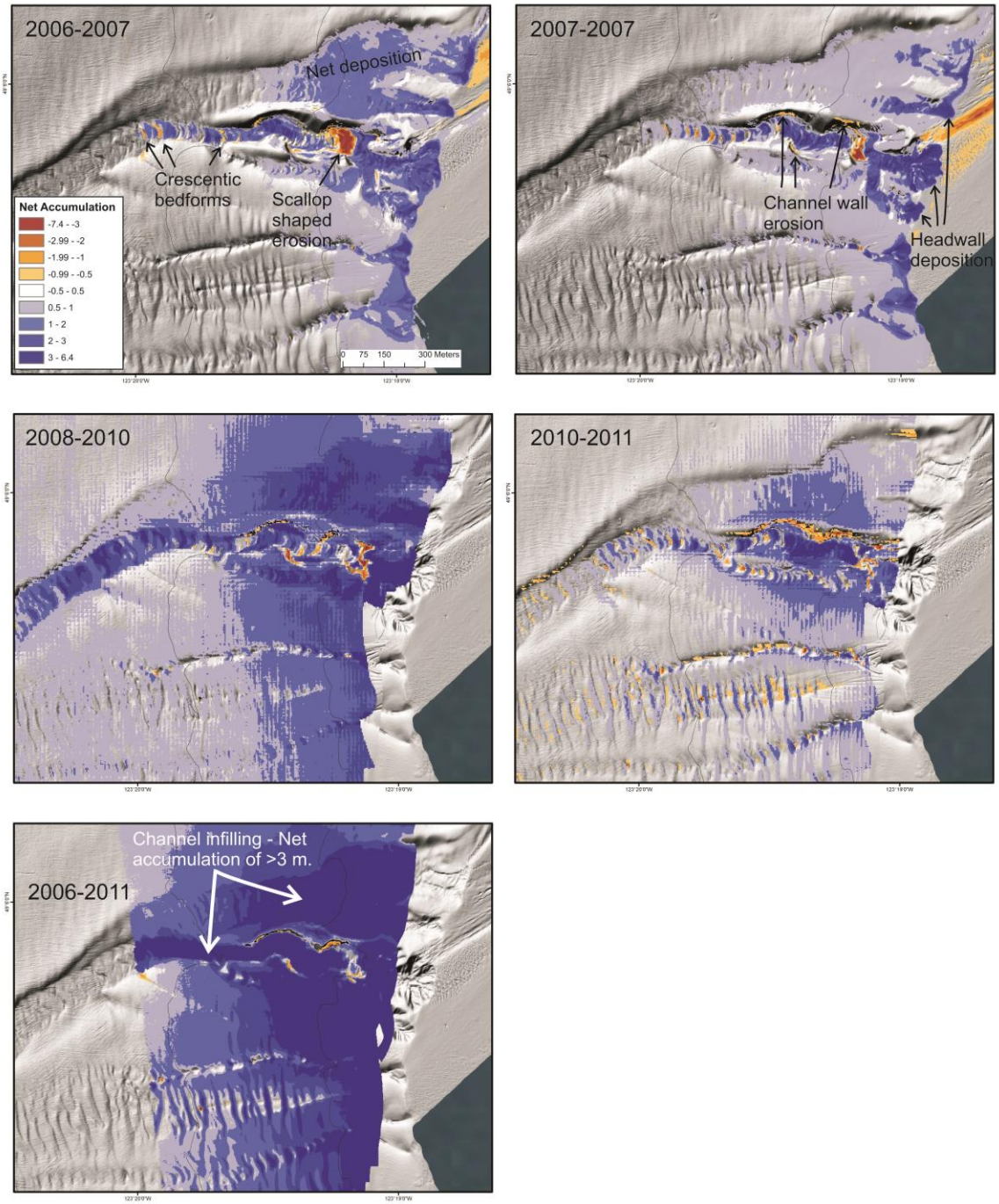

Fig. 3.3A. Bathymetric difference maps of upper channel region. Cold colours represent net deposition and warm colours represent net erosion.

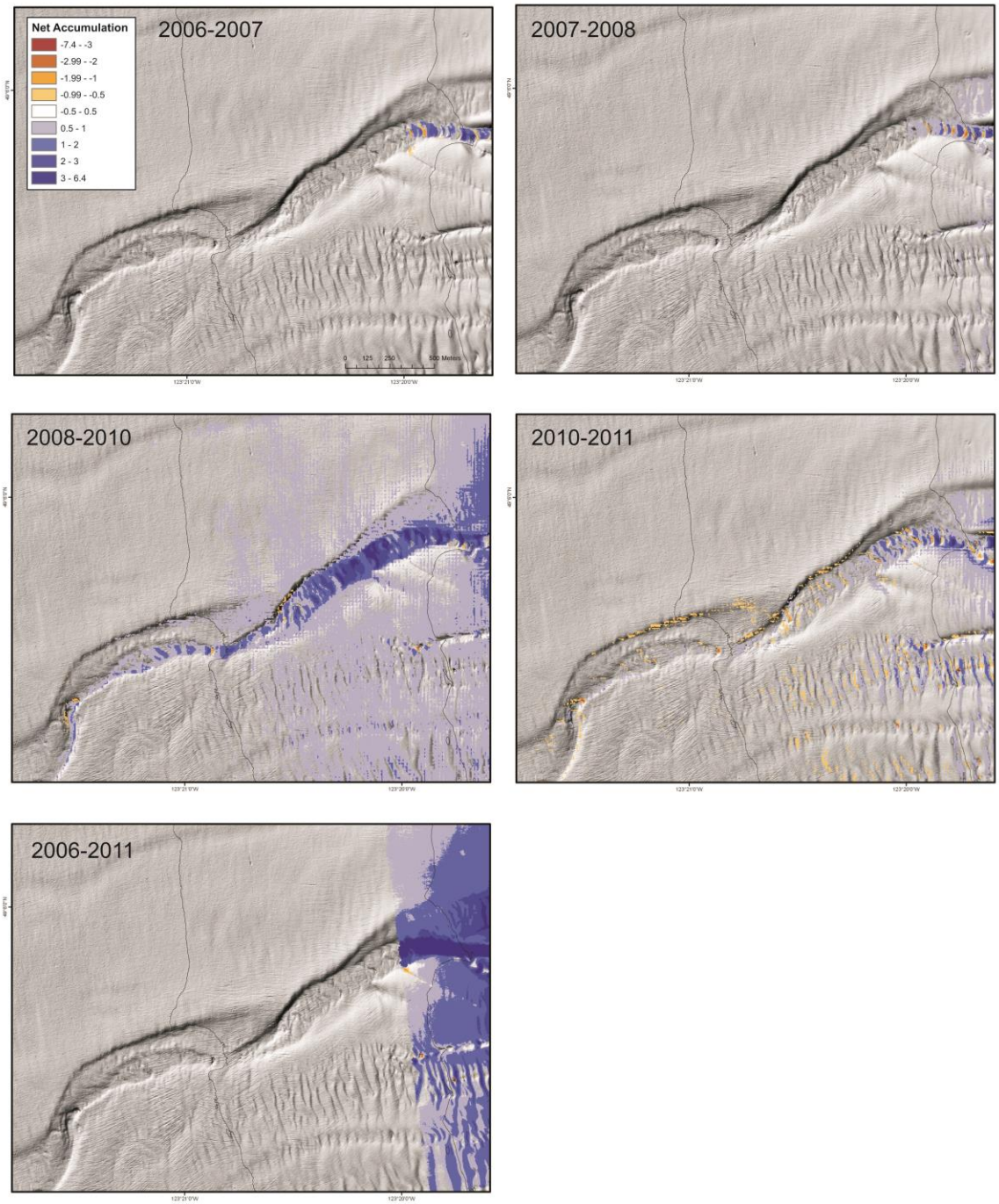

Fig. 3.3B. Bathymetric difference maps of mid-channel region. Cold colours represent net deposition and warm colours represent net erosion.

The second site of net erosion is around the channel walls of the south tributary (Fig. 3.3A). Amounts of net erosion ranging between 1 and 2 m are common, especially on the southern flank of the interfluves which separates the north tributary from the south

tributary. Images from Tully cruise 2011006 ROV dive reveal a fresh erosion surface along the south flank with exposed parallel laminations and blocks of wasted material which lie at the base of the interfluves (Fig. 3.4). Net accumulation appears to be prevalent in all other areas of the tributary channels. The north tributary is characterized by accumulation of greater than 3 m between 2006 and 2011. Amounts of net accumulation in the tributary headwalls between 2006-2007 and 2007-2008 are greater than two meters. Rates of accumulation in the tributary channels are generally higher than the adjacent non-channelized margins of the seafloor.

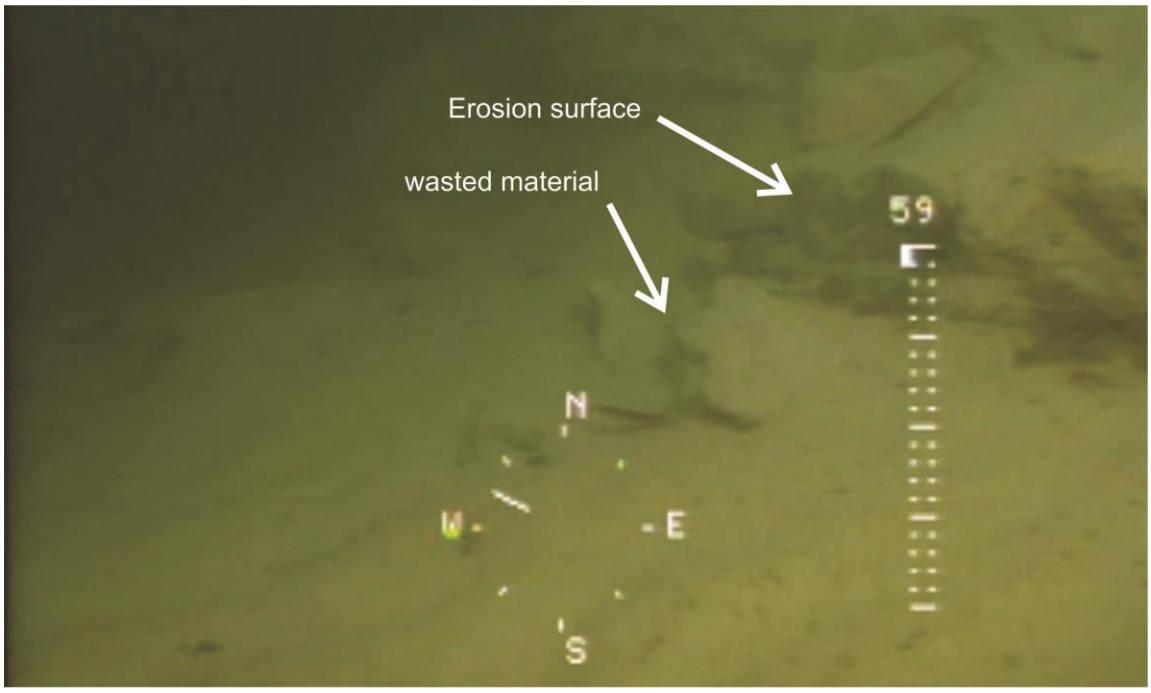

Fig. 3.4. Erosion surface and wasted blocks observed in south tributary from ROV 'Ocean Explorer'. Wasted blocks are roughly 10 cm in height. Image taken from the north wall of the south tributary.

3.1.3 Confluence of Tributaries and Further Downslope

Beyond the point where the two tributaries converge, the channel is mainly characterized by net deposition in recent surveys (Fig. 3.3B). With increasing distance from the river mouth, the thickness of accumulation in the channel decreases until the south bend.

Beyond the south bend, no net change in accumulation can be detected. Changes between 2008 and 2011 range from 0.5 to greater than three meters of accumulation over much of the channel. The difference map of 2008-2011 shows bedforms with similar morphologies as those observed in the south tributary. Net loss of sediment in crescent-shaped bedforms ranges between 0.5 and 2 m. The 2010-2011 difference map shows net erosion along the N wall of the channel of between 0.5 and 2 m, but the resolution of the 2010 survey is low when compared to the resolution of the 2011 survey (5 m vs. 2 m), creating some uncertainty.

3.1.4 Gullied Margin South of the Main Submarine Channel

A series of gullies have incised the delta crest south of the Main Submarine Channel (Fig. 3.1). Gully heads are roughly 200 m apart and begin roughly 200 m south of the south tributary channel. The gully which is immediately south of the Main Submarine Channel appears to have a more extensive headscarp, and the gully itself is deeper until it reaches the field of sediment waves where the gully gradually becomes no longer recognizable. The head of this gully has experienced net deposition (2006-2007, 2007-2008), but the rest of the gully appears to have no net change in sediment accumulation. A series of rills in a feather-like morphology extend upslope from the upper 300 m of the gully toward the delta crest (Fig. 3.1). These rills are only observed in the 2011 multibeam survey. Similar rills appear at the top of a smaller gully immediately to the south. The feather-like morphology of the southern gully is truncated by that of the northern gully. The depressions have relief up to 1 m. One other feature which has not been described previously is an interchannel gully which extends diagonally from a position 100 m north

of the 1st gully to the Main Submarine Channel just beyond the confluence of the tributary channels (Fig. 3.1). This feature is present in all surveys from 2006 to 2011 and has experienced a lower amount of net deposition than the surrounding area. The relief of this feature is 1 m at its deepest point, which is closest to the Main Submarine Channel.

3.1.5 Levee Relief

There is a prominent positive relief feature adjacent to most sections of the Main Submarine Channel that has been previously identified as a levee. The levee is on the north side of the channel from the confluence of tributary channels until the point where the Main Submarine Channel bends to the south. Beyond the bend, the levee is more prominent on the south bank (Fig. 3.1). Beginning just beyond the confluence of tributary channels and extending until the southward bend in the channel, the levee is on the north bank of the channel. In water depths between 105 and 180 mbsl, the positive relief feature reaches over 5 m above the local topography (Fig. 3.5). The slope toward the channel is generally between 5º and 10º, and reaches as high as 27º at 135 mbsl (Fig. 3.6). The slope away from the channel is generally between 2 and 5º and reaches a maximum slope of 7º at 110 mbsl. Measuring from the thalweg to the crest of the levee, the greatest change in relief is at depths less than 90 mbsl, and where the channel is deepest. At 90 mbsl the change in relief is 14 m. In places where the levee has greater relief compared with non-channelized local topography, the adjacent channel is not as deep and the change in relief between thalweg and crest is 10 to 13 m. Below 150 mbsl the change in relief is generally 5 to 10 m. A similar but smaller positive relief feature is present on the south bank of the channel where the channel bends toward the south. The

south levee crest is less pronounced than that of the north levee. South levee relief is at a maximum of 6 m at 180 mbsl.

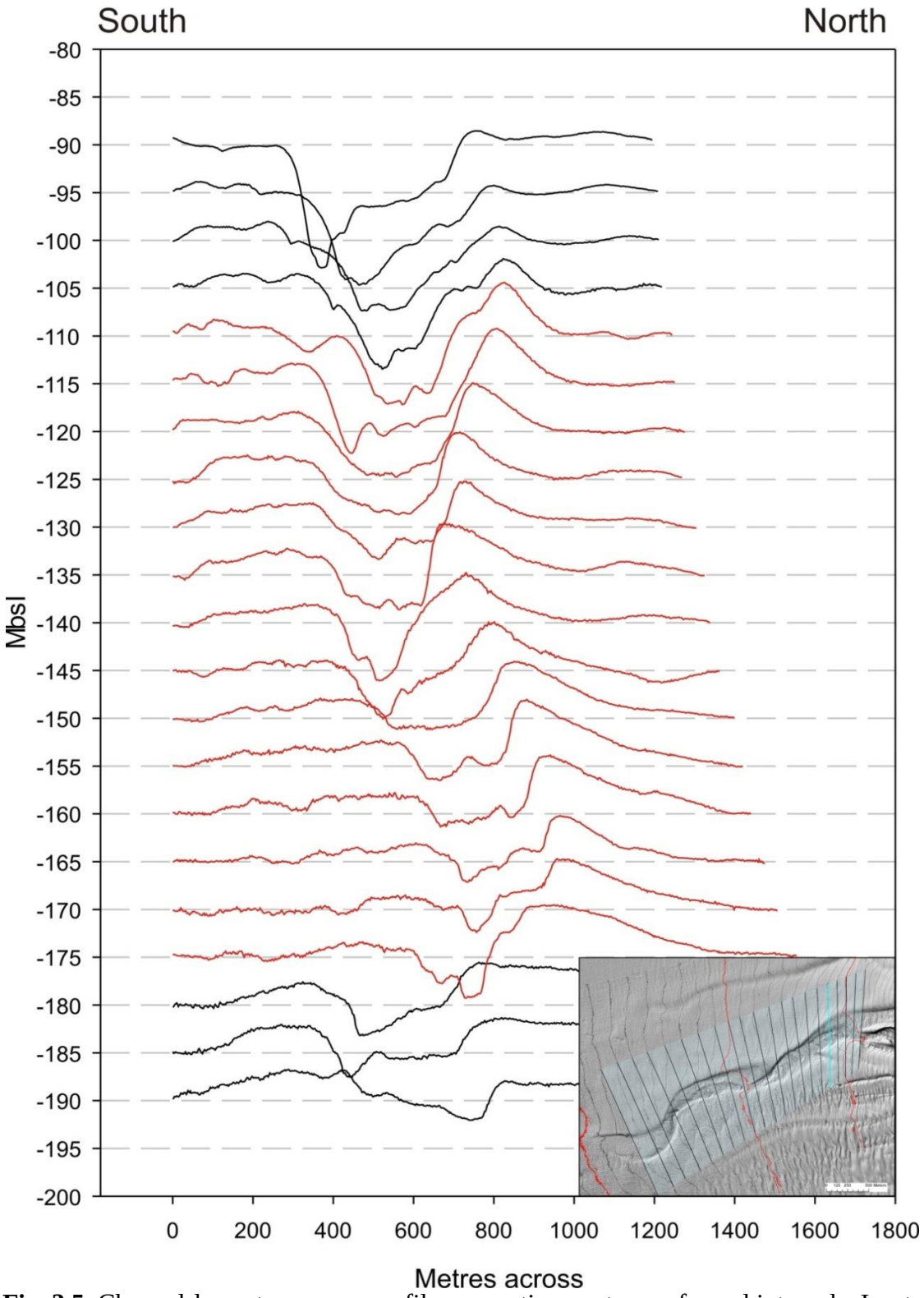

Fig. 3.5. Channel-levee transverse profile connecting contours of equal intervals. Inset map shows profile transects. Red channel profiles show depths where channel relief is greater than 10 m.

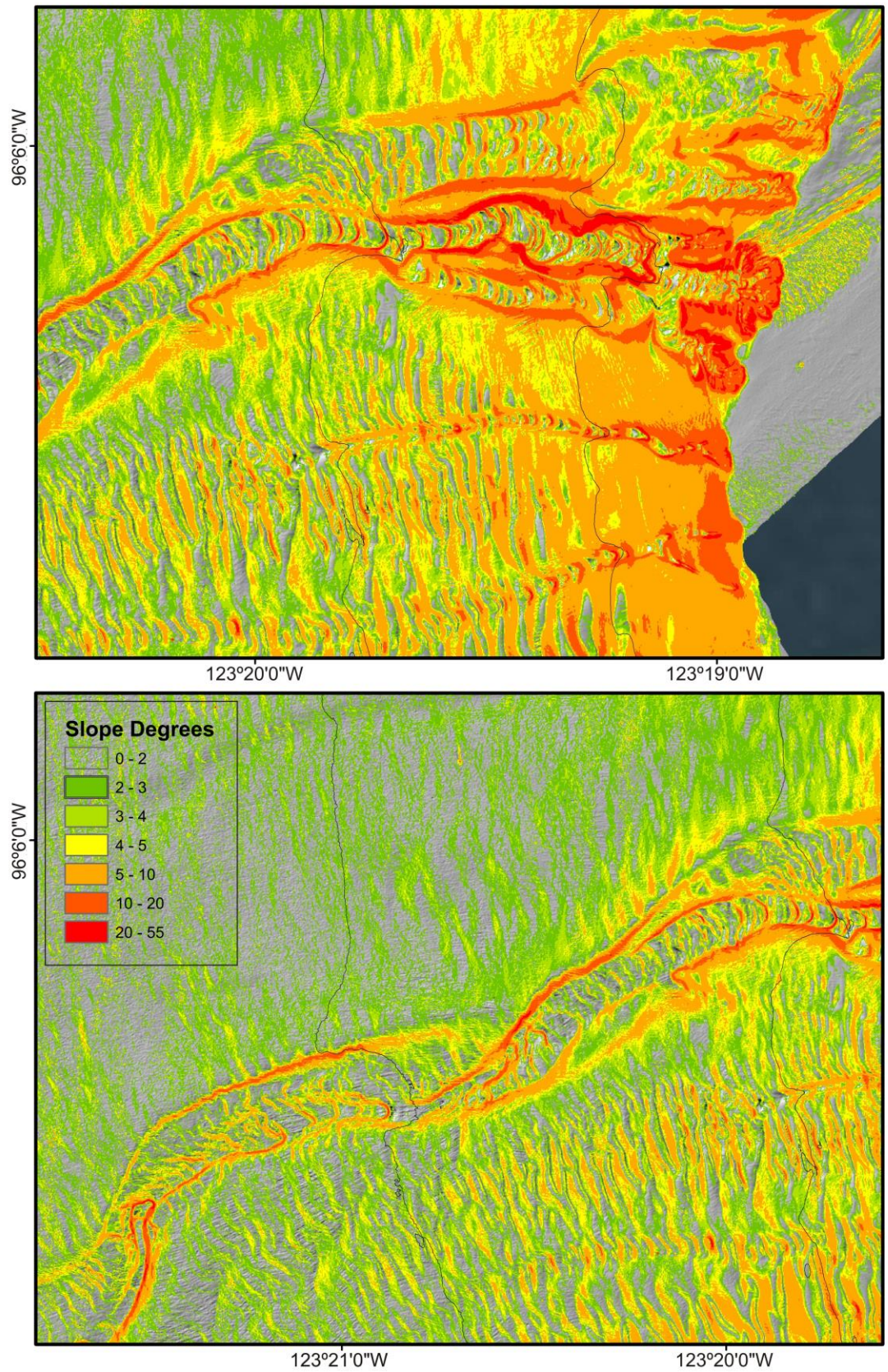

Fig. 3.6. Slope maps of upper and mid-channel regions.

3.1.6 Acoustic Backscatter

Backscatter data show concentrations of high backscatter in three main regions: inside the channel, on the banks of the channel, and the fan deposit (Fig. 3.7). Within the channel, highest backscatter values occur between water depths of 150 and 200 mbsl and in the distributary channels in water depths greater than 200 mbsl. There is an area of high backscatter on the north side of the channel between 150 and 200 mbsl which extends 1 km north to the relict channel. On the southern margin of the channel in depths of 150 to 200 mbsl there is a narrow area of high backscatter which extends less than 300 m to the south. The area of highest backscatter intensity is at the fan in water depths of 200 to 250 mbsl. There is a cone shaped area of approximately $5 \times 10^6 m^2$ which extends westward 2.9 km from the end of the Main Submarine Channel, and has a maximum width of 2.6 km.

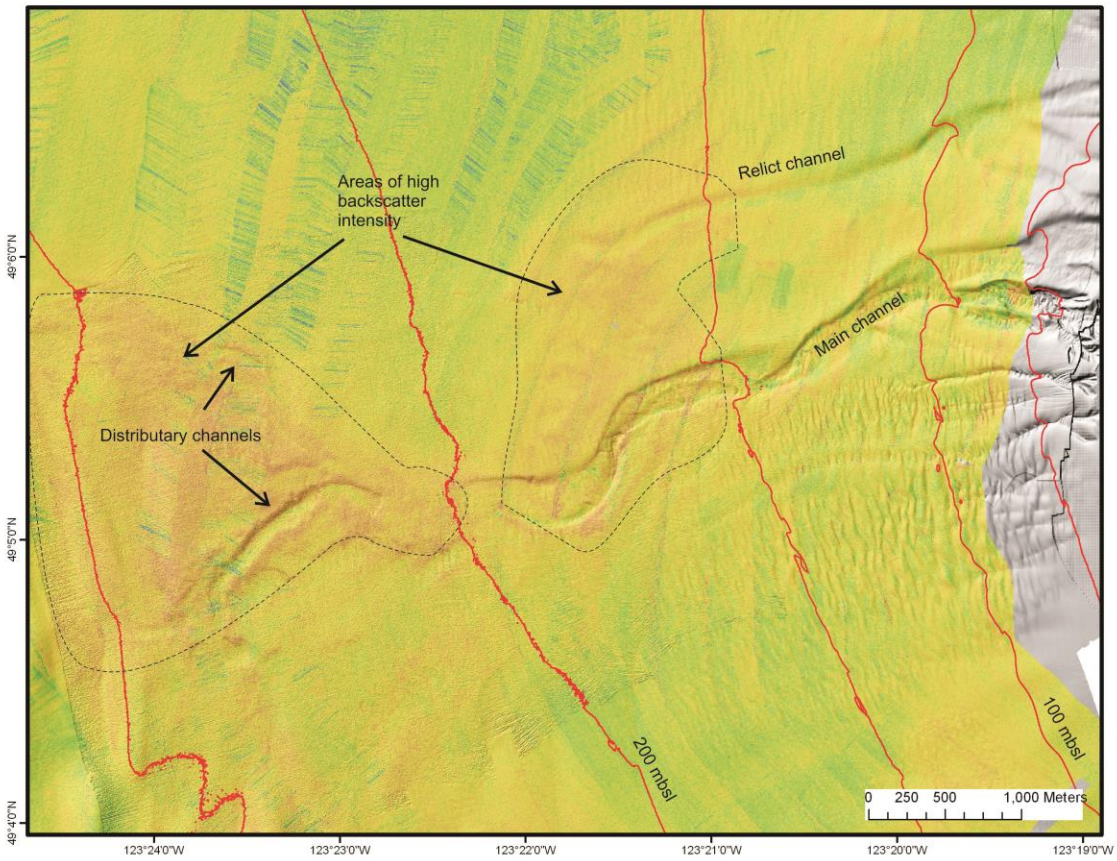

Fig. 3.7. Acoustic backscatter of the Main Submarine Channel showing areas of high backscatter intensity in yellow-brown which is focused around the channel and fan areas.

3.1.7 Seismic Interpretation

Seismic images of the subsurface beneath the channel system reveal 3 general acoustic units: a chaotic basal unit, a channel fill unit and a sub-parallel levee unit (Fig. 3.8A,B,C and 2.1). All three units can be observed in seismic transects which range in depth from 130 to 190 mbsl.

The chaotic basal unit is the basal unit which lies beneath the channel and extends north and south for the full reach of the channel. Reflectors in this unit are discontinuous. The transition between this unit and the overlying levee facies is marked by a high amplitude

reflector, which is seen in all seismic profiles of the channel system. This transition occurs between depths of approximately 2.5 and 3.5 mbsf.

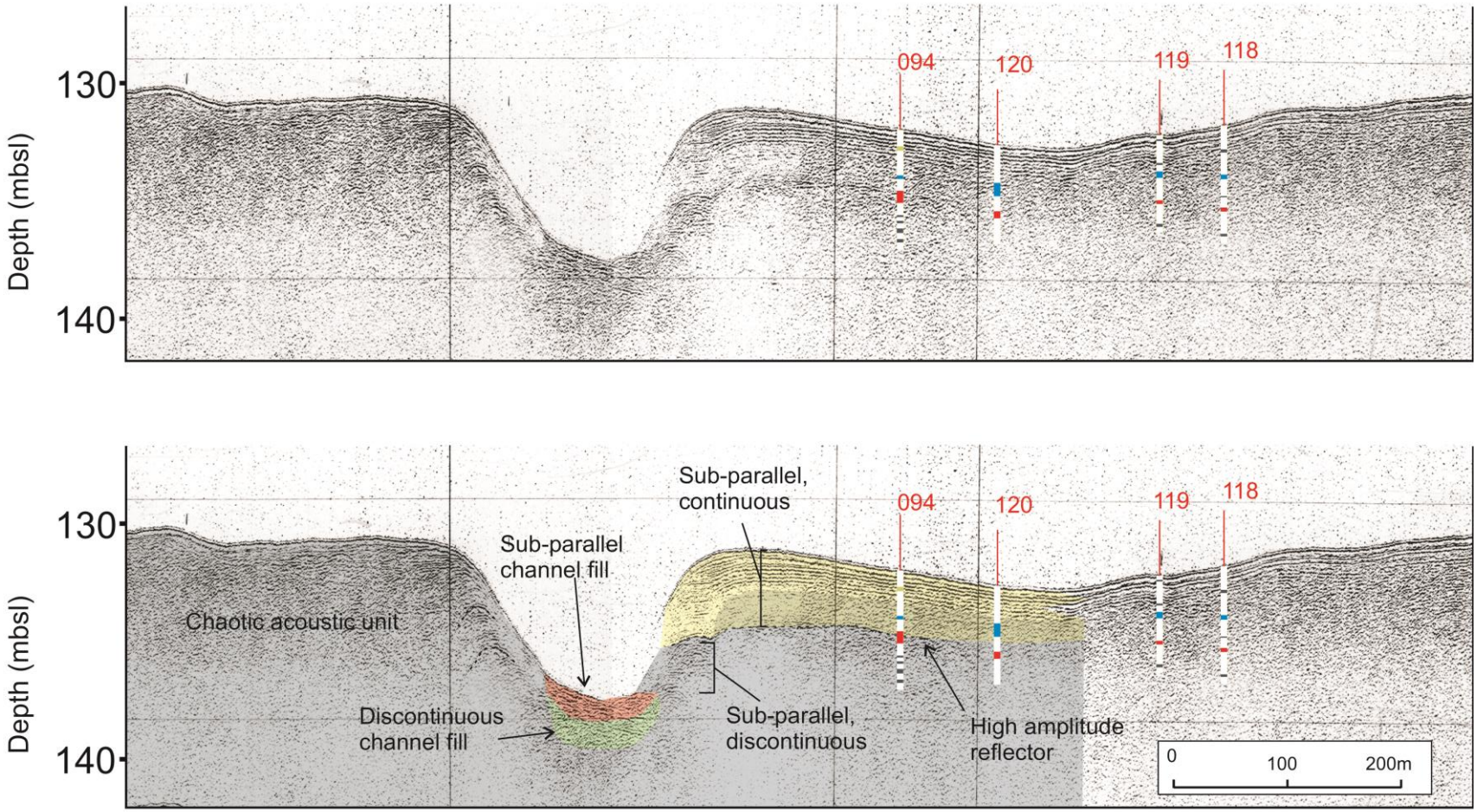

Fig. 3.8A. Huntec 92006PGC 340/0630. Transect 2 showing acoustic units and core locations. Yellow, blue and red bands on cores represent depth of sand bed sets. Grey bands are Facies 5 sand beds. Location of seismic line shown in Fig. 2.1.

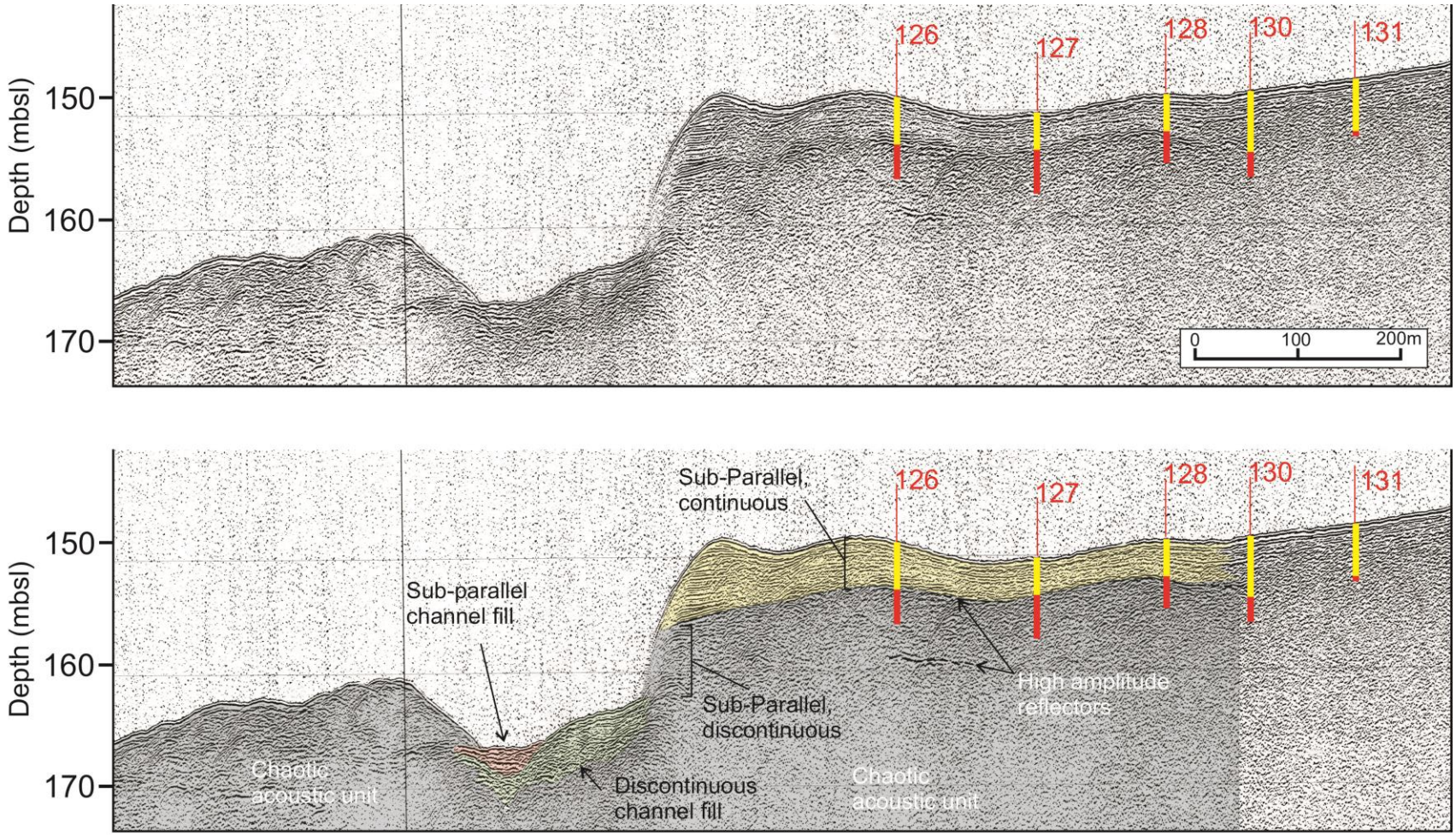

Fig. 3.8B. Huntec 92006PGC 324/1410. Transect 3 showing acoustic units and core locations. Yellow core section represents muddy sediment with few sand beds; red core section is characterized by sand beds. Location of seismic line shown in Fig. 2.1.

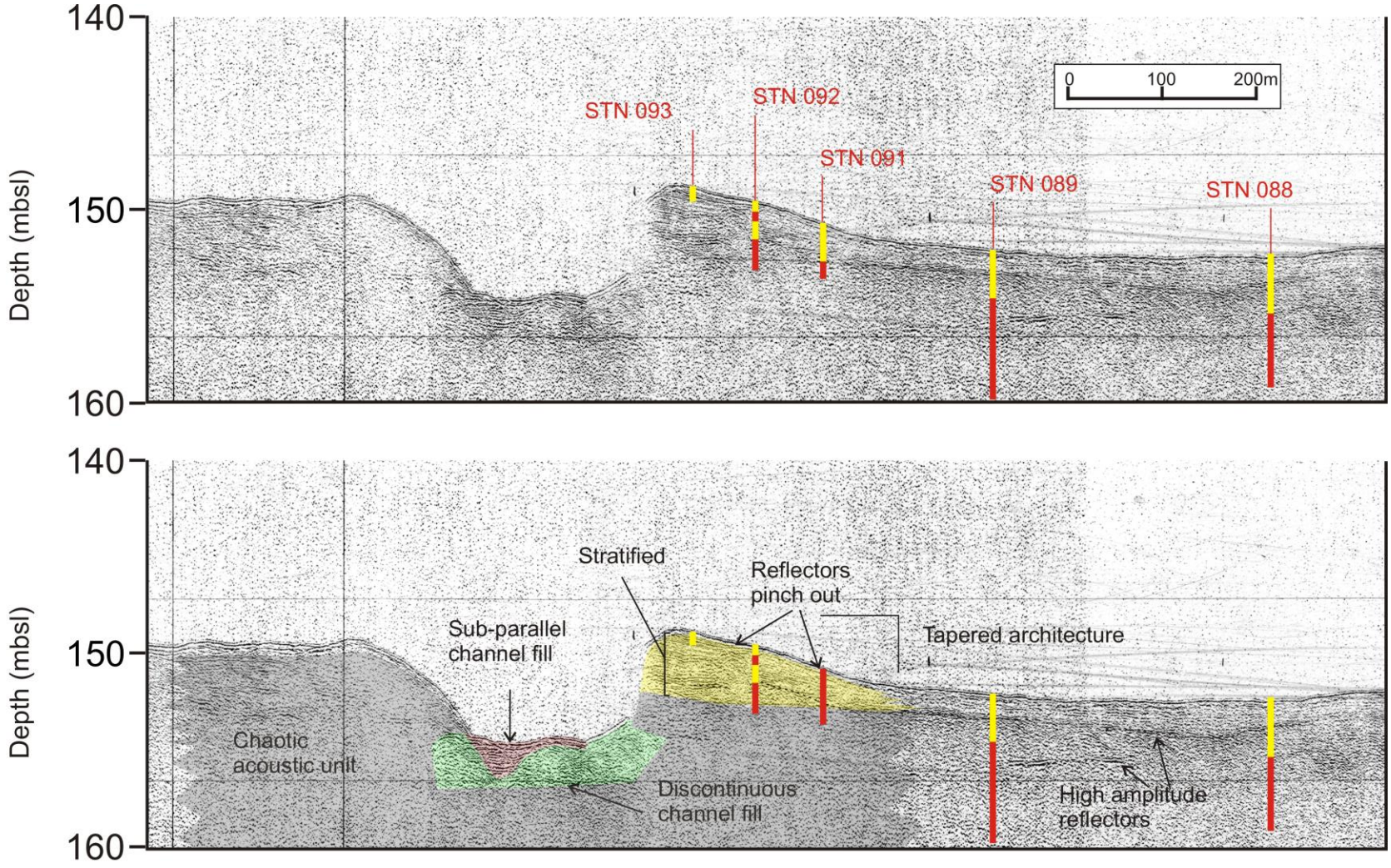

Fig. 3.8C. Huntec 92006PGC 340/0713. Transect 4 showing acoustic units and core locations. Yellow core section represents muddy sediment with few sand beds; red core section is characterized by sand beds. Location of seismic line shown in Fig. 2.1.

The channel fill unit is found at the base of the channel in most seismic profiles and is as thick as 3 m in transect 3. There are two facies in the channel fill unit; sub-parallel channel fill and discontinuous channel fill. Sub-parallel reflectors are generally high amplitude, occur in places where the channel bottom is flat, and may occupy a depression within surrounding discontinuous channel fill. Reflectors of the discontinuous channel fill are high amplitude and are generally curvilinear with convex structure. The discontinuous channel fill occupies most of the channel sub-bottom and transitions to the chaotic acoustic unit laterally where channel walls become steep (Fig. 3.8).

The levee unit is present on the north bank of the channel and is characterized by sub-parallel reflectors. In seismic transects, which are oriented 90º to the channel axis, a clear tapering architecture is visible where the levee is thickest proximal to the channel axis and thins with distance (Fig. 3.8C). In some cases individual reflectors are observed pinching out with distance from the channel. Some reflectors within the levee system have higher amplitudes than surrounding reflectors. The tapering architecture of the levees tends to extend for several hundred metres and then passes into sub-parallel, non-tapering horizons that are laterally extensive and are present in most parts of the delta front.

3.2 Facies Description

Facies 1 to 7 are shown in Fig. 3.9. Facies type summaries of all cores are shown in Fig. 3.10A,B,C,D.

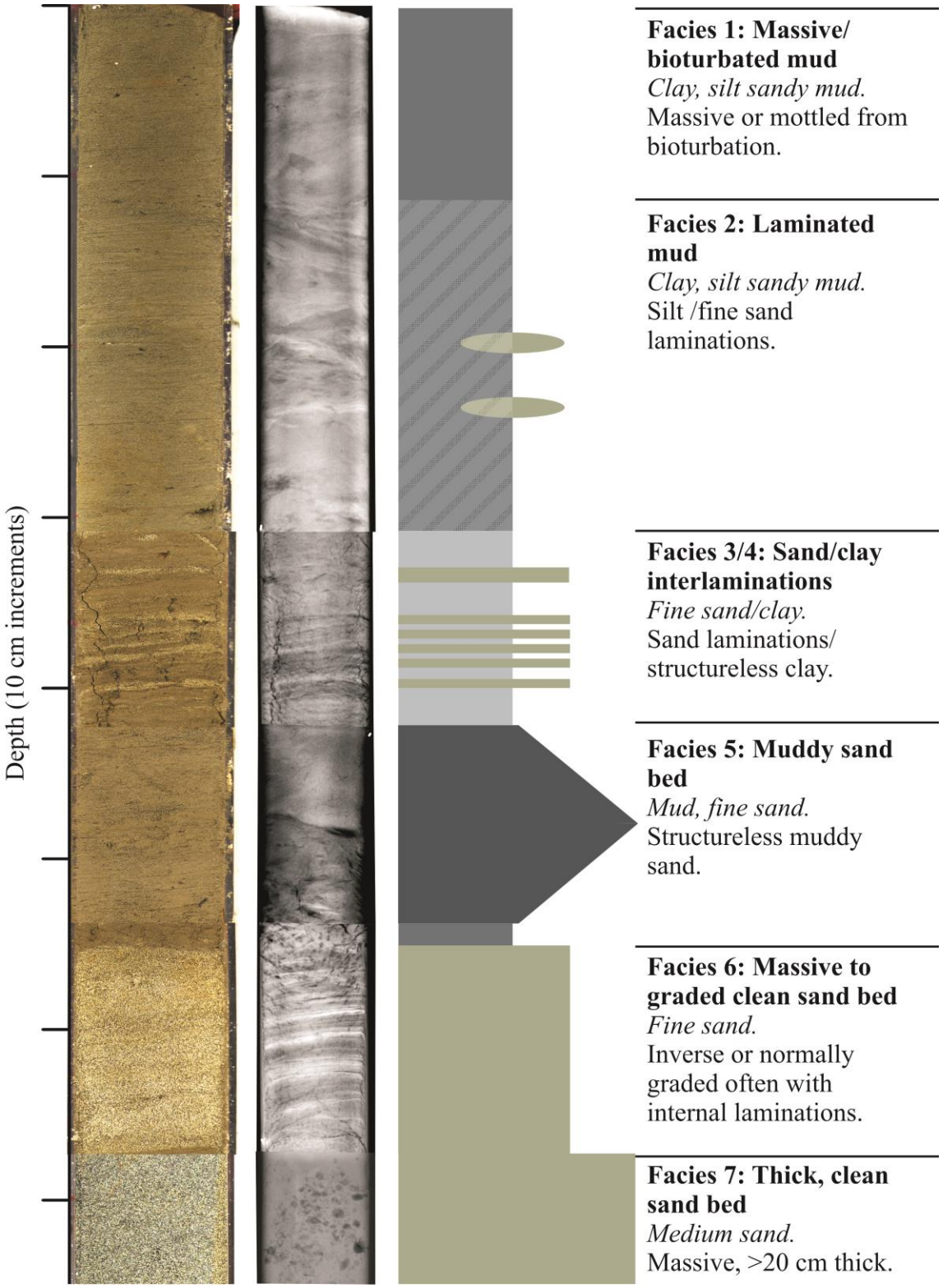

Fig. 3.9. Composite facies log showing facies 1 to 7. Left image is high resolution photograph, middle is x-radiograph and right is a graphic log.

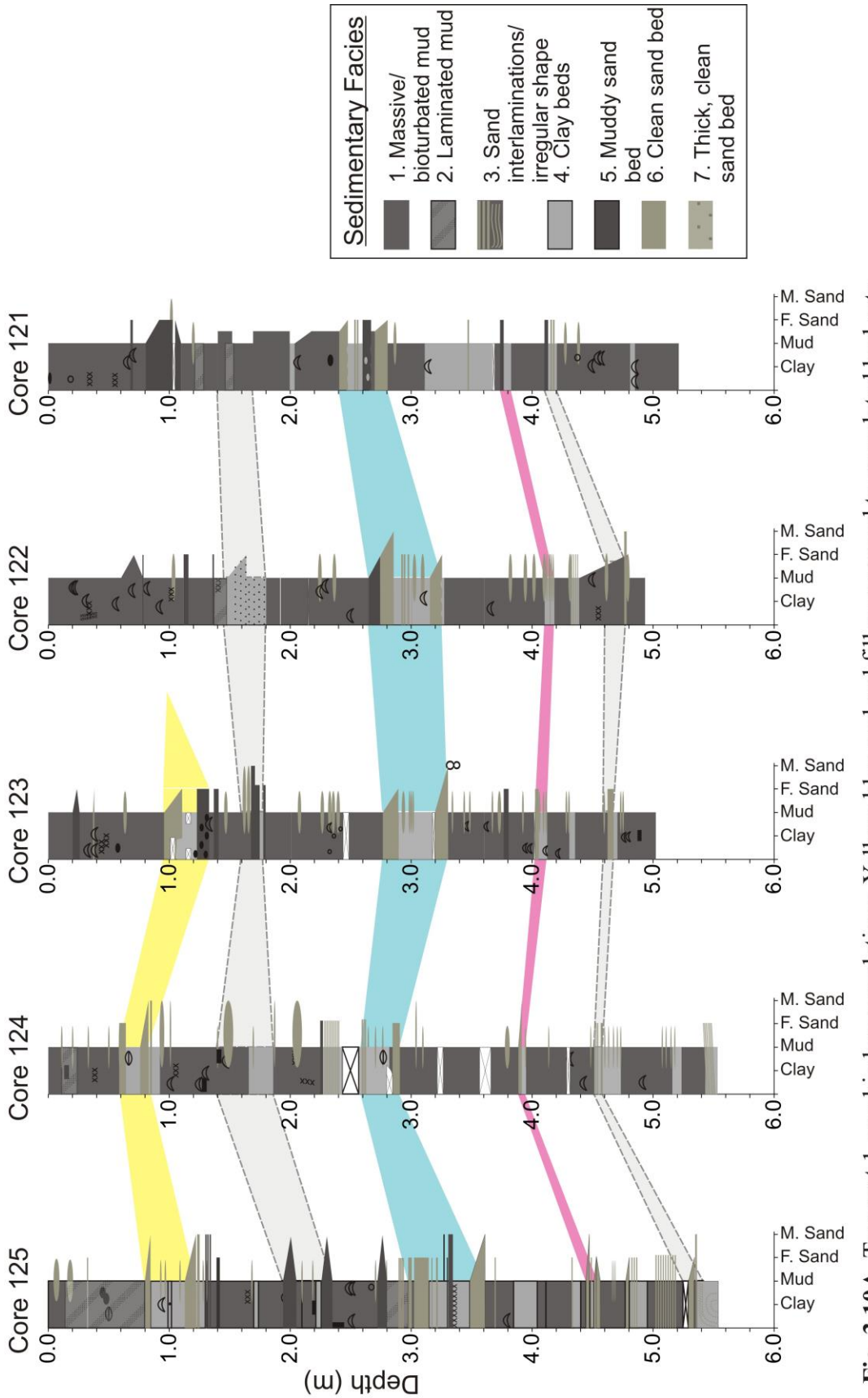

Fig. 3.10A. Transect 1 graphic log correlations. Yellow, blue and red fill correspond to correlated bed sets.

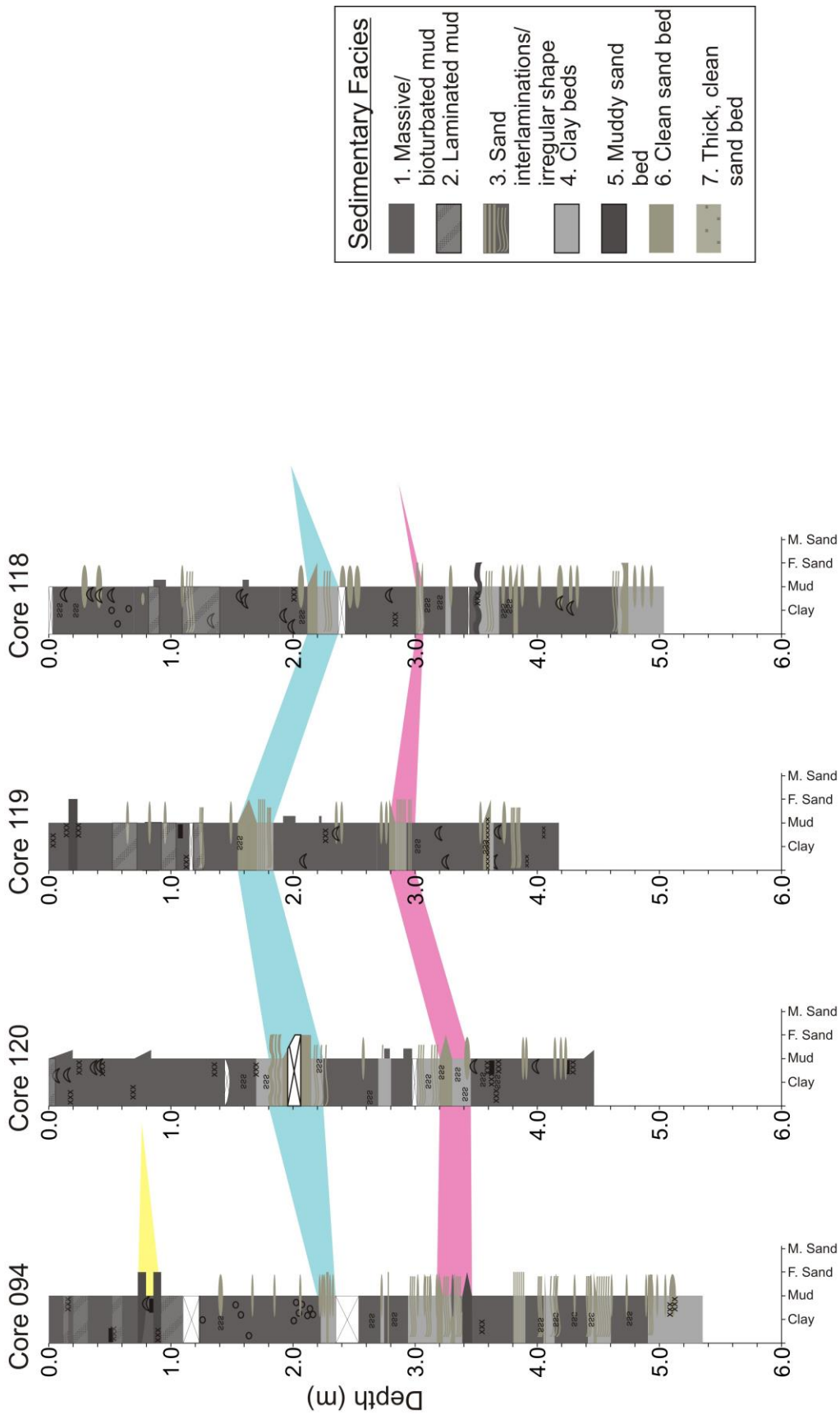

Fig. 3.10B. Transect 2 graphic log correlations. Yellow, blue and red fill correspond to correlated bed sets.

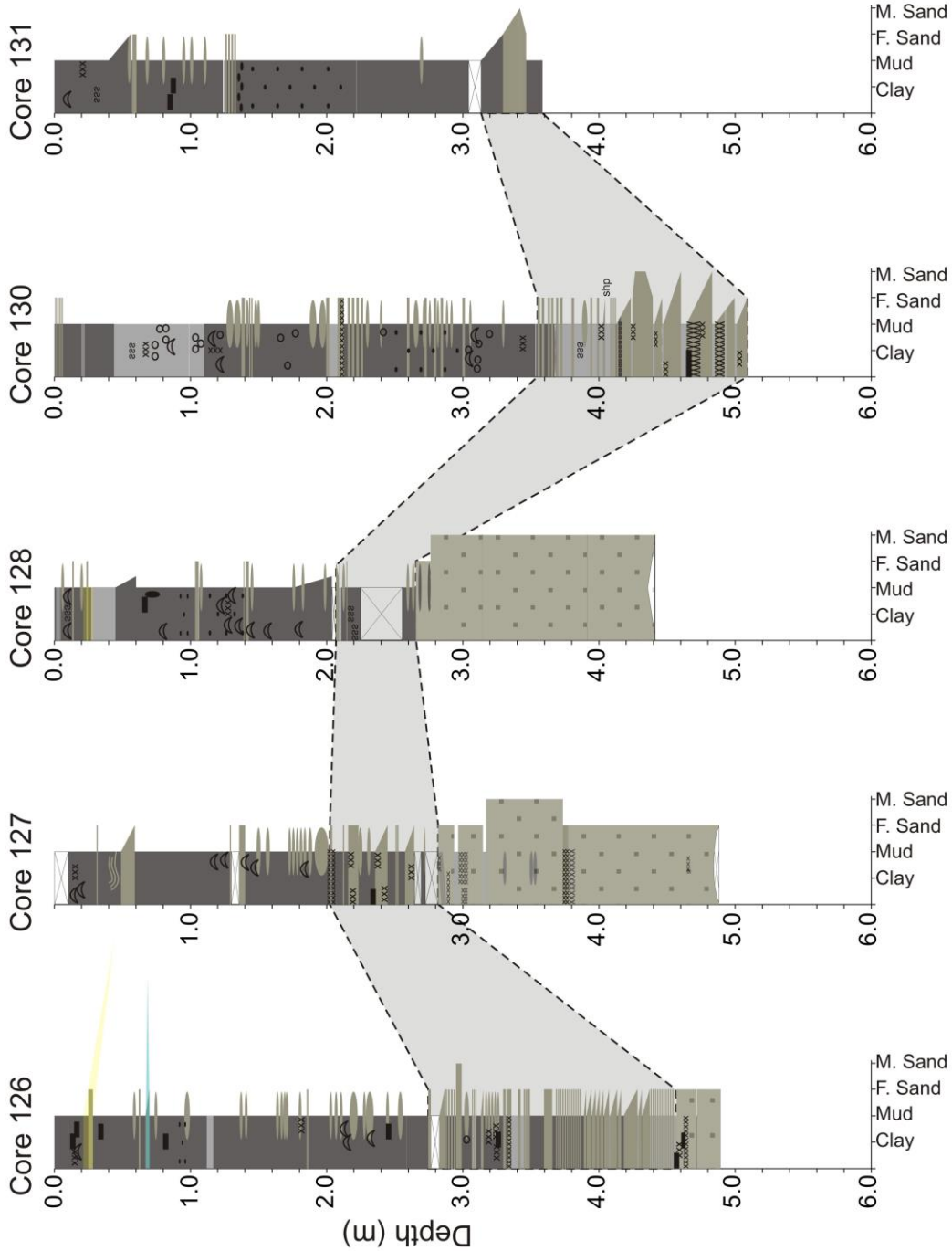

Fig. 3.10C. Transect 3 graphic log correlations. Yellow and blue correspond to correlated bed sets. Grey fill with dashed outline corresponds to the interbedded sand bed unit.

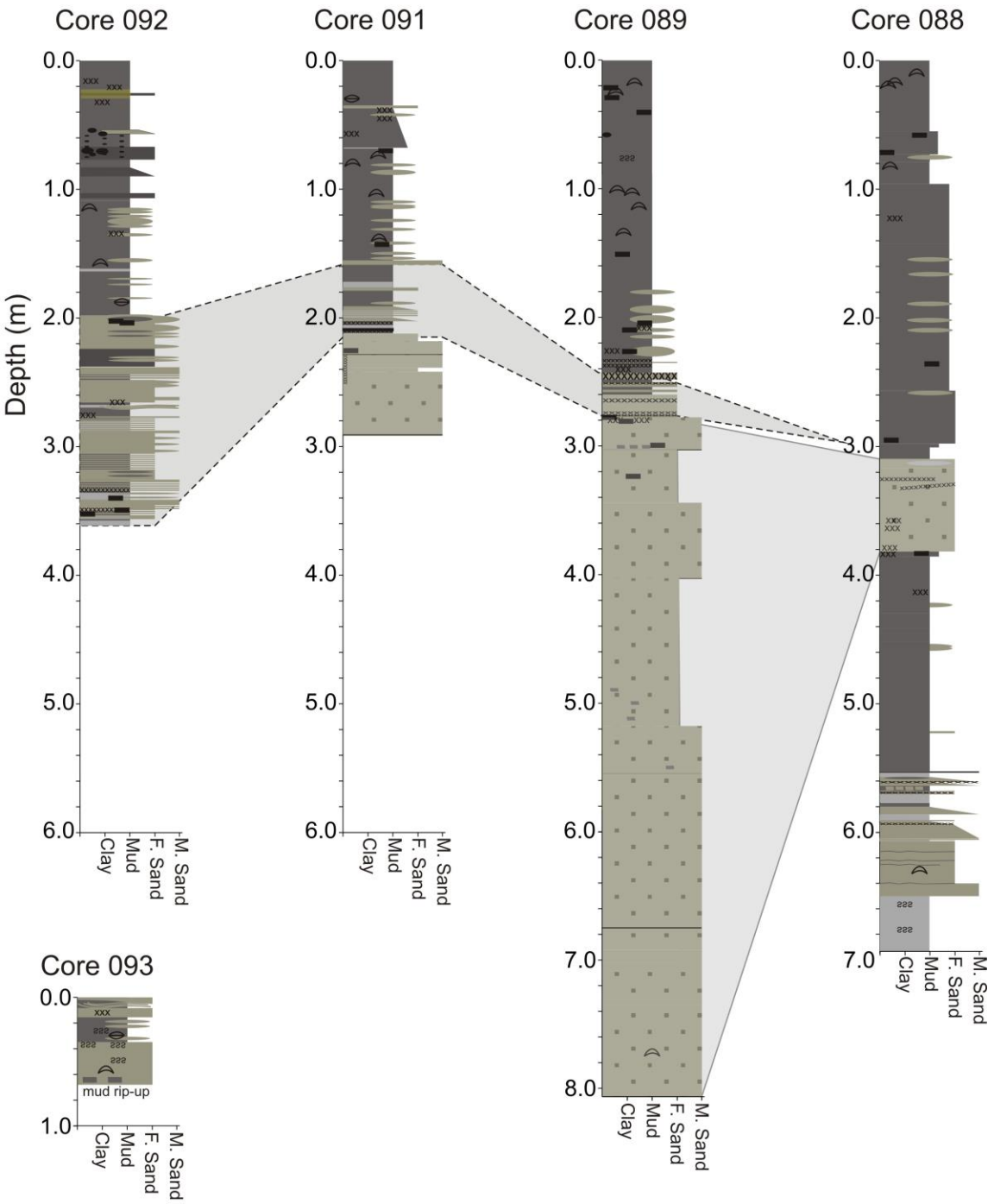

Fig. 3.10D. Transect 4 graphic log correlations. Grey fill with dashed outline corresponds to the interbedded sand bed unit. Grey fill with solid outline corresponds to the basal facies 7 sand unit.

3.2.1 Facies 1 (F1): Massive/bioturbated Mud.

F1 consists of clay-rich to fine sandy mud and may have patches, or mottles of silt or sand in a finer matrix. This facies is generally internally massive where mottles are not present. Mottles may be sandy mud with poorly defined boundaries, or may be clean sand with sharp boundaries. They are generally elongated and may have rounded or angular boundaries. Horizontal and vertical burrows are well preserved in places and are visible in x-radiographs. The extent of bioturbation varies from minimal, below a detectible amount, to extensive, with a high density of overlapping burrows. Organic matter is common in this facies including disseminated fine woody debris and bivalve shell fragments.

3.2.2 Facies 2 (F2): Laminated Mud.

Like F1, F2 consists of clay-rich to fine sandy mud but has preserved laminations. There are two end members of the mud facies; F1 is at one end with no primary structure and facies 2 has preserved primary structure. In places with poor core or x radiograph quality the two end members cannot be differentiated. In F2 muds, well preserved silt laminations up to 0.5 cm thick are generally either plane parallel or wavy/subparallel. Convolute laminations with a high degree of curvature are present in places but their occurrence is rare. In places where silt laminations share the same grain size as the surrounding silty mud matrix, structure is discrete and only observable in x-radiographs of F2. Laminated muds generally occur in beds greater than 10 cm thick and range from 4 to 99 cm in thickness. Sediment core quality plays an important role in the identification of lamination due to poor x-radiograph image quality of dry and cracked cores.

3.2.3 Facies 3 (F3): Mud with Sand Interlaminations.

Muddy sediments of F3 contain sand laminations up to 1 cm thick that are texturally distinctive from F1 and F2, and are easily identified by visual inspection of split cores. Most sand laminae are plane parallel, although some laminations may be discontinuous or lenticular in nature. This facies includes millimetre scale laminations of fine woody debris. Interlaminations occur in intervals up to 43 cm thick. Elongated horizontal sandy mottles in F1 may indicate bioturbation or soft sediment deformation of F3 laminations.

3.2.4 Facies 4 (F4): Clay Beds

This unit consists of structureless gray clay in intervals up to 5 cm thick. Beds may have minor silt components, but contrast with F1 by a lack of any internal sand content. This facies is associated with sets of sand beds and sand laminations. Clay beds are often present at the top of fining up sand beds and are often preserved beneath sharp based sand beds of Facies 6 where interlaminations of clay and sand are common. Interlaminations of F3 and F4 occur in beds sets as thick as 40 cm. Interlaminations and interbeds are well preserved with a lower amount of bioturbation than F1. Immediately after cores were split the clay beds had a distinct grey colour which distinguished them from other facies, but the colour changed to brown when oxidized. The colour is slightly lighter than the brown of F1 and F2 in places, but this is not always the case.

3.2.5 Facies 5 (F5): Muddy Sand.

F5 is characterized by fine sand with a substantial mud component. Bottom and top contacts are often characterized by inverse grading and normal grading, respectively, and internal structures are rare. This facies often does not visually stand out from F1 or F2

and upper and lower boundaries can be difficult to distinguish. Peaks in bulk density and magnetic susceptibility and high relative stiffness compared to other muddy intervals are distinguishing characteristics when relative change in grain size is minimal. Muddy sand beds are generally less than 5 cm thick, but may be as thick as 20 cm. F5 beds occur as individual beds or in sets of multiple beds with Facies 6 sand beds.

3.2.6 Facies 6 (F6): Massive to Graded Clean Sand Bed.

This facies comprises beds of well sorted fine to medium sands and lacks the interstitial mud component of F5. Beds often have a sharp basal contact, and a fine sandy base that fines up to a muddy or clay rich cap. Some beds are medium grained sand at the base and fine upwards. The sand component of the fining up beds ranges from 2 to 20 cm and the clay/mud cap rarely exceeds several centimetres. Basal coarsening-up is also common, in most cases coarsening for less than 0.5 cm then fining up. Internal plane parallel laminations are common and are especially clear in x-radiographs. Rare cross laminations can be observed in x-radiographs (Fig. 3.12A Core 122, 1.).

Massive sand beds generally still have sharp basal contacts and share similar thickness with the structured sand beds. Laminations of fine woody debris may be present, usually at the top of a sand bed, but in some cases can be found internally or even at the base of sand beds. Core quality may be compromised where cracking has occurred at the contact between sand and mud beds. These cracks make it difficult to distinguish the nature of the interfacies contact. Clean F6 sand beds are often interbedded with F1, F2 or F4 in packages between 10 and 60 cm thick and as thick as 200 cm when immediately above Facies 7.

3.2.7 Facies 7 (F7): Thick (>20 cm), Clean Sand Beds.

This facies is characterized by thick beds of medium grained sand with no apparent structure. These beds appear at the base of the piston core. Core 88 is the only F7 bed (65 cm thick) that was penetrated through to the underlying mud unit. The thickest F7 sand bed is 525 cm. In many cases it is possible that sand was drawn up the piston core making beds appear much thicker than in reality. Tops of the massive sand beds are bioturbated with no preserved structure or contacts. Beds of coarse woody debris are in places up to 10 cm thick with individual wood and bark pieces up to 1 cm thick. Rounded mud clasts are present in a few cores.

3.3 Correlations

In cores from transects one and two, three sets of mappable sand beds are identified and are referred to as ‘yellow’, ‘blue’ and ‘red’ bed sets (not descriptive of actual sediment colour). Bed sets are shown in Figs. 3.11 to 3.13 and summarized in tables 3.1 to 3.3. In both transects 1 and 2, the yellow bed set is discontinuous, only being observed in the first few cores. The blue bed set is the largest both in terms of number of sand beds and in terms of individual bed thickness. The red bed set is continuous, but beds are fewer and are not as thick as in the blue set.

3.3.1 Yellow Bed Set

The yellow bed set in transect 1 is characterized by multiple F6 beds interbedded with F3 and F4 beds (Fig. 3.11). The yellow bed set is only present in Cores 123 to 125 and begins at depths ranging from 59 to 96 cm (Table 3.1).

Core 125 has two F6 sand beds interbedded with F4 beds (Fig. 3.11). The bottom clay bed is beneath the first sand bed. The clay bed is laminated with discontinuous muddy sand laminations, but appears relatively unbioturbated. The first sand bed has a sharp base which grades up to a poorly defined top (Fig. 3.11, Core 125, 1.). The clay bed above the first sand beds is mottled and has a few granules dispersed throughout. The second sand bed has sharp boundaries, is normally graded, and has internal laminations (Fig. 3.11, Core 125, 2.). The top of the second sand bed is bioturbated.

Core 124 has two F6 sand beds interbedded with F4 clay (Fig. 3.11). The bottom clay bed is beneath the first sand bed. This clay bed has thin, continuous, millimetre scale muddy sand laminations and a large sand mottle at 92 cm. The first sand bed has a sharp base, which grades up to a poorly defined, bioturbated top (Fig. 3.11, Core 124, 1.). The clay

bed between the two sand beds is highly bioturbated with discontinuous sand laminations and sand mottles. There is a discontinuous sand lamination containing granule size clasts at 71 cm. The second sand bed is discontinuous with sharp but irregular boundaries (Fig. 3.11, Core 124, 2.). This bed is highly bioturbated with mottles of muddy sand in the overlying sandy mud bed.

Core 123 has two sand beds, one F6 and one F5, which are separated by a F4 clay bed (Fig. 3.11). The first sand bed is F5 muddy sand with no defined boundaries (Fig. 3.11, Core 123, 1.). There is a clean sand mottle with irregular boundaries at the base of the first sand bed and granule-sized clasts dispersed throughout the sand bed. The clay bed between sand beds has a higher sand component than most clay beds associated with sets of F6 sand beds. This clay bed is bioturbated with mottles of sand and no recognisable sand laminations. The second sand bed is cracked at the base, obscuring the boundary, and fines up to a gradational top contact (Fig. 3.11, Core 123, 2.). No structure is observed in the second sand bed.

Cores 122 and 121 have sandy mud concentrations from 60 to 80 cm and 80 to 100 cm, respectively, but lack the clean F6 sand of yellow bed set sand beds of this transect. Core 94 contains two F5 sand beds at approximately 80 cm, but with no clean F6 sand bed (Fig. 3.11). Consequently, core 94 was not included in the yellow bed set. Yellow beds cannot be traced to this approximate depth of 70 to 90 cm in other cores of transect 2.

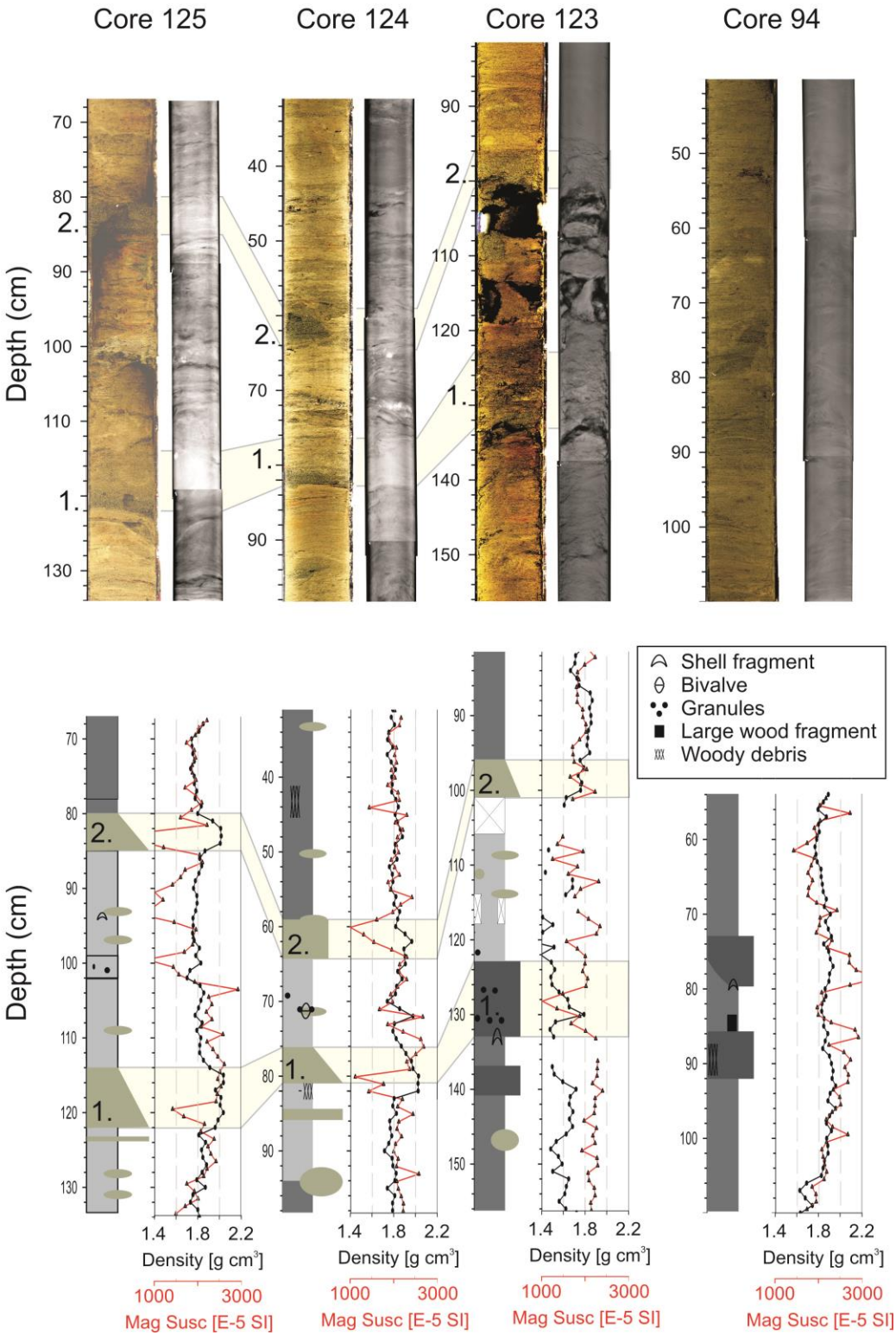

Fig. 3.11. Figure showing correlations of yellow bed sets in transects 1 and 2. Top shows high resolution photograph and x-radiograph. Bottom shows corresponding graphic logs and physical properties (black curve-gamma ray density; red curve-magnetic susceptibility). Yellow band shows correlation of sand beds. Sand beds described in text are numbered.

Table 3.1. Yellow bed set depth, number of sand beds and bed thickness.

	Station	Depth (cm)	Number of sand beds	Bed thickness (cm)
Transect 1	125	75 to 125	2	5, 8
	124	59 to 81	2	5, 6
	123	96 to 133	2	5, 10
	122	n/a	n/a	n/a
	121	n/a	n/a	n/a
Transect 2	94	73 to 92	2	7, 6
	120	n/a	n/a	n/a
	119	n/a	n/a	n/a
	118	n/a	n/a	n/a

3.3.2 Blue Bed Set

Transect 1 blue bed set is characterized by multiple F6 sand beds interbedded with F3 and F4 clay beds with sand laminations (Fig. 3.12A). The blue bed set begins at a subsurface depth of 240 to 300 cm in transect 1. This bed set has the thickest sand beds encountered in all cores along the transect (Table 3.2).

Core 125 has four sand beds with two thick F6 beds at the top and bottom of the bed set (Fig. 3.12A). The bottom sand bed has a sharp base with some minor irregularities (Fig. 3.12A, Core 125, 1.). Upper fine sand grades to very fine sand with internal planar laminations. The top contact is difficult to define. The second sand bed is an F5 muddy sand with poorly defined boundaries and no apparent structure (Fig. 3.12A, Core 125, 2.). The third sand bed is the thickest and has a sharp base (Fig. 3.12A, Core 125, 3.). The third sand bed coarsens up for approximately 1 cm then fines up in the top 2 cm. There is no apparent gradation in the middle. Planar laminations are present throughout the third sand bed, and the top has a sharp but slightly irregular contact. The fourth sand bed has gradational and irregular boundaries, and internal planar laminations (Fig. 3.12A, Core 125, 4.). The top of the fourth sand bed appears bioturbated. The F4 clay interbeds are bioturbated between 338 and 348 cm, and exhibit sandy mud mottles and thick F3 sand

laminations grouped around 315 to 338 cm. The sand laminations are continuous and well preserved.

Core 124 has a F6 sand bed which is overlain by F4 clay with sand laminations (Fig. 3.12A). The sand bed has a sharp base with one nearly vertical elongated sand intrusion that extends down into the clay-rich F1 mud below (Fig. 3.12A, Core 124, 1.). Internal structure is characterized by sub-planar laminations. The sand bed fines up and has a gradational top. There is a 4 cm gap at the top of the sand bed which obscures its upper contact. A large bivalve shell fragment is visible at 282 cm in the x-radiograph. The F4 clay bed overlying the F6 sand bed in core 124 has sand mottles and discontinuous sand laminations.

Core 123 has two large F6 sand beds with interbedded F4 clay (Fig. 3.12A). The first sand bed has a sharp base that was disturbed during the coring process (Fig. 3.12A, Core 123, 1.); sand was drawn down with the core liner 4 cm into the clay rich F1 mud below the sand bed. The first sand bed comprises fine sand and fines up to a gradational top. Internal planar laminations are visible from 326 to 332 cm; above this the structure of the sand bed appears to have been homogenized by bioturbation. Above the first sand bed, there is a bioturbated clay bed with one sand lamination preserved at 300 cm. The second sand bed is similar to the first with a sharp base, fining up texture, a gradational top, and internal planar laminations (Fig. 3.12A, Core 123, 2.). The top contact of the second sand bed is difficult to define as there is a distinct shift from clean sand to muddy sand at 282 cm (Fig 3.12A). The boundary of the change from clean to muddy sand is irregular, and likely represents the depth of penetration of bioturbation.

Core 122 has two F6 sand beds with interbedded F4 clay (Fig. 3.12A). The first sand bed has a sharp base, and fines up to a gradational top (Fig. 3.12A, Core 122, 1.). Internal structure is characterized by cross lamination from 322 to 326 cm. The second sand bed is sharp based, with 1 cm of basal coarsening, then an overall fining up into a bioturbated, gradational top (Fig. 3.12A, Core 122, 2.). There is a transition from clean sand to muddy sand at 275 cm. Internal laminations are not visible in x-radiograph, however they are highlighted by a lamination of fine woody debris at 277 cm (Fig. 3.12A, Core 122, 2.). The clay bed between sand beds is bioturbated with mottles of sand and a few preserved muddy sand laminations between 293 and 296 cm.

Core 121 has three sand beds with interbedded clay (Fig. 3.12A). The first sand bed is F6 with a sharp base, basal coarsening up for 1 cm, then fines up to a gradational top (Fig. 3.12A, Core 121, 1.). The top is obscured by cracks in the core. Cross bedding is preserved, and is apparent in x-radiograph (Fig. 3.12A, Core 121, 1.). The second sand bed is F5 muddy sand is bioturbated and has gradational boundaries (Fig. 3.12A, Core 121, 2.). The third bed is F6 with a sharp base, coarsening up for 1 cm then fining up to a gradational top (Fig. 3.12A, Core 121, 3.). No internal structure is apparent. Bioturbated clay is interbedded with the sand beds and has mottles of sand and a few preserved muddy sand laminations between 254 and 256 cm.

Transect 2 blue bed sets are characterized by F6 sand beds associated with F3 and F4 clay-rich mud and sand laminae (Fig. 3.12B). The blue bed set is at a depth of 155 to 222 cm in transect 2 and the thickest F6 sand beds are found in this group (Table 3.2). Core 94 has one 2 cm F6 sand bed which overlies a F4 clay bed (Fig. 3.12B). The sand bed has bioturbated, irregular boundaries, and shows no signs of gradation or internal

structure. The clay bed beneath the sand bed is bioturbated with sand mottles and discontinuous sand laminations. Sand from the sand bed appears to have been transported down into the clay bed forming an irregular shaped mottle. Traces of interlaminated clay and sand are preserved above the sand bed, but bioturbation has eliminated most of the original structure.

Core 120 and 119 both have one F6 sand bed which are the thickest sand beds of transect 2. The sand bed in core 120 is disturbed, and exhibits little original structure. A sharp base is obscured by cracks and sediment may have been reworked after the coring process. A small interval of sand which is in contact with the underlying clay unit shows preserved primary internal planar lamination. Above this no structure or gradation is observed. The top contact is sharp and appears to be well preserved. The sand bed is overlain by a F4 clay bed that exhibits signs of bioturbation including muddy sand mottles and discontinuous muddy sand laminations. The sand bed in core 119 is sharp-based, and coarsens up from very fine sand to medium fine sand over 2 cm. The sand bed then fines up to a bioturbated, gradational top. Planar laminations are preserved at the bottom 3 cm of the sand bed, but only traces of laminations remain in the bioturbated upper portion. The sand bed overlies a clay bed which is interlaminated with fine sand laminations. F1 fine sandy mud overlies the sand bed, and appears structureless.

Core 118 has one F6 sand bed. The F6 sand bed is sharp based, fines up from medium to fine sand, and has a gradational top. Internal structure is difficult to detect due to the poor x-radiograph quality (Fig. 3.12B). The F6 sand bed overlies a F4 clay bed which has discontinuous sand laminations. The sand bed is overlain by F1 bioturbated fine sandy mud.

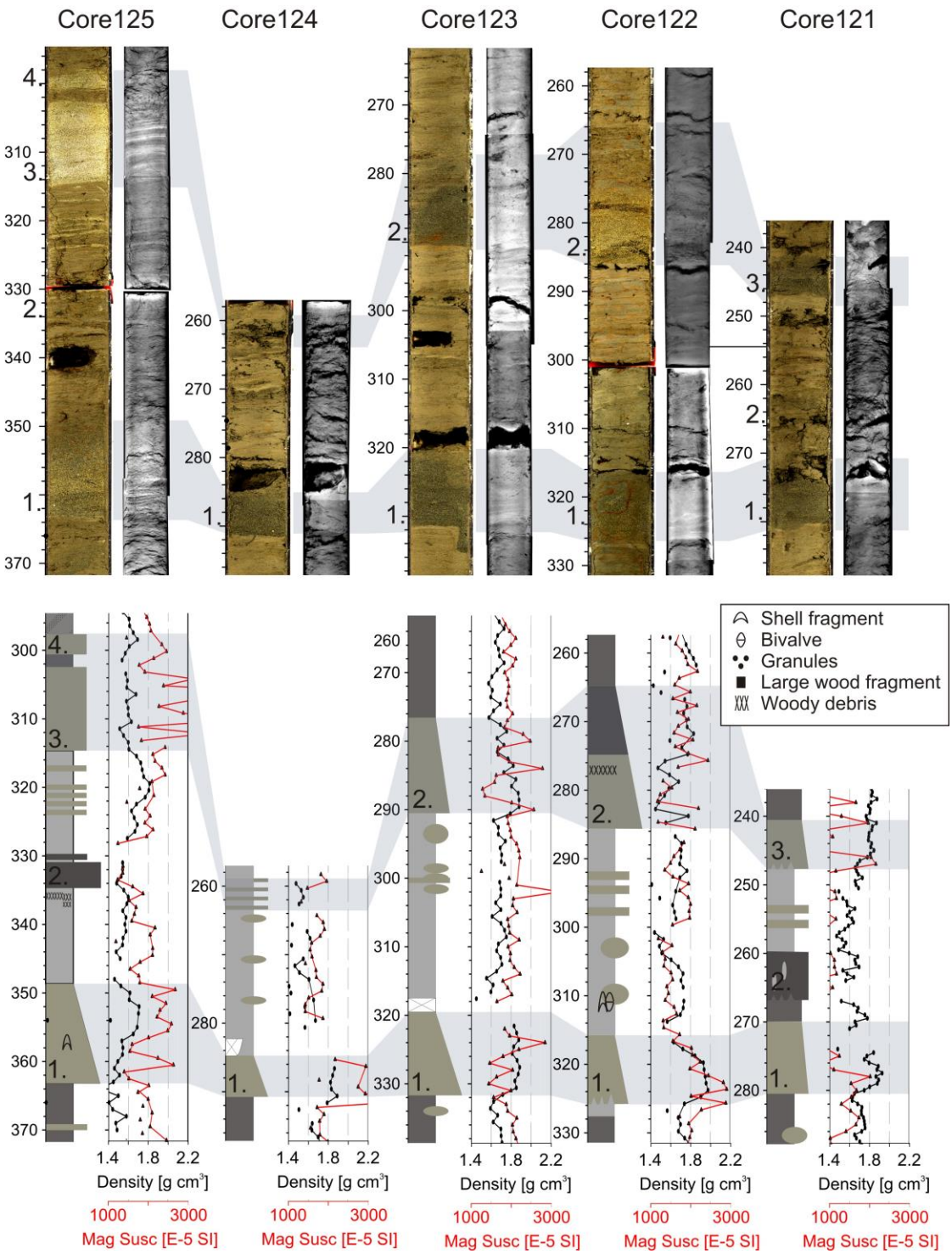

Fig. 3.12A. Figure showing correlations of blue bed sets in transect 1. Top shows high resolution photograph and x-radiograph. Bottom shows corresponding graphic logs and physical properties (black curve-gamma ray density; red curve-magnetic susceptibility). Blue band shows correlation of sand beds. Sand beds described in text are numbered.

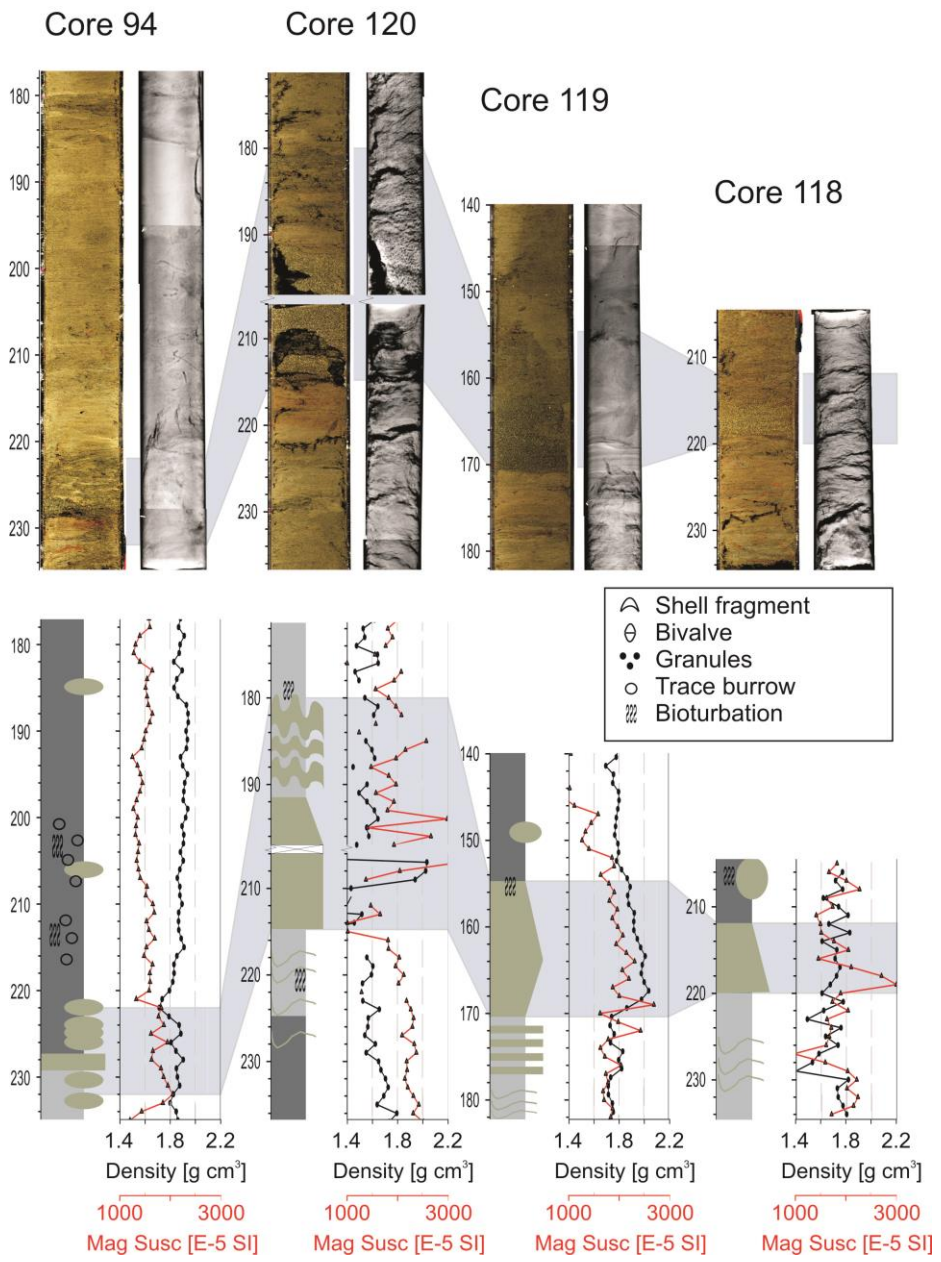

Fig. 3.12B. Figure showing correlations of blue bed sets in transect 2. Top shows high resolution photograph and x-radiograph. Bottom shows corresponding graphic logs and physical properties (black curve-gamma ray density; red curve-magnetic susceptibility). Blue band shows correlation of sand beds.

Table 3.2 Blue bed set depth, number of sand beds and bed thickness

	Station	Depth (cm)	Number of sand beds	Bed thickness (cm)
Transect 1	125	298-363	4	3, 12, 3, 15
	124	259-291	1	6
	123	275-330	2	13, 11
	122	265-326	2	20, 9
	121	241-281	3	6, 7, 11
Transect 2	94	222-232	1	2
	120	180-214	1	13
	119	155-171	1	16
	118	212-220	1	8

3.3.3 Red Bed Set

Transect 1 red bed set is characterized by F6 sand beds that overlie bioturbated F3 and F4 clay beds with sand laminations (Fig. 3.13A,B). The red bed set begins at roughly 4 mbsf, except core 125, where it begins at 4.5 mbsf (Table 3.3). The characteristic F6 sharp based, clean sand beds do not extend past core 123, but correlations have been extended to intervals of high sand concentration at similar depth.

Core 125 has two F6 sand beds separated by F4 clay, with mm-scale sand laminations (Fig. 3.13A). The first sand bed shows basal coarsening, then fines up with an irregular, bioturbated top (Fig. 3.13A, Core 125, 1.). Internal planar laminations are visible throughout the bed. The F3 clay bed is bioturbated except for a 2 cm thick patch of fine sand laminations immediately beneath the second F6 sand bed. The second F6 sand bed has a sharp base and is composed of fine sand (Fig. 3.13A Core 125, 2.). The bed fines up to an irregular, bioturbated top. The sand bed shows internal planar laminations.

Core 124 has one F6 sand bed which overlies F3 clay (Fig. 3.13A). The sand bed has a sharp base and fines up to a gradational upper boundary. Traces of internal structure are detectable in the x-radiograph (Fig. 3.13A), but the bed appears disturbed, possibly by the coring process. At the base of the clay bed there is an elongated horizontal muddy sand mottle with a thickness of 2 cm and poorly defined boundaries. It is possible that this is a

disturbed sand bed that was disturbed either by the coring process or by bioturbation. Planar laminations have been preserved below this mottle, observable in x-ray image. The clay bed between the sand bed and the mottle does not have any other substantial sand features.

Core 123 has one F6 sand bed over bioturbated clay (Fig. 3.13A). The sand bed has a sharp base and comprises fine sand. The fine sand fines up. The top contact of the F6 sand bed has been destroyed by a large crack in the sediment core. Internal planar laminations are present, but obscured by a crack in the core. The F4 clay bed has wavy, discontinuous sand laminations and lenses.

There is no sand bed in core 122 (Fig. 3.13A); instead the red bed set has been correlated to a bioturbated interval with a high concentration of sandy mottles within a clay bed. The mottles are irregular and clean. There are some discontinuous sand laminations at 414 cm which appear to be the only remnants of primary structure.

Core 121 has a F5 muddy sand bed over a mottled clay bed (Fig. 3.13A). The sand bed has very poorly defined contacts and no apparent internal structure. It appears as though the coarsest sand is near the top of the sand bed, indicating basal coarsening. The clay bed has a few irregular fine muddy sand mottles.

Transect 2 red bed set is also characterized by F6 sand beds which overlie F3 and F4 clay beds with sand laminations (Fig. 3.13B). The depths below seafloor for cores 94, 120, 119 and 118 are 318, 321, 279 and 300 cmbsl, respectively (Table 3.3).

Core 94 has three sand beds, the deepest being F5 muddy sand (Fig 3.13B, Core 94, 1.). Cracks in the core make it difficult to discern any sort of internal structure in the first sand bed. The second sand bed is F6 and has a sharp base and fines up to an irregular,

bioturbated top. Some traces of internal planar lamination remain, but bioturbation has destroyed much of the primary structure. The third sand bed is also F6 and has prominent basal coarsening up. The base is sharp and very fine sand is abruptly overlain by lower medium sand at 322 cmbsf. The lower medium sand then fines up. Internal planar laminations are observed throughout this sand bed in x-radiography (Fig. 3.13B). The F3 and F4 clay beds with sand laminations are bioturbated.

Core 120 has one F6 sand bed which has an irregular base (Fig. 3.13B). Basal coarsening up occurs through roughly the first centimetre where laminations of fine woody debris is preserved. Above the first centimetre, the bed fines up. Internal planar laminations are clearly visible in x-radiograph (Fig. 3.13B). The top boundary of the F6 sand bed is bioturbated. The F4 clay bed, which is under the sand bed, has clean sand mottles, one of which is nearly vertical and has sharp edges. Sand laminations are discontinuous with irregular contacts at best.

Core 119 has one F6 sand bed over a bioturbated F4 clay bed. The sand bed coarsens up from the base, for 3 cm, from very fine sand to upper fine sand with a gradational base and sharp top. A lamination of fine woody debris and an unusual diagonal orientation is present at the top of the bed. Internal planar laminations can be observed in x-radiograph (Fig. 3.13B). The F4 clay bed is mottled, and also exhibits laminae that are elongate, discontinuous and oriented diagonally. Sand laminations appear to be more continuous at the base of the clay bed; however cracks in the sediment core obscure the laminations.

Core 118 has one F6 sand bed over F3 clay. The sand bed is only 2 cm thick and has an irregular, but sharp base with no apparent gradation. Discontinuous laminations of fine woody debris give the appearance of internal lamination, although no lamination is

discernable in x-radiography (Fig. 3.13B). The clay bed is bioturbated and sandy from 303 to 307 cm with only a few mm-scale sand clasts from 302 to 303 cm.

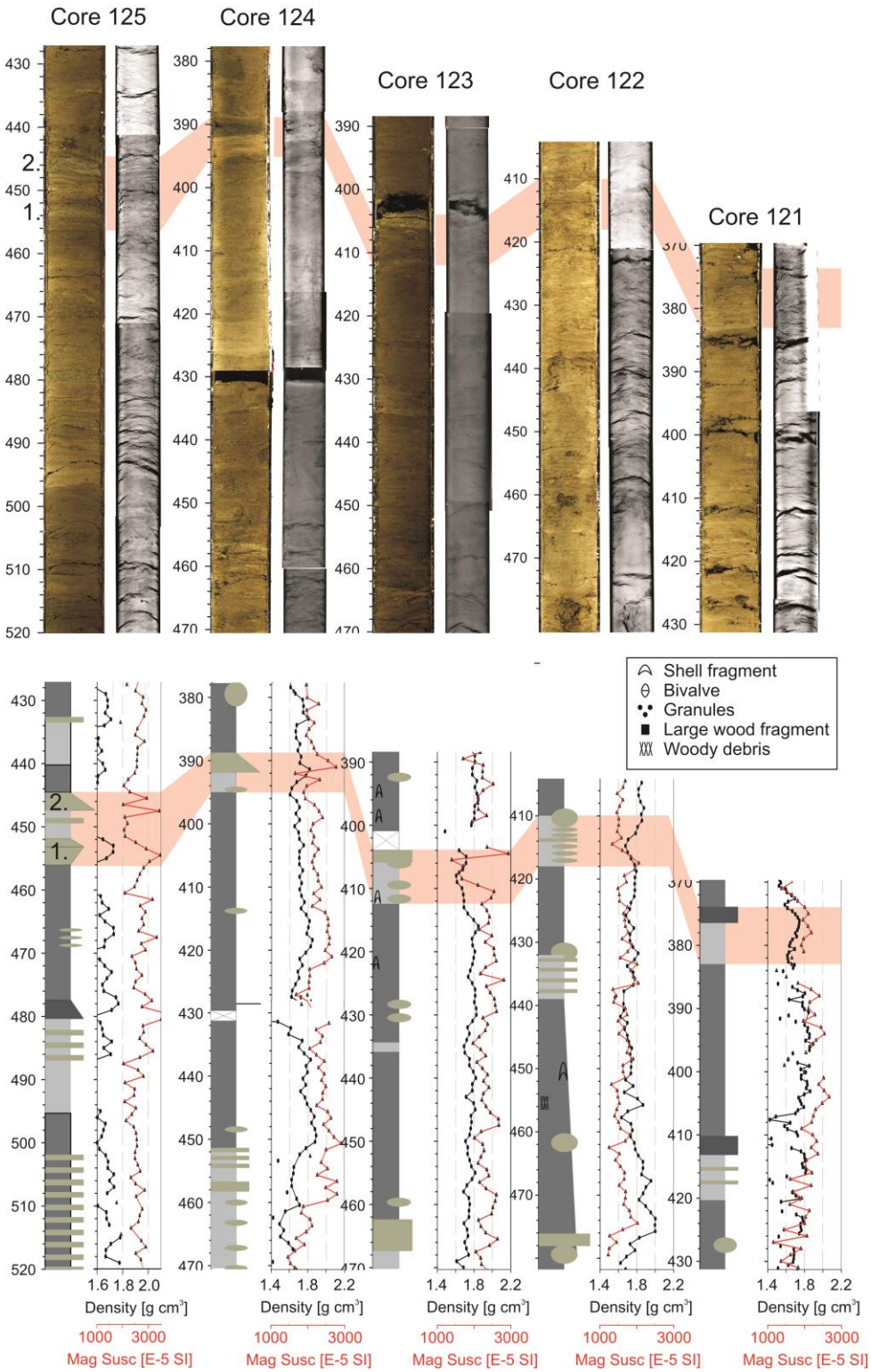

Fig. 3.13A. Figure showing correlations of red bed sets in transect 1. Top shows high resolution photograph and x-radiograph. Bottom shows corresponding graphic logs and physical properties (black curve-gamma ray density; red curve-magnetic susceptibility). Red band shows correlation of sand beds. Sand beds described in text are numbered where more than one bed is described.

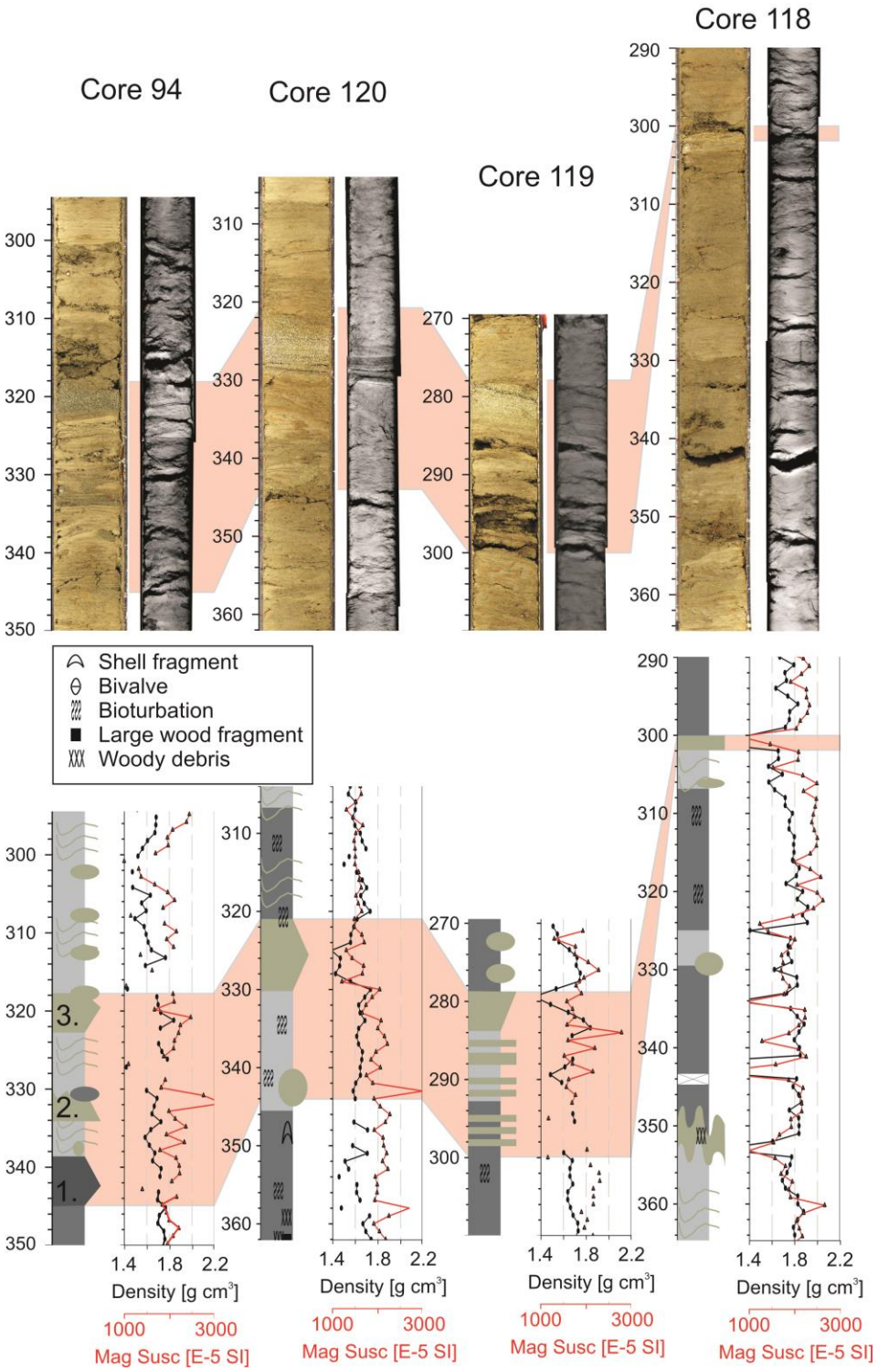

Fig. 3.13B. Figure showing correlations of red bed sets in transect 2. Top shows high resolution photograph and x-radiograph. Bottom shows corresponding graphic logs and physical properties (black curve-gamma ray density; red curve-magnetic susceptibility). Red band shows correlation of sand beds. Sand beds described in text are numbered where more than one bed is described

Table 3.3 Red bed set depth, number of sand beds and bed thickness

	Station	Depth (cm)	Number of sand beds	Bed thickness (cm)
Transect 1	125	445-456	2	3, 4
	124	389-395	1	3
	123	404-412	1	2
	122	410-418	0	laminations
	121	374-383	1	3
Transect 2	94	318-345	3	5,5,5
	120	321-344	1	9
	119	278-300	2	6,1
	118	300-302	1	2

3.3.4 Summary of Bed Sets

Yellow

- F5 and F6 sand interbedded with F4 clay at comparable depths in cores 125, 124 and 123. The yellow bed set is not continuous across the transect 1 and only appears in core 94 of transect 2.
- F6 beds are sharp based, grade up and are bioturbated at the top. Only core 125 shows internal planar laminations
- The only F5 bed is in core 123 and has no defined boundaries with dispersed granules throughout.
- F4 beds beneath the sets of sand beds are well preserved with laminations of fine sand while the clay bed between sand beds is bioturbated with sand mottles and discontinuous laminations

Blue

- F5 and F6 sand interbedded with F4 clay at comparable depths. Transect 1 has multiple thick sand beds while transect 2 has only one thick sand bed. These are the thickest sand beds of transects 1 and 2.

- F6 sand beds are sharp based, fine grained and may coarsen upward from the base and transition to fining up to a gradational top or may lack the coarsening up base. Internal structure includes planar and cross laminations, and tops may be bioturbated.
- F5 sand beds have gradational tops and bases and are often bioturbated.
- F4 clay beds may have preserved F3 sand laminations but are often bioturbated with sand mottles.

Red

- F5 and F6 sand interbedded with F4 clay at comparable depths. Transect 1 and 2 generally have one sand bed except cores 125 and 94 which are the most proximal to the levee crest of their respective transects. The red bed set shows a higher degree of bioturbation than the blue bed set.
- F6 sand beds are sharp based, fine grained and usually coarsen upward from the base. A transition to fining up to a gradational top occurs in most sand beds. Many beds show planar laminations, and tops which may be bioturbated.
- F5 sand beds have gradational top and base and are often bioturbated.
- F4 clay beds are bioturbated with sand mottles and rarely have preserved F3 sand laminations.

3.3.5 Other Bed Bets

In transects three and four, the yellow, blue and red sets are not easily distinguishable and could not be correlated in most cores. Transects three and four have two different bed

groupings, ‘interbedded sand bed’ unit and ‘basal F7 sand bed’ unit. These two bed sets are not present in the first two transects.

3.3.5.1 Interbedded Sand Bed Unit

This unit consists of a set of F6 sand beds found immediately above F7 basal sands (Fig. 3.14). Sand beds are interbedded with F4 clay and F1 mud. This set is absent or poorly represented in cores 128, 131, 91 and 89 (Table 3.4). Thicker sequences of interbedded F6 sand beds with a greater number of sand beds occur nearest to the levee crest and become poorly represented with distance from the levee (Fig. 3.10C). Core 130 is an exception to this, exhibiting a high number of F6 sand beds at a great distance from the levee crest. Some cores (88, 92, 130, 131) do not have the basal sand as core penetration stopped somewhere in the interbedded sand bed unit (Fig. 3.10D). In most of these cores, the interbedded unit is thick with thick sand beds. As with the tops of the basal sand units, beds of woody debris are common in the sand beds of the interbedded units. There is a high amount of bioturbation, with sandy mottles in the interval between the interbedded sand and the red set sand beds. High concentrations of sand mottles could represent sand beds which have been destroyed by burrowing organisms.

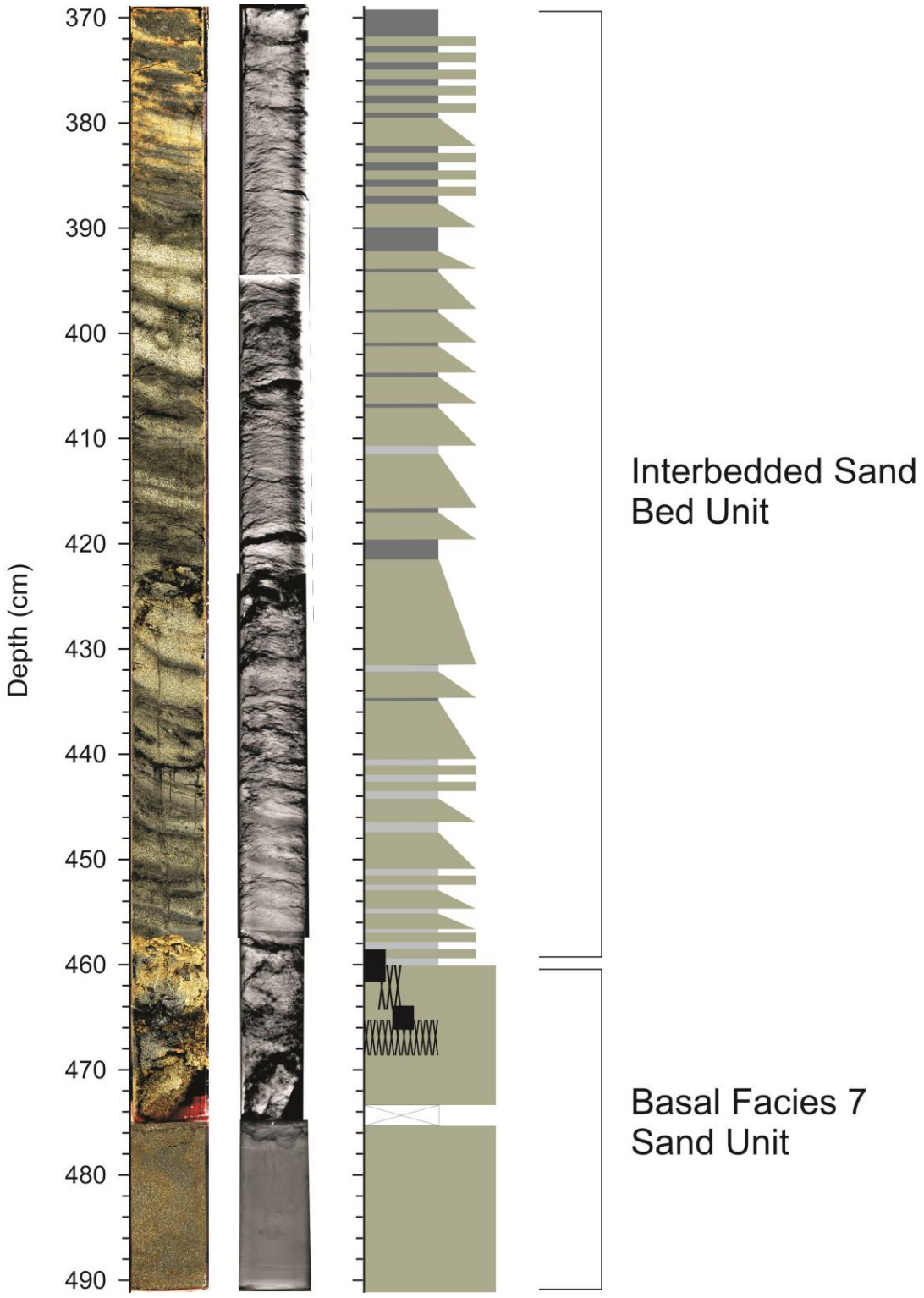

Fig. 3.14. High resolution photograph, x-radiograph and graphic log from core 126 showing the Interbedded Sand Bed Unit and the Basal Facies 7 Sand Unit.

3.3.5.2 Basal Facies 7 Sand Unit

Cores from transects 3 and 4 are farther from the river mouth and penetrated thick sand sequences which were not observed in transect 1 and 2. The sand sequences are characterized by thick F7 sand beds, usually followed by a thick sequence of F6 sand beds interbedded with F4 clay and F1 mud (Table 3.4, Fig. 3.14). Cores 127, 128 and 89 show basal sand beds greater than 160 cm in thickness (Fig. 3.10C, D). Cores 126 and 91 have F7 sand beds with thicknesses of 33 cm and 78 cm, respectively. F7 sands are absent in cores 130, 131, 92 and 88. Upper boundaries and internal structures are disturbed at contacts with F1 and F4 muds and clays where expansion has occurred and large voids are present. Top contacts of F7 sand beds have not been preserved, so the relationship between this facies and the overlying interbedded sand beds is unknown. Preserved structure can only be observed where beds of woody debris are present. The primary occurrences of the beds of woody debris are at the tops of F7 units, near the contact with overlying units. One bed of woody debris is found 1 m beneath the top of a F7 bed, which is likely the deepest sign of original structure within a F7 bed.

Table 3.4 Interbedded sand bed unit and basal F7 sand beds.

	Interbedded Sand Bed Unit			Basal Facies 7 sand	
Core	Depth (cm)	Number of beds	Bed thickness	Depth (cm)	Thickness (cm)
126	283-457	23	1-6 cm	457	33
127	202-265	5	1-9 cm	265	236
128	204-229	1	2 cm	229	169
130	413-510	7	7-20 cm	n/a	n/a
131	n/a	n/a	n/a	n/a	n/a
92	200-365	8	8-26 cm	n/a	n/a
91	158-215	4	2-6 cm	215	78
88	n/a	n/a	n/a	n/a	n/a
89	181-280	9	2-7 cm	298	525

3.4 Sediment Accumulation Rates

3.4.1 Sedimentation

The inclusive and exclusive sediment accumulation rates are presented to infer the reasonable range of values based on the ^{210}Pb sediment accumulation rate model. The inclusive sediment accumulation rate uses ^{210}Pb activities from all subsamples (S-n) of the core, thus being the least manipulated number. The exclusive sediment accumulation rate excludes subsamples which have higher sand content, and are interpreted as transported or reworked intervals. Intervals of potentially transported sediment were identified based on visual sedimentary characteristics, pinch test results, high values of bulk density, and magnetic susceptibility. In general subsamples were taken from mud intervals, but in some cases, intervals with high sand content were subsampled and analyzed as an attempt to constrain a typical steadily declining trend in ^{210}Pb activities with depth. Some of the subsamples were extracted from: intervals between F6 sand beds, among sand laminations, or from otherwise reworked material in the absence of more suitable sand-free subsample locations. These subsamples were at high risk of showing anomalous ^{210}Pb activities (e.g. core 126: 260 to 380 cm). Sediment accumulation rates (cm yr^{-1}) were calculated from the slope of the linear regression of the natural logarithm of excess ^{210}Pb activity. ^{210}Pb activity is measured in disintegrations per minute per gram (dpm g^{-1}). Subsample information including intervals and activities is presented in Appendix A.

3.4.1.1 Core 123

The profile of the ln of excess ^{210}Pb activity of core 123 is shown in Fig. 3.15 and the estimated sedimentation rates are shown in Tables 3.5A and 3.5B. The points in the ln(excess ^{210}Pb) activity scatter plot are non-linear and generally decrease from 0.707 to -

0.332. The slope of all points is -0.0022 which results in a sediment accumulation rate of 14.2 cm yr $^{-1}$. The largest deviation from the slope line is S-7 at a corrected depth of 238 cm (Fig. 3.14). This subsample was taken from a F3 clay bed among the blue bed set of F6 sand beds (Fig. 3.14). S-3 and S-4 were taken close to sand intervals and also show the largest deviation from the average. The exclusive slope excludes S-3, S-4, S-10 and S-11 based on their proximity to sand intervals (Table 3.5A). Removing these four subsamples changes the slope to -0.0025 which results in a sediment accumulation rate of 12.5 cm yr^{-1} (Table 3.5B).

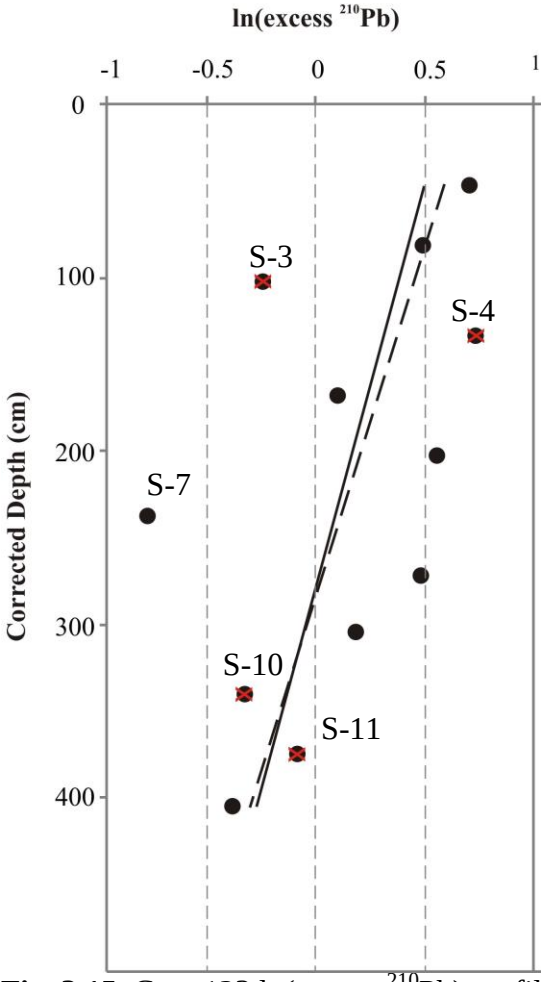

Fig. 3.15. Core 123 ln(excess ^{210}Pb) profile. Discrete points are the measured values. Subsamples excluded from the exclusive curve are marked with a red x. Inclusive slope line is solid and exclusive is dashed.

Table 3.5A. Core 125 - Justification for exclusion of subsampled intervals.

Excluded subsamples	Justification
3	Base of sand bed (yellow bed set)
4	Base of F3 with sand lamination
10	Sand mottles
11	Top of sand bed

Table 3.5B. Core 123 - Inclusive and exclusive sediment accumulation rates.

	Slope (cm^{-1})	Sediment accumulation rate (cm yr^{-1})	r^2 value
Inclusive	-0.0022	14.15 +/- 1.23	0.28
Exclusive	-0.0025	12.45 +/- 1.16	0.33

3.4.1.2 Core 125

The profile of the ln of excess ^{210}Pb activity of core 125 is shown in Fig. 16 and the estimated sedimentation rates are shown in Tables 3.6A and 3.6B. The points in the ln(excess ^{210}Pb) activity scatter plot are non-linear and generally decrease from 0.628 to -0.801. The slope of all points is -0.0024 which results in a sediment accumulation rate of 13.0 cm yr^{-1}. The largest deviation from the slope line is S-8 at a corrected depth of 308 cm. This subsample was taken from a F3 clay bed which has prominent clay/mud laminations and appears to be reworked sediment. S-2, S-3, S-5, S-10 and S-11 are also far from the slope line. All of these except for S-10 were from intervals high in sand content and were thus excluded from the exclusive slope. Sample S-8 was also excluded. Removing these five points changes the slope to -0.0031 which results in a sediment accumulation rate of 10.0 cm yr^{-1} and increases the R^2 value considerably.

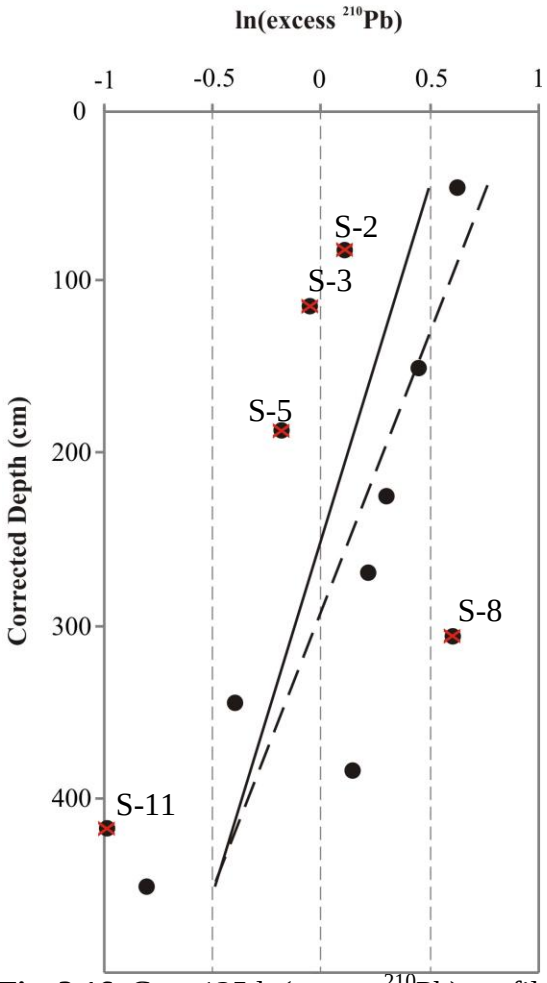

Fig. 3.16. Core 125 ln(excess ^{210}Pb) profile. Discrete points are the measured values. Subsamples excluded from the exclusive curve are marked with a red x. Inclusive slope line is solid and exclusive is dashed.

Table 3.6A. Core 125 - Justification for exclusion of subsampled intervals.

Excluded subsamples	Justification
2	Sand mottles
3	Sand bed
5	Top of sand bed
8	Clay/mud laminations. Reworked.
11	Sand laminations

Table 3.6B. Core 125 - Inclusive and exclusive sediment accumulation rates.

	Slope (cm^{-1})	Sediment accumulation rate (cm yr^{-1})	r^2 value
Inclusive	-0.0024	13.0 +/-1.09	0.40
Exclusive	-0.0031	10.0 +/-0.81	0.75

3.4.1.3 Core 126

The profile of the ln of excess ^{210}Pb activity for core 126 is shown in Fig. 3.17 and the estimated sedimentation rates are shown in Tables 3.7A and 3.7B. The points in the ln(excess ^{210}Pb) activity scatter plot have a higher degree of scatter in core 126 and decrease from 1.308 to -2.230. Due to its location proximal to the delta crest this core is very sandy, even at most depths with no defined sand beds. This accounts for the high degree of scatter. Below a depth of 280 cm (S-13 to S-17) there is a greater concentration of sand beds and many of the subsamples from this section of the core were categorized as reworked sediment. For this reason, all samples below 280 cm (corrected depth) have been omitted from the calculation of the inclusive sediment accumulation rate. The exclusive slope excludes points S-3, S-6, S-8, S-9, and S-10 on the basis of proximity to sand/reworked intervals. The points for the exclusive curve have a slope of -0.0078 resulting in a sediment accumulation rate of 4.0 cm yr^{-1}. The inclusive slope is -0.007 resulting in a sediment accumulation rate of 4.4 cm yr^{-1}.

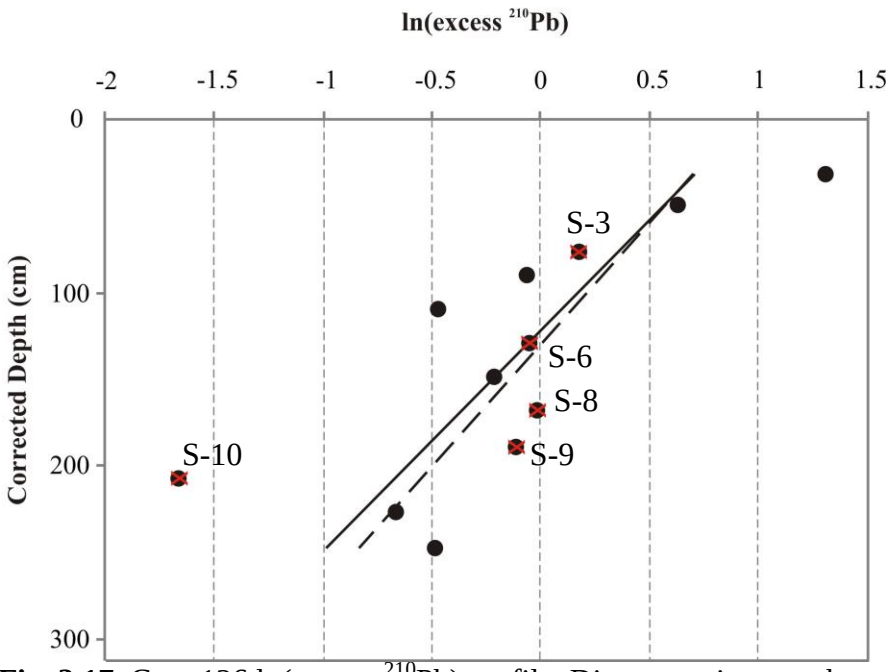

Fig. 3.17. Core 126 ln(excess ^{210}Pb) profile. Discrete points are the measured values. Subsamples excluded from the exclusive curve are marked with a red x. Inclusive slope line is solid and exclusive is dashed.

Table 3.7A. Core 126 - Justification for exclusion of subsampled intervals.

Excluded subsamples	Justification
3	Clay/mud laminations
6	Sand Mottle
8	Sand Mottle
9	Sand Mottle
10	Sand Mottle
13-17	Repetitive sand beds

Table 3.7B. Core 126 - Inclusive and exclusive sediment accumulation rates.

	Slope (cm^{-1})	Sediment accumulation rate (cm yr^{-1})	r^2 value
Inclusive 1-12	-0.0078	4.0 +/-0.18	0.59
Exclusive	-0.007	4.4 +/-0.30	0.68

3.4.1.4 Core 127

The profile of the ln of excess ^{210}Pb activity for core 127 are shown in Fig. 3.18 and the estimated sediment accumulation rates are shown in Tables 3.8A and 3.8B. The points in

the ln(excess ^{210}Pb) activity in the core 127 scatter plot have a linear pattern and decrease from 0.960 to -1.941. The slope of all points is -0.0122 which results in a sediment accumulation rate of 2.6 cm yr $^{-1}$. As with core 126, there is a high concentration of sand intervals in core 127 below a depth of 180 cm. Below this depth the points become scattered, especially below 220 cm. The exclusive slope includes all points above and excludes all points below 180 cm corrected depth (S-8 to S-12). The slope of this line is -0.0128 with a sediment accumulation rate of 2.4 cm yr $^{-1}$.

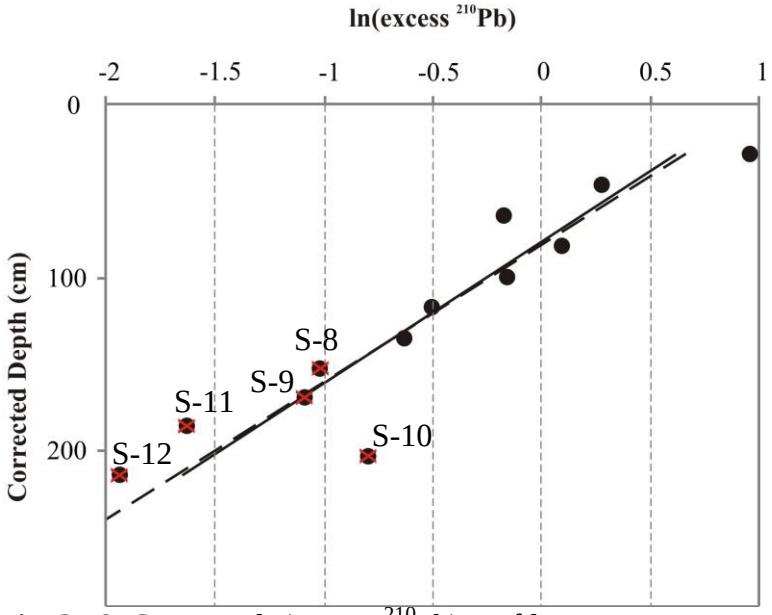

Fig. 3.18. Core 127 ln(excess ^{210}Pb) profile. Discrete points are the measured values. Subsamples excluded from the exclusive curve are marked with a red x. Inclusive slope line is solid and exclusive is dashed.

Table 3.8A. Core 127 - Justification for exclusion of subsampled intervals.

Excluded subsamples	Justification
8	Sand mottles
9	Sand mottles
10	Base of sand bed
11	Sand lamination
12	Sand beds (4 cm clay between thick sand beds)

Table 3.8B. Core 127 - Inclusive and exclusive sediment accumulation rates.

	Slope (cm^{-1})	Sediment accumulation rate (cm yr^{-1})	r^2 value
Inclusive	-0.0122	2.6 +/-0.10	0.86
Exclusive	-0.0128	2.4 +/-0.18	0.84

3.4.2 Estimated ages of sand beds

Ages based on sediment accumulation rates must be used with caution, as the ^{210}Pb dating method establishes a range of dates for any particular interval of sediment (Johannessen and Macdonald 2012). Our model assumes that no sediment transport or mixing has occurred across F6 sand beds and that there has been a constant accumulation rate through time. Analytical error increases with depth and even the selection of an exclusive sediment accumulation rate as opposed to the inclusive rate introduces a certain amount of bias. Ages are presented here in three different scenarios: 1) a range of dates based on exclusive sediment accumulation rates of all cores; 2) a large range of dates based on inclusive and exclusive sediment accumulation rates; and, 3) a discrete date which falls within this range and represents the specific age produced by the ^{210}Pb model (Fig. 3.19).

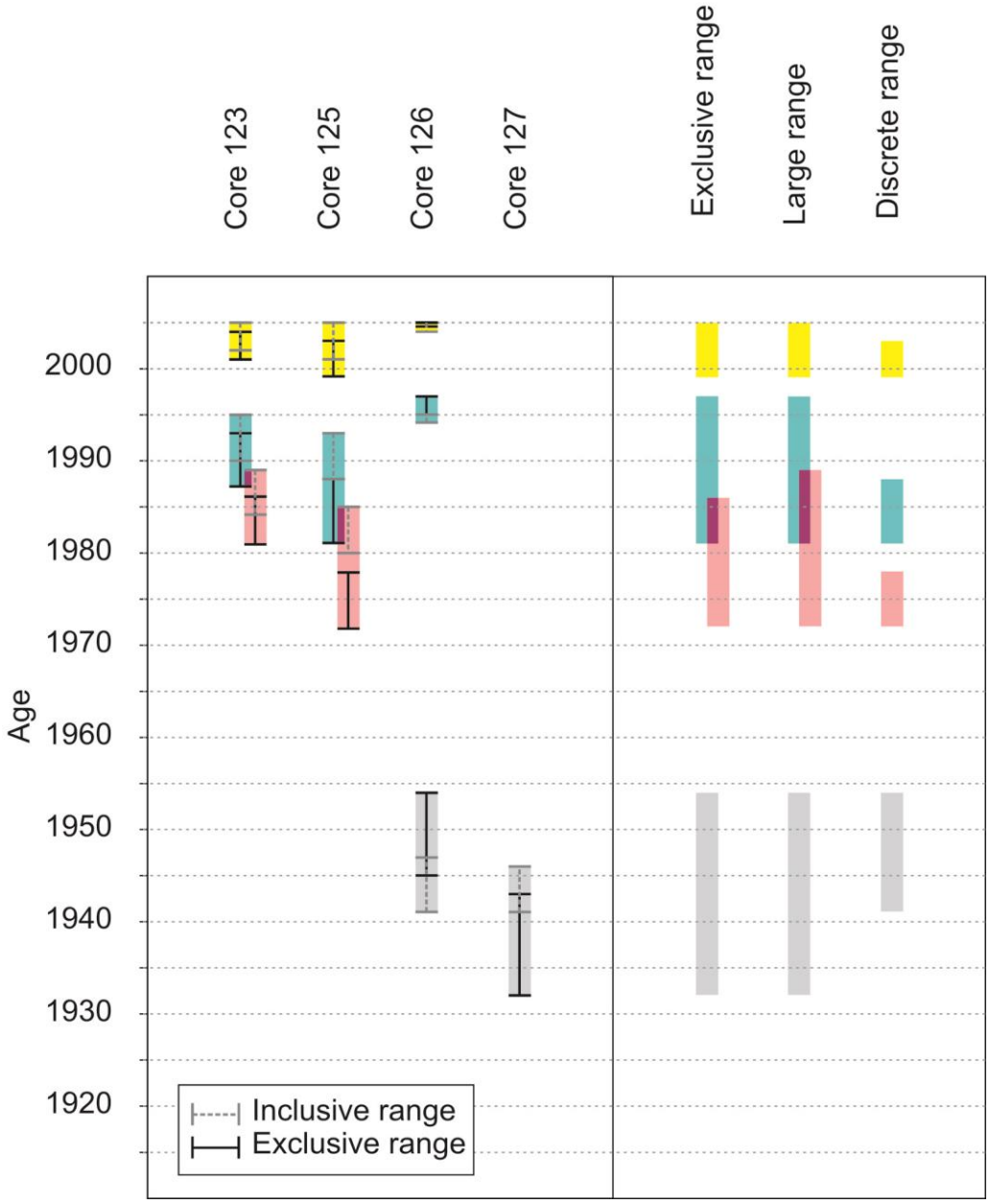

Fig. 3.19. Age ranges of bed sets are coloured yellow, blue and red and the range for tops of interbedded sand bed units are coloured grey. The exclusive range is based on the exclusive sediment accumulation rate of all four dated cores. The large range is based on both exclusive and inclusive sediment accumulation rates. The discrete range is based on the discrete ages resulting from exclusive sediment accumulation rate calculations from core 125 for yellow, blue and red bed sets and from core 126 for the top of the interbedded sand bed unit and uses the least amount of caution. Inclusive and exclusive range bars show the range of multiple beds within a bed set.

1. Exclusive sediment accumulation rate

Exclusive sediment accumulation rates of cores 123 and 125 are used to determine the age range of sand bed sets. Results are listed in Table 3.9A and shown in Fig. 3.20A and 3.20B. Sediment accumulation rates of cores 126 and 127 are used to determine the age of the top of the interbedded sand bed unit and are shown in Table 3.9B and Figs. 3.20C.

Table 3.9A. Ages of bed sets in transect 1 based on exclusive sediment accumulation rates.

	Yellow		Blue		Red	
Core	Base	Top	Base	Top	Base	Top
123	2002 ± 0.7	2003 ± 0.9	1989 ± 2.2	1991 ± 2.0	1984 ± 2.8	1984 ± 2.8
125	2000 ± 0.7	2003 ± 1.0	1983 ± 2.4	1986 ± 2.2	1975 ± 3.2	1975 ± 3.1
Range	2000-2003 ± 1.0		1983-1991 ± 2.4		1975-1984 ± 3.2	

Table 3.9B. Ages of bed sets in transect 3 based on exclusive sediment accumulation rates.

Core	Yellow	Blue	Red	Interbedded
126	2005 ± 0.4	1996 ± 1.0	n/a	1950 ± 4.4
127	n/a	n/a	n/a	1938 ± 5.9

2. Large-range inclusive and exclusive sediment accumulation rates

Comparisons of ages based on inclusive and exclusive sedimentation rates provides the largest range of ages for sand beds and shows the limitations of the ^{210}Pb dating technique. Results are listed in Table 3.10.

Table 3.10. Age ranges of bed sets in transects 1 and 3 calculated including inclusive and exclusive sediment accumulation rates. Ranges include statistical error.

	Yellow		Blue		Red		Interbedded	
Core	Base	Top	Base	Top	Base	Top	Base	Top
123	2002	2005	1987	1995	1981	1989	n/a	n/a
125	1999	2005	1981	1993	1972	1985	n/a	n/a
126	2004	2005	1994	1997	n/a	n/a	1941	1954
127	n/a	n/a	n/a	n/a	n/a	n/a	1932	1946
Range	1999-2005		1981-1997		1972-1989		1932-1954	

3. Discrete date based on exclusive sediment accumulation rate from best data.

Although it is dangerous to assign a discrete date to a specific interval, approximation is required in order to summarize the age of each event. This is done so as to project ages from cores which have been analyzed for excess ^{210}Pb to those cores which have not been analyzed. To do this, the exclusive sediment accumulation rate from core 125 is used to represent the upper portion of the sediment record (down to the red bed set) (Table 3.11). Core 127 is used to represent the top of the interbedded sand bed unit which is not present in core 125. The ln(excess ^{210}Pb) curve for core 125 has more data points which are closer to the average slope and has a higher R^2 value than that of core 123. Likewise, core 127 has a linear profile and higher R^2 value compared to those of core 126.

Table 3.11. Ages of bed sets in transect 1 and 3 based on exclusive sediment accumulation rates of core 125 and 127.

	Yellow		Blue		Red		Interbedded
Core	Base	Top	Base	Top	Base	Top	Top
125	2000 ± 0.7	2003 ± 1.0	1983 ± 2.4	1986 ± 2.2	1975 ± 3.2	1975 ± 3.1	n/a
127	n/a	n/a	n/a	n/a	n/a	n/a	1938 ± 5.9
Range	2000-2003 ± 1		1983-1986 ± 2.4		1975 ± 3.2		1938 ± 5.9

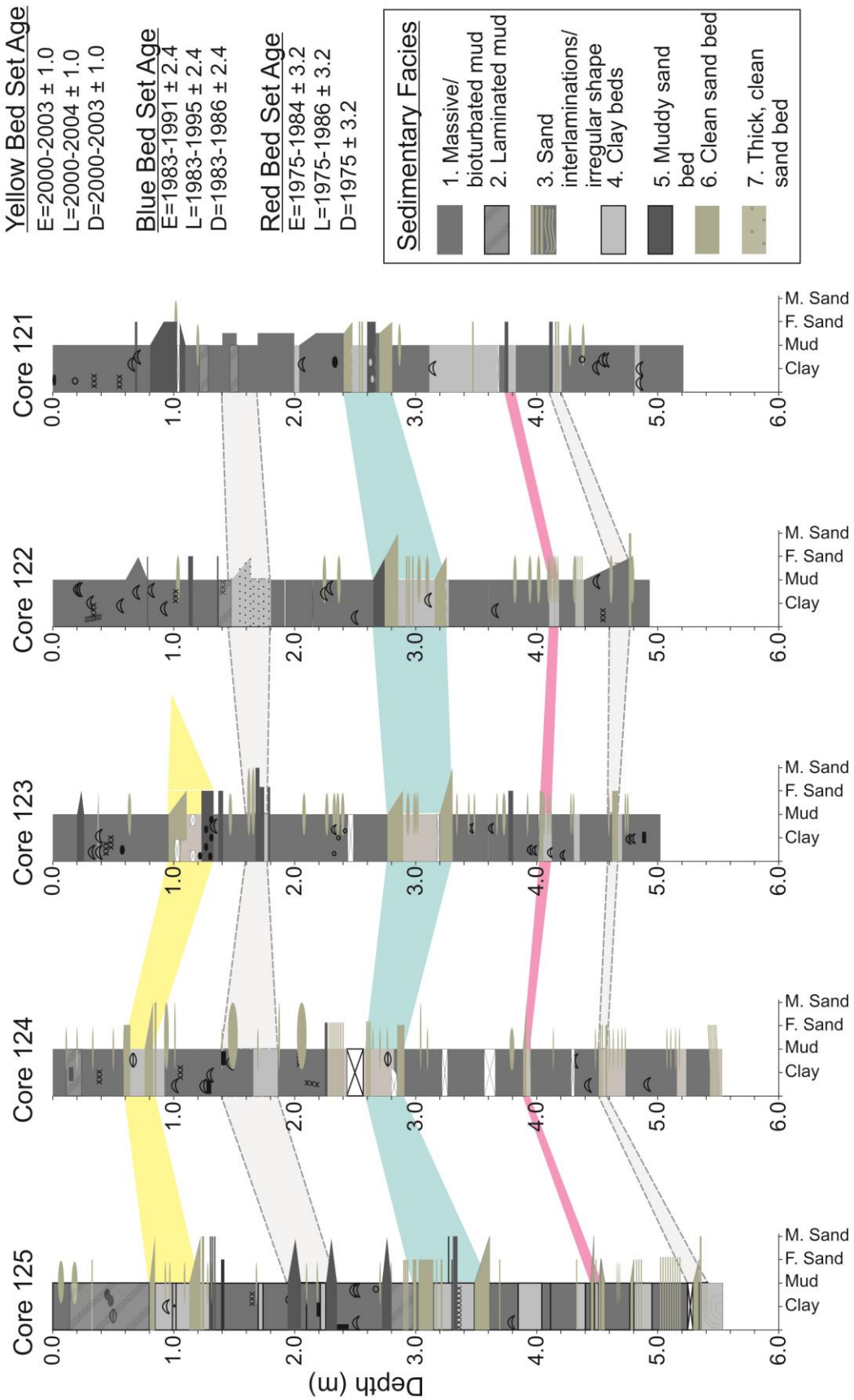

Fig. 3.20A. Transect 1 - Ages of sand bed sets based on sediment accumulation rates from three scenarios; E - exclusive, L - large range and D - discrete.

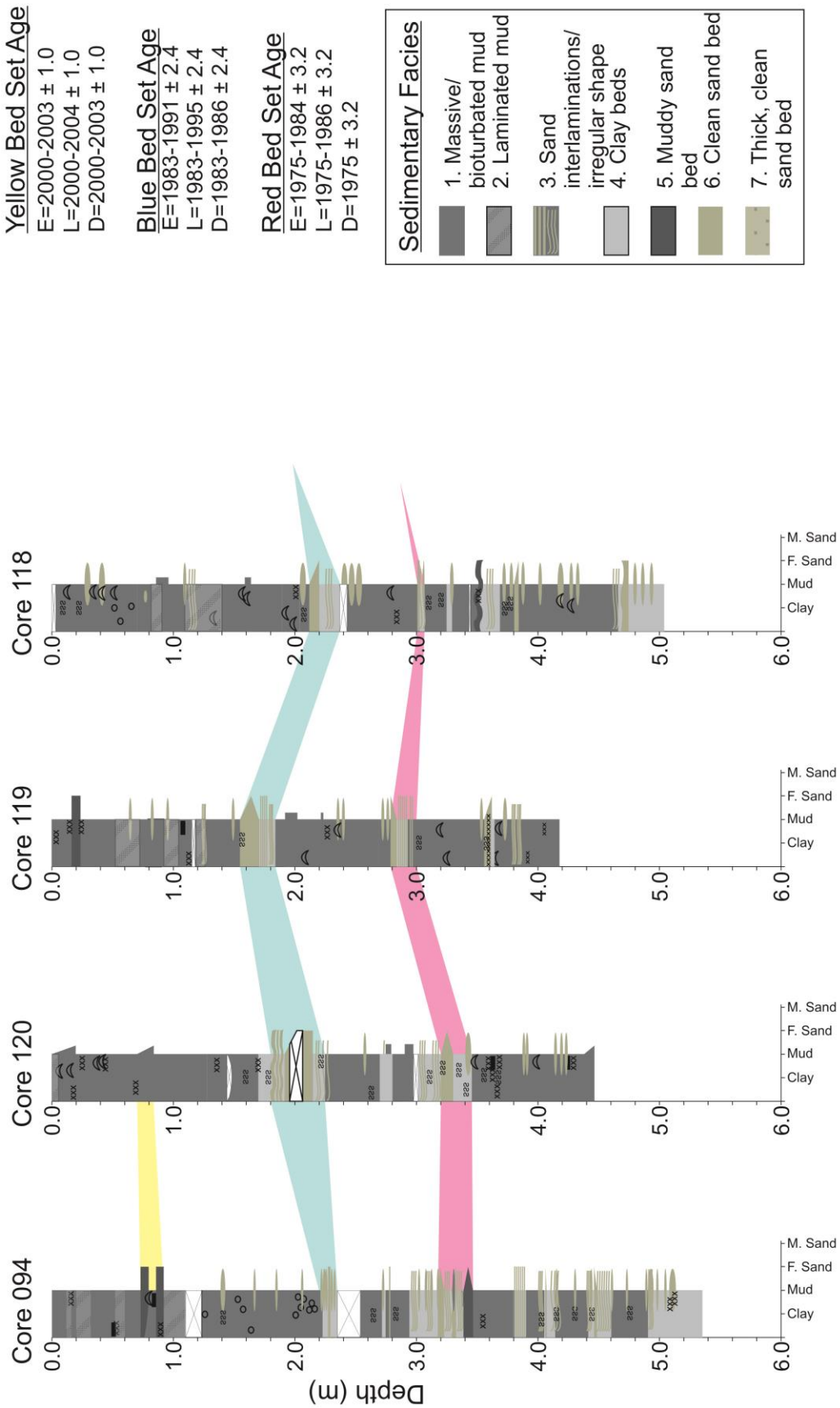

Fig. 3.20B. Transect 2 - Ages of sand bed sets based on sediment accumulation rates from three scenarios; E - exclusive, L - large range and D - discrete.

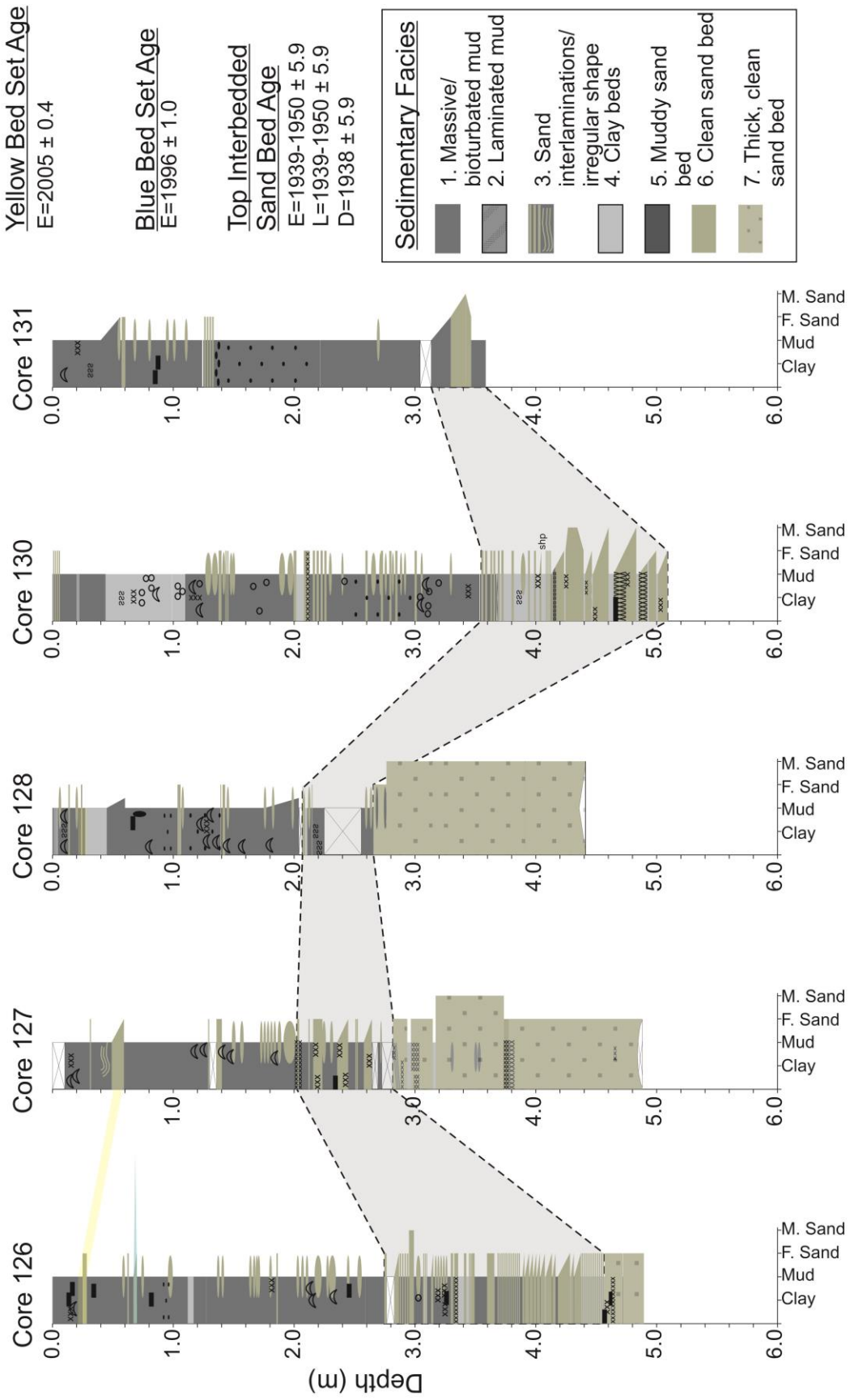

Fig. 3.20C. Transect 3 - Ages of sand bed sets based on sediment accumulation rates from three scenarios; E - exclusive, L - large range and D - discrete.

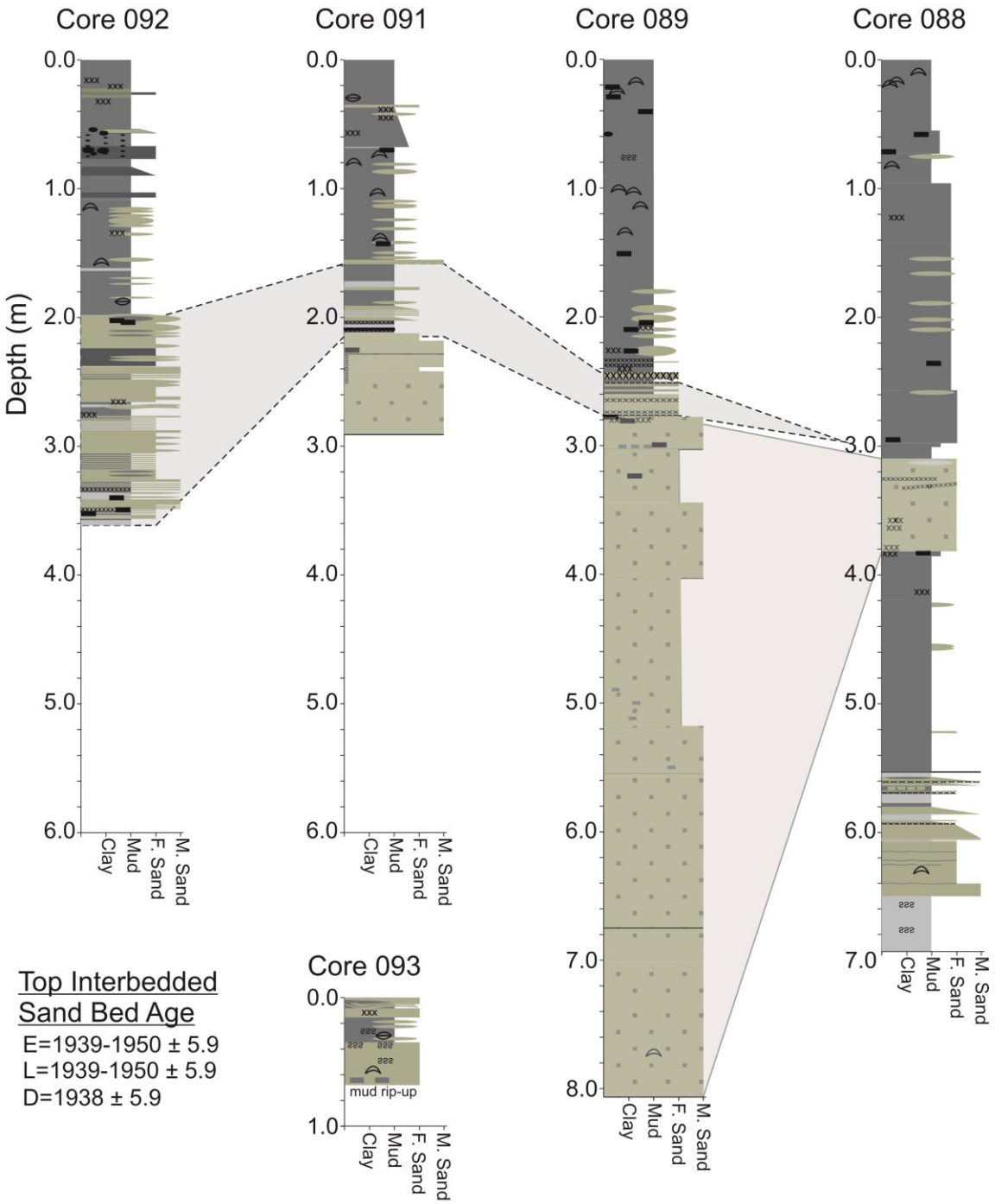

Fig. 3.20D. Transect 4 - Ages of sand bed sets based on sediment accumulation rates from three scenarios; E - exclusive, L - large range and D - discrete.

3.4.3 Projecting sediment accumulation rates

Using the red bed set as a datum in transect 1 and 2, ages from known cores were projected onto the depth at which the red bed set occurs in cores which were not dated

(Fig. 3.21, Table 3.12). In transects 1 and 2, the red bed set is the deepest sand bed which occurs in all cores and was correlated to an age of approximately 1975 based on the exclusive sediment accumulation rate at core 125. For transect 3 and 4 the top of the interbedded sand unit was used as the datum at an approximate age of 1938 based on the sediment accumulation rate at core 127. Sediment accumulation rates were calculated by dividing the thickness of mud above the respective datum over the projected approximate age. The discrete ages were used to project dates onto other cores and as such, projected sediment accumulation rates are rough approximations.

Table 3.12 Projected sediment accumulation rates calculated from discrete ages. Rates include mud intervals from top of core down to the common datum.

Core	Datum	Projected sediment accumulation rate (cm yr^{-1})
125	Red bed set	10.0*
124	Red bed set	10.4
123	Red bed set	9.3
122	Red bed set	10
121	Red bed set	8.8
94	Red bed set	7.5
120	Red bed set	8.2
119	Red bed set	7.0
118	Red bed set	7.9
126	Top interbedded sand unit	3.7
127	Top interbedded sand unit	2.4*
128	Top interbedded sand unit	2.8
130	Top interbedded sand unit	4.8
131	Top interbedded sand unit	4.3
92	Top interbedded sand unit	2.7
91	Top interbedded sand unit	2.9
89	Top interbedded sand unit	3.6
88	Top interbedded sand unit	4.2

* Sediment accumulation rate used to project onto other cores at depth of common datum

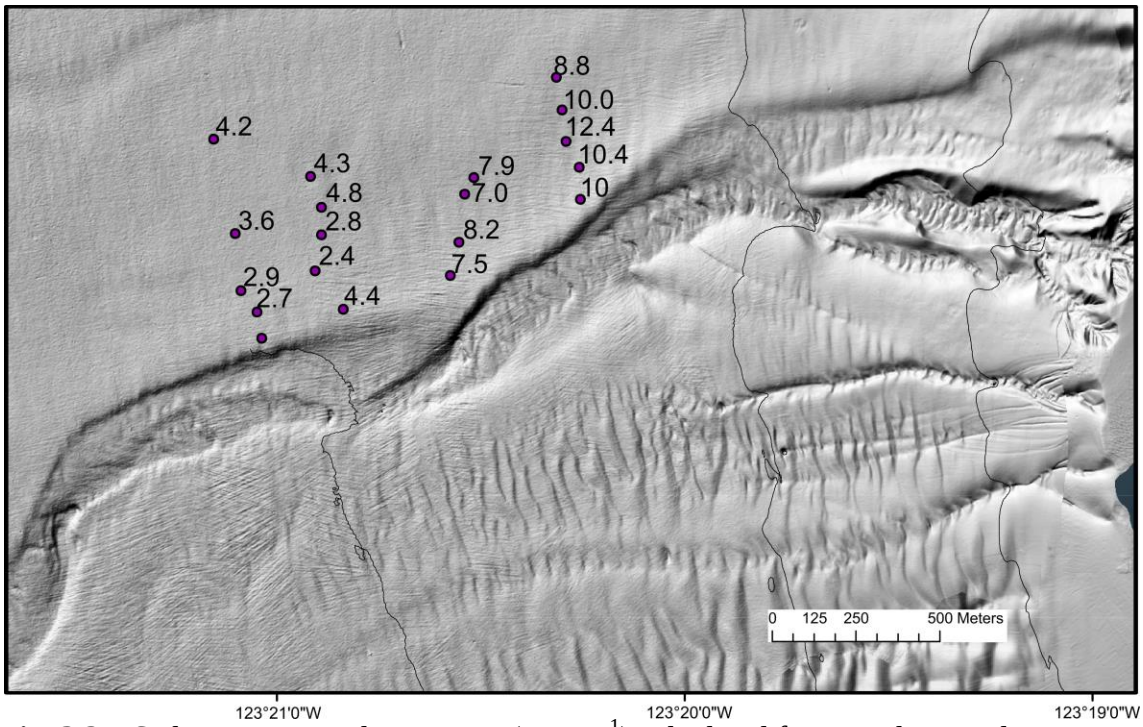

Fig. 3.21. Sediment accumulation rates (cm yr $^{-1}$) calculated from mud intervals using exclusive rates. Transect 1 and 2 calculated from red group with a calculated approximate age of 1975. Transect 3 and 4 calculated from top of interbedded sand unit (grey correlation fill) with a calculated approximate age of 1938.

3.4.4 Total Sediment Accumulation Rates

A total sediment accumulation rate, which includes the thicknesses of sand intervals, is calculated at each core location. This is done by using the age at a constant datum and counting the total amount of material deposited on top of the datum (Table 3.13). The red bed set was used as the datum for transects 1 and 2, and the top of the interbedded sand bed unit were used as the datum for transects 3 and 4. Sand accumulation rates were also calculated using the same datums but by adding the thickness of F5 and F6 sand beds (Table 3.13). Sand accumulation rates apply to the intervals above the interbedded datum; interbedded and massive sand beds below this datum contain much higher amounts of sand and would have a higher total accumulation rate. Cores tend to fit into two separate groups of sediment accumulation rates (Fig. 3.22): transects 1 and 2 tend to have mud

accumulation rates greater than 6 cm/y^{-1} and sand accumulation rates greater than 0.5 cm/y^{-1}. Core 118 plots at 0.3 cm/y^{-1}. Transects 3 and 4 fall into a group with mud accumulation rates less than 6 cm/y^{-1} and sand accumulation rates less than 0.5 cm/y^{-1}.

Table 3.13. Total sediment accumulation rates calculated from discrete ages. Rates include sediment from top of core down to the common datum.

Core	Datum	Total sediment accumulation rate (cm yr^{-1})	Sand accumulation rate (cm yr^{-1})	Mud accumulation rate (cm yr^{-1})
125	Red bed set	12.6	2.6	10.0*
124	Red bed set	11.0	0.6	10.4
123	Red bed set	11.0	1.7	9.3
122	Red bed set	11.5	1.5	10
121	Red bed set	10.4	1.6	8.8
94	Red bed set	8.4	0.9	7.5
120	Red bed set	8.6	0.6	8.2
119	Red bed set	7.6	0.6	7.0
118	Red bed set	8.2	0.3	7.9
126	Top interbedded sand unit	3.8	0.1	3.7
127	Top interbedded sand unit	2.6	0.2	2.4*
128	Top interbedded sand unit	2.9	0.1	2.8
130	Top interbedded sand unit	4.9	0.1	4.8
131	Top interbedded sand unit	4.3	0.0	4.3
92	Top interbedded sand unit	3.0	0.3	2.7
93	Top interbedded sand unit	2.9	0.0	2.9
89	Top interbedded sand unit	3.6	0.0	3.6
88	Top interbedded sand unit	4.2	0.0	4.2

* Sediment accumulation rate used to project onto other cores at depth of common datum

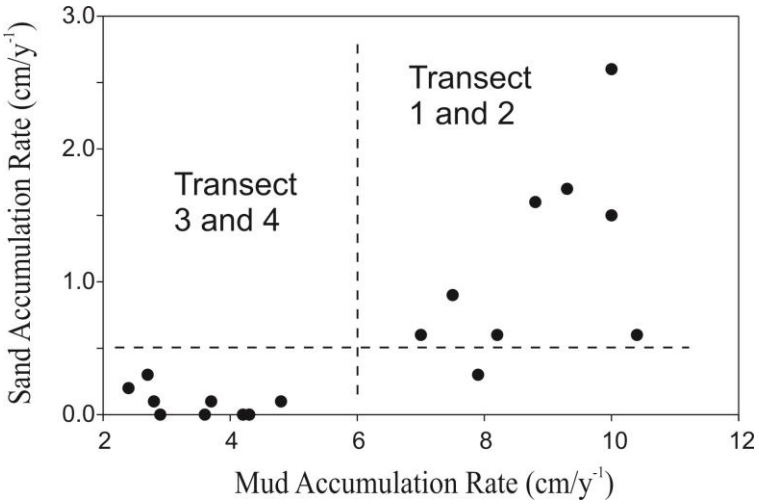

Fig. 3.22. Plot of mud accumulation rates vs. sand accumulation rates based on rates from table 3.13. Transects 1 and 2 separate into a group with mud accumulation rates greater than 6 cm/y^{-1} and sand accumulation rates greater than 0.5 cm/y^{-1}. Core 118 plots at 0.3 cm/y^{-1}. Transects 3 and 4 fall into a group with mud accumulation rates less than 6 cm/y^{-1} and sand accumulation rates less than 0.5 cm/y^{-1}.

3.4.5 Frequency of sand beds

Frequencies of sand beds were calculated from discrete ages from core 125 and average overall one occurrence approximately every 2 to 3 years since 1968 (Table 3.14A). Sets of F6 sand beds (yellow, blue and red bed sets) occur approximately every 10-15 years and F5 events occur approximately every 4 to 5 years on average. From calculated approximate dates of 1956 to 1973 from core 94, sand beds occur approximately every 4 years (Table 3.14B).

Table 3.14A. Approximate ages of sand beds calculated from the exclusive sediment accumulation rate of core 125. Bed sets are highlighted yellow, blue and red.

Bed Number	All beds
1	2003
2	2000
3	1999
4	1998
5	1993
6	1991
7	1987
8	1986
9	1986
10	1985
11	1983
12	1975
13	1975
14	1973
15	1968

Table 3.14B. Approximate ages of sand beds calculated from the exclusive sediment accumulation rate of core 94. Bed sets are highlighted red.

Bed Number	All beds
13	1973
14	1968
15	1965
16	1961
17	1956

3.5 Seismic Chronostratigraphy of Levee Deposits

3.5.1 Transect 2

The red bed set in core 94 corresponds to the high amplitude reflector separating the sub-parallel levee unit from the underlying chaotic acoustic unit (Fig. 3.8A). This depth has been dated to approximately 1975. Below the high amplitude reflector the chaotic acoustic unit does not show any coherent reflectors that can be correlated to the sand beds in cores 94, 120, 119 and 118. Above the high amplitude reflector, sub-parallel levee reflectors are laterally and vertically continuous, but do not correspond directly to the thick F6 sand beds of the yellow or blue bed set.

3.5.2 Transect 3

The top of the interbedded sand bed unit in cores 126, 127, 128 and 130 corresponds to the high amplitude reflector that separates the sub-parallel levee unit and the chaotic acoustic unit (Fig. 3.8B). The high amplitude reflector does not extend past core 130 on the seismic image, although core 131 has a sand bed corresponding to the same depth. This depth has been dated between 1938 and 1950. A high amplitude reflector is identified at a depth of 8.4 mbsf in the seismic image, but this was not intercepted by any of the cores along this transect.

3.5.3 Transect 4

The high amplitude reflector, identified at the base of the levee unit in other transects, is discontinuous in transect 4 (Fig. 3.8C). Cores 91 and 92 have sand intervals which correspond to a high amplitude reflector. This depth has been dated between 1938 and 1950.

4 Discussion

4.1 Long Term Sedimentation

Core 126 has the most complete record of sedimentation, and includes the time equivalent record of core 125 down to a depth of 200 cm. The lower portion (below 200 cm) of core 126 and others of transect 3 reveals a different pattern of sedimentation than the sets of sand beds observed from approximately 1967 and above in transects 1 and 2. This deep interval is characterized by interbedded F6 sand beds, and F1 and F4 mud beds, all of which overlie massive F7 sand beds. Core 126 shows cyclic bedding of sand beds 1 to 6 cm in thickness with less than one year's accumulation of mud between. The top of the interbedded unit is calculated to correspond to approximately 1938 based on the sediment accumulation rate at core 127. Although the age of the F7 sand bed cannot be unequivocally determined — the calculation involves a high count of sand beds which dramatically increases the chances of error — we do know that the combined time which passed between the interbedded sand beds is approximately 14 years or more based on the thickness of interbedded mud and clay intervals. If the top of the interbedded unit represents approximately 1938 ± 5.9 this provides an approximate age range of 1918-1929 for the top of the F7 sand bed. We know that the bed cannot be much older than 100 years because samples from mud intervals just above the sand bed show that the ^{210}Pb activities have not reached background levels. If the basal facies 7 sand beds represent the beginning of channel inception, based on ^{210}Pb dating, the channel system is interpreted to be approximately 100 years old.

The fixing of the main arm of the Fraser River in its current position between 1912 and 1932 has resulted in the submarine channel being supplied with a continuous

supply of sandy river discharge. Sedimentation from the Fraser River is focused on the Sand Heads area creating a loading or over steepening of the slope at the delta crest. The sediment is deposited at very high rates and as a result is underconsolidated and is prone to failure (McKenna et al., 1992). When slides occur at the delta crest, the failed material flows down slope and cohesive blocks of sandy mud disintegrate (McKenna et al., 1992). The disintegrated material transforms into turbidity currents which flow down the delta front. Repeated events result in the formation of a channel/levee complex (Fig. 4.1).

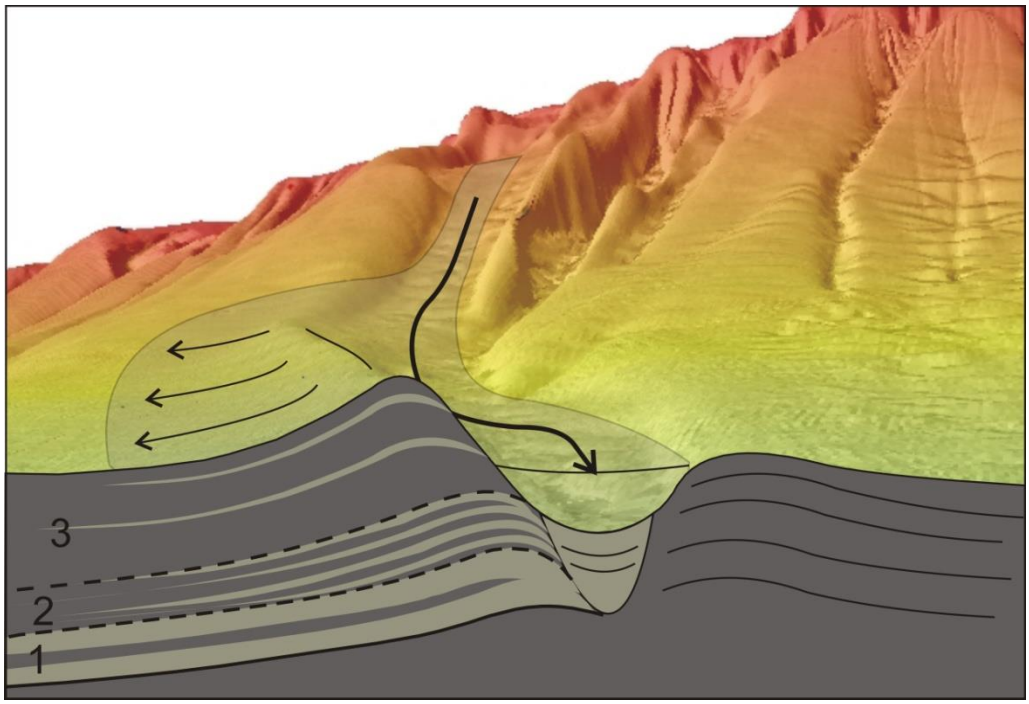

Fig. 4.1. Levee construction occurs when repeat turbidity currents overspill the Main Submarine Channel, leaving sand beds on the banks. Three phases of levee growth occur; the first is characterized by low channel relief where continuous overspill events result in thick coarse sand beds. The second phase is a period where levees have grown resulting in an increase of channel relief. Overspill events still occur regularly, but much of the flow is channelized and sand beds not as thick or coarse as in phase 1. In the third phase, channel relief has become higher than the typical flow height resulting in sediment bypass and long periods characterized by no overspill with deposition dominated by muddy plume fallout.

4.1.1 Levee Construction

A general fining up sequence of the Fraser levee structure can be summarized by three phases. These three phases represent a progression through time before and after the installation of the Steveston Jetty. Phase 1 consists of a basal phase which is characterized by thick beds of fine to medium F7 sand. Phase 2 is a transitional phase characterized by repetitive interbedded F6 sand with mud intervals Phase 3, the youngest phase comprises sand beds that are less frequent, thinner and finer grained (Fig. 4.1). The 3 phase trend is consistent with the work of Manley et al. (1997) and Piper and Normark (1983) who describe the evolution of a channel levee system. The process begins before the channel has reached substantial relief and the turbidity current is unconfined allowing the lower and coarser portions of the current to spill over the banks of the channel. With subsequent events, levee growth occurs, and channel relief increases. Channel confinement of later turbidity currents results in the bypassing of coarser material, which remains in the channel, while finer sediment from the upper portion of the current overtops channel walls and overspills onto the levees via flow stripping. Coarser material remains at the base of the channelized turbidity current, is transported down the channel, and is deposited at the base of the slope on the fan (Hill, 2012).

Thick F7 beds are only present at depths corresponding to some time between the 1910s and 1930s in sediment cores. These deposits represent the early stage of channel-levee growth, at which time the low relief of the system allowed for frequent overbank spilling of thick and coarse sand beds from the base of turbidity currents (Figs. 4.1 and 4.2). As levees became higher and channel relief increased, coarse sediment became confined in the channel and overspill events became less frequent. This occurred after deposition of the interbedded sand beds, the tops of which have been dated to an approximate range of

1938 to 1950. The interbedded unit was likely deposited when levees were in an early growth stage and overspill events were frequent. The repetitive interbedded unit terminates and the sand dominated sediment record transitions to thick mud intervals representing long periods where no overspill events occurred. Red, blue and yellow bed sets are interpreted to have been deposited when larger than normal turbidity currents travelled downslope, overtopped the levees and deposited fine sand on the levees. For example, a turbidity current with a height of 8 m would produce overspill deposits when the channel relief was low (Fig. 4.2). With increased levee construction, resulting in the heightening of channel relief up to 10 m, the same 8 m turbidity current would be no longer capable of depositing material on the channel banks. This is an important concept to recognize when considering the source of the turbidity current and how the channel conditions and depositional style change over time. The reduced number of sand beds in the upper phase of the levee deposit does not indicate that slides are less frequent during the most recent phase of deposition, but likely reflects the fact that more slides are confined to the channel and bypass the delta slope. For this reason the frequency of events calculated from cores of transect 1 and 2 represent a minimum number of events and sediment deposited from relatively large events.

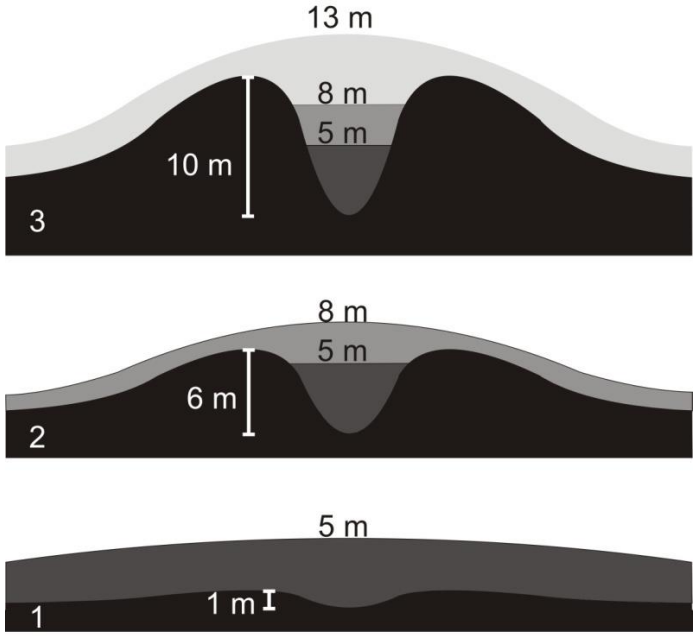

Fig. 4.2. Three conceptual phases of levee growth showing flows of different heights. A 5 m flow results in continuous overspill in phase 1 with low channel relief but is confined to the channel during phase 2 and 3. Present channel relief in the Fraser Main Submarine Channel is 10 m. Thick mud units in the levee deposits indicate that typical flows do not overspill the channel.

If channel confinement of the typical turbidity current is indeed occurring with no overspill onto the levees, this constrains the typical height of the flows. An inference can be made that the majority of the turbidity currents are thinner than the present channel relief of 10 m.

4.1.2 Effect on Local Sedimentation Rate

Results from this study imply that the greatest effect on the local sediment accumulation rate is distance from the river mouth. Sedimentation from river plume suspension fallout decreases seaward. Calculated sediment accumulation rates can only be applied to the Sand Heads submarine channel system and the surrounding area which is directly influenced by sedimentation from the main arm of the Fraser River.

Levee growth occurs with repeated channel overspill events, resulting in higher amounts of sand than areas of the delta front which experience sediment bypass. Sand beds are concentrated particularly on the outer bank of a channel bend (Fig. 4.3). Calculated sediment accumulation rates exclude sand thickness and are inferred to represent river suspension fallout. Amounts of sand on the channel banks are controlled by two factors: proximity to the levee crest, decreasing distally; and proximity to bends in the submarine channel.

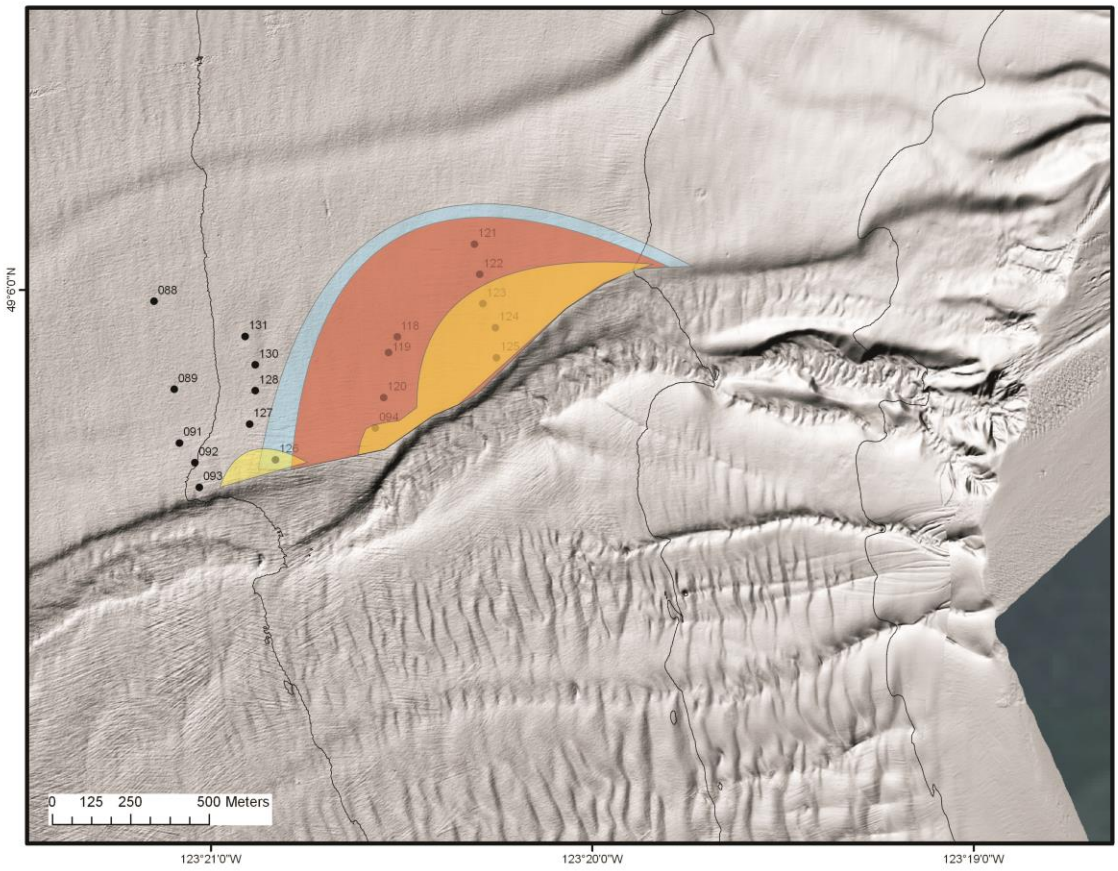

Fig. 4.3. Lateral coverage of bed sets. Sand beds are concentrated at bends in the channel. Yellow, blue and red polygons show extent of yellow, blue and red bed sets as determined by core correlations.

4.2 Event Beds

Ambient sediment deposition in the study area is characterized by sandy mud which is deposited from river plume suspension fallout (Evoy et al., 1994). F1 and F2 are interpreted to represent gravitational settling of sandy mud, which occurs continuously. Sand beds are interpreted as event deposits, characterized by relatively rapid deposition. A single event may have a duration of hours or days and deposit large volumes of sand. F5 and F6 sand beds have characteristics of Bouma-type turbidites (Bouma, 1962). Sharp-based clean sand beds that fine up characterize F6. The basal portion of the turbidite is clean with an increased mud interval toward the top. The classic Bouma sequence of massive sand, laminated sand with a silt or clay cap representing $T_{a,}$ T_b and T_e is present in multiple beds in most cores. Muddy sand turbidites with no apparent internal structure characterize F5 sand beds which in some cases have inversely graded bottoms transitioning to normally graded tops.

4.2.1 Source of Sand Beds

Variations in sand deposition can be attributed to either separate sources or changing flow characteristics. The Fraser Delta front has a history of submarine slide events which likely generated turbidity currents (McKenna et al., 1992; Evoy et al., 1994; Hill, 2012). These slides occur at the head of the Sand Heads channel system and consist primarily of sand and silt that is transported down slope through the channel. Dense, sediment laden river flow from flood events of the Fraser River are also capable of transporting large amounts of sediment down the delta front in the form of turbidity currents.

4.2.1.1 Submarine Slide Events

Our knowledge of slide events is based on bathymetric change at the lip of the delta and upper parts of the channel tributary system. Studies of repeat bathymetric surveys of this

area as old as 1970 reveal several large slides that have resulted in the delta crest shifting landward by up to 350 m (McKenna et al., 1992). Erosional features have been observed at the headwalls of the tributary channels between 2002 and 2006 (Hill, 2012). Changes in sedimentation in the tributary channels, including the infilling of the north tributary and the activation of a large south tributary, have also resulted in the wasting of large volumes of sediment. Surveys have not been conducted frequently enough to know if mass wasting events occur instantaneously as single events or as a sequence of events. Channelized turbidity currents with heights greater than channel relief, overspill onto the levees through flow stripping or run up. In places where the outer bank has a greater bend than the channel axis, flow acceleration can occur as a result of centrifugal force around bends. This may lead to flow stripping of the upper part of the channelized flow (Piper & Noramark, 1983; Migeon et al., 2004). Smaller turbidity currents that do not have a height greater than that of the channel relief are also capable of depositing coarse material, particularly on the levees at channel bends, if inertial run up over tops the channel wall (Hay, 1987). In both cases, the dense base of the turbidity current contains the coarser material while finer silts and clays are suspended at a greater height within the current. When deposition occurs the coarse basal material falls out of suspension first followed by the settling out of the finer material. This results in deposition of clean, relatively coarse sand with a sharp base, grading up to sandy mud and covered by ambient river plume fallout.

4.2.1.2 River Flood Events

The second potential source of the sand beds is high density suspended sediment flows from river discharge. Although the concentration of suspended sediment in the Fraser River is below the calculated amount required to produce hyperpycnal conditions (Mulder and Syvitski, 1995), new data supporting favourable conditions for such events is being provided by the VENUS Delta Dynamics Lab (DDL). The DDL provides real time, high frequency measurements of the water column of the upper delta front in 41 and 101 m water depth on an unchannelized margin of the delta front, south of the Main Submarine Channel (Lintern and Hill, 2010). Measurements made during spring freshet conditions, when river discharge exceeded 9,000 $m^3 s^{-1}$, record events with anomalously low salinity, high temperature and high turbidity at 1.5 m above seafloor for durations up to several hours (Ayranci et al., 2012). A destructive event which displaced the DDL during spring freshet conditions in 2012 registered readings of increased turbulence and flow velocity before communication with the cabled observatory was cut (Lintern 2013, in prep). Multibeam bathymetry data indicate that no significant slide occurred to account for this destructive event. These events are mainly concentrated during spring freshet, however, they have been recorded on an irregular basis. They do not necessarily occur annually (Ayranci et al., 2012). Deposits from river discharge events may be different than slide events and may be characterized by inverse grading followed by normal grading representing a hydrograph of a river flood event (Mulder et al., 2003). This style of deposition occurs when the intensity of discharge waxes and wanes over a period of time. Changes in discharge manifest sedimentologically by a coarsening up in grain size, correspond to increasing transportive energy, and transition to fining up when transportive energy decreases. F5 deposits have inversely graded bases and normally

graded tops which can be correlated from proximal to distal transects and may be the deposit from this sort of event.

4.2.2 Changing Flow

Different deposit types, including F5 and F6 sand beds, may also reflect changing flow conditions from a single source. Flow styles can be simplified as ignitive where they erode and entrain new material, or dissipational where they decelerate and deposit their suspended load (Parker, 1982). The erosive force, which results in the entrainment of new sediment, depends ultimately on the following conditions: slope angle, sediment concentration and bed stress. There is a critical threshold for values above which erosion occurs and the turbidity current grows, but if these conditions are not met the turbidity current will die out (Parker, 1982).

There are two substantial changes in slope on the delta front which decrease from average gradients of 8.4° to 5.3° to 2.3° (Fig. 3.2). Sediment cores were collected from the margin with a 2.3° slope and range in distance from the slope break from 694 to 1720 m. Flow transformation would likely occur at different proximities to the source depending on initial sediment concentration. A liquefied block of wasted material from a slide at the lip of the delta would supply a far greater concentration of suspended sediment than a river flood and the resulting turbidity current would be capable of remaining in a high density, erosive state farther down slope than a river discharge induced turbidity current. Flow transformation would most likely result from a combination of decreasing slope and initial sediment concentration. A decrease in velocity at slope breaks could result in a reduction in bed stress, reducing the ability to entrain new sediment. With a low initial

sediment concentration, sediment would not take long to fall out of suspension and the turbidity current would collapse.

Another possibility is that F5 muddy sand beds result from turbidity currents generated by smaller volume slides, and represent the distal deposits or overspill of only the upper portion of the turbidity current. Slides involving smaller volumes of failed sediment may liquefy and result in a turbidity current with comparable sediment concentrations to that of a larger volume of sediment. However, small volume slides might not reach as far down slope or, due to a lower height, only the upper, less dense portion of the turbidity current would be capable of overspilling. In the case of a limited amount of overspilling from a low volume flow, a more dilute, muddy sand bed would be deposited. If some F5 beds were deposited by small slides, a new way to distinguish between river-flood-generated F5 beds and slide-generated F5 beds would be required. Coring closer to the source would likely reveal F6 sand beds, which would correlate to the distal F5 sand beds, and coring levee deposits where the levee height is not as great might reveal more clean F6 sand beds. Flood generated F5 beds would be expected to be more laterally continuous and may correlate to F5 beds on the unchannelized margin of the delta front.

There are numerous examples of turbidite-deposited F6 sand beds from the blue and red bed set. These sharp based, clean sand beds are interpreted as deposits from the upper flow regime, and represent the basal, high density portion of the turbidity current (Lowe, 1982). These high concentrations are interpreted to be sourced from larger sized slides from the delta crest. The F6 sand beds of possible turbidite origin in the yellow bed sets

cannot be correlated to other F6 sand beds more distally from the river mouth or from the channel axis because they likely represent smaller slide events. Distal F5 sand deposits can be correlated to the F6 sand beds of the yellow bed set at roughly the same depth in transect 1. F5 muddy sand beds with inversely graded bases and normally graded tops are interpreted to be deposited from turbidity currents generated by river flood events that are of a lower sediment concentration than those generated from slide events.

4.3 Lithological Correlation

Lithological correlations of sand beds across transects 1 and 2 can be made with a high level of confidence based on visual inspection (Fig. 3.10A,B). Along strike of a single transect, sand beds occur at nearly the same depth below the sea floor. Sand beds from the blue bed sets are thickest and share distinct structural and textural properties. Sand beds in the red bed set are thinner than the blue bed set. Along each transect, the red bed set exhibits sand beds of similar thickness, and share similar sedimentary structures and textural properties. The yellow bed set is present only in cores proximal to the levee crest and does not correlate along the transect (Fig. 3.10A). With sand bed intervals removed, the correlation lines of the yellow bed set are very straight from cores 122 to 125 suggesting that all core locations share a comparable sedimentation rate (Fig. 4.4). The same properties are found in transect 2, which is more distal from the river mouth (Fig. 3.10B).

Correlations along transect 3 are much more difficult to make as there are fewer sand beds in the upper half of the cores (Fig. 3.10C). The tops of F7 sand beds can be correlated in cores 126, 127 and 128, and this surface can be used as a reference horizon for correlation. In cores 126 and 127, the F7 sand beds are overlain by thick units of

interbedded sand and mud beds. This thick sequence, however, is not present in all cores along the transect. Above the interbedded unit, sand beds are generally thin and do not occur at similar depths or thicknesses from core to core. The properties used to correlate beds along transects 1 and 2 could not be identified in transect 3, and for this reason correlation of transect 3 to more proximal transects based on visual means is not possible. The discontinuity of the yellow and blue bed sets and the lack of identifiable beds corresponding to the red bed set in transect 3 implies that the lateral extent of deposition is limited and that the depositional process which emplaced sand beds in the position of transects 1 and 2 did not carry as far as transect 3 (Fig. 4.3). This style of sedimentation is interpreted to represent overspill which is focused at the channel bend as opposed to continuous overspill. Continuous overspill would only occur when flow height is greater than channel relief, resulting in laterally continuous sand beds.

4.4 ^{210}Pb Model

Repeat multibeam surveys reveal sediment accumulation rates at the mouth of the river of greater than 1 m yr $^{-1}$ (Hill 2012). Closer to the study area, Hart et al., (1998) used ^{137}Cs dating to conclude that sediment accumulates at 10 cm yr $^{-1}$ on the upper slope, approximately 3 km from the river mouth, and quickly drop to 3 cm yr $^{-1}$ approximately 4 km from the river mouth (Hart et al., 1998). Sediment accumulation rates in this study fall within the expected amount with regards to distance from river mouth, agreeing well with those calculated by ^{137}Cs analysis.

Sediment accumulation rates can be applied to cores with a reasonable amount of confidence due to the close agreement between sediment accumulation rate calculations. The selection of the exclusive sediment accumulation rate instead of the inclusive sediment accumulation rate was done because subsamples have a high probability of including reworked sediment. Exclusive sediment accumulation rates have a regression line with a better fit, and correspondingly higher r^2 values. Reworking of sediment typically involves the mixing of newer material with older material which would result a deviation from a linear ln(excess ^{210}Pb) regression. If the deviation is related to a higher excess ^{210}Pb activity than the linear regression curve, the inclusion of the data point would result in a decreased calculated sediment accumulation rate. The variation between inclusive and exclusive sediment accumulation rates for single cores is between 8 and 12% for cores 123, 126 and 127 and is 23% for core 125.The low variability in sediment accumulation rates suggests that there is little sensitivity in the inclusion or exclusion of data points.

Variation in sediment accumulation rates between cores along single transects is also low. The agreement along transects shows that the sediment accumulation rates are consistent. This is expected for core sites positioned approximately 100 to 200 m apart. It was previously unknown if proximity to the channel would result in higher sediment accumulation rate, but the excess ^{210}Pb activities suggest that this is not an important factor for sediment accumulation. Local variations are expected to occur along transect with bathymetric relief.

The most important variable influencing sediment accumulation rate is distance from the river mouth. Transect 3 is located 780 m further from the river mouth than transect 1 and

has sediment accumulation rates which are on average 70% lower. These differences are to be expected as sediment accumulation rates generally decrease exponentially with distance from a river mouth source (Nemec, 1995). The agreement of sediment accumulation rates of cores along transect implies that this sedimentation rate is applicable to other sites at the same distance from the river mouth. As the most important controlling factor for sediment accumulation rate is the river source of sediment, these sediment accumulation rates cannot be applied to sites on the southern Fraser Delta front.

The primary consideration for potential sources of error with the sediment accumulation rate model is sediment reworking. The most conspicuous problem is mud bed erosion. Most F6 sand beds have sharp bases which imply erosion of the underlying mud interval may have occurred. The mud intervals are interpreted to represent a constant rate of sedimentation so it would be beneficial to constrain the amount of erosion which has occurred. The only way to estimate the amount of erosion during emplacement of each sand bed is to look at the beds that have been correlated to each other to determine if there are substantial gaps in the sediment record. To do this all sand beds were mathematically removed (Fig. 4.4), their positions are marked with event markers and the sediment thickness of mud intervals between markers was examined. Localized erosion would be evident between cores of similar sediment accumulation rates if mud beds were thinner between erosive sand beds, making intervals appear shorter relative to adjacent cores. Sharp based F6 sand beds have been shown to be limited in lateral extent. They are interpreted to have been emplaced by events involving overspill from the channel, and erosion is most likely to be observed proximal to the channel where erosive energy would

be greatest. The yellow sets of sand beds has F6 sand beds which pinch out or correlate to F5 sand beds with distance from the levee crest. More erosion is expected to occur under the F6 sand beds of cores 125, 124 and 122 than under the F5 sand beds in cores 122 and 121. The thickness of mud is the same between sand bed markers of the blue bed sets and yellow bed sets in cores 123 and 125 indicating that if erosion occurred under F6 sand beds there were no major differences in the amount of erosion between the levee crest and 200 m away from the levee crest. Likewise, F5 beds in cores 121 and 122, which occur at the same depth as the F6 yellow bed sets, have the same thickness of mud between them and the top of the blue bed sets. This consistency in thickness of mud intervals between sharp based F6 beds and graded F5 beds implies that there is no substantial amount of erosion associated with these beds. Other mud intervals are consistent in thickness along transect, providing no reason to suggest that erosion is a substantial issue in transect 1 and 2. The same statement cannot be made for transect 3, however, as correlations from core to core cannot be made with the same level of confidence.

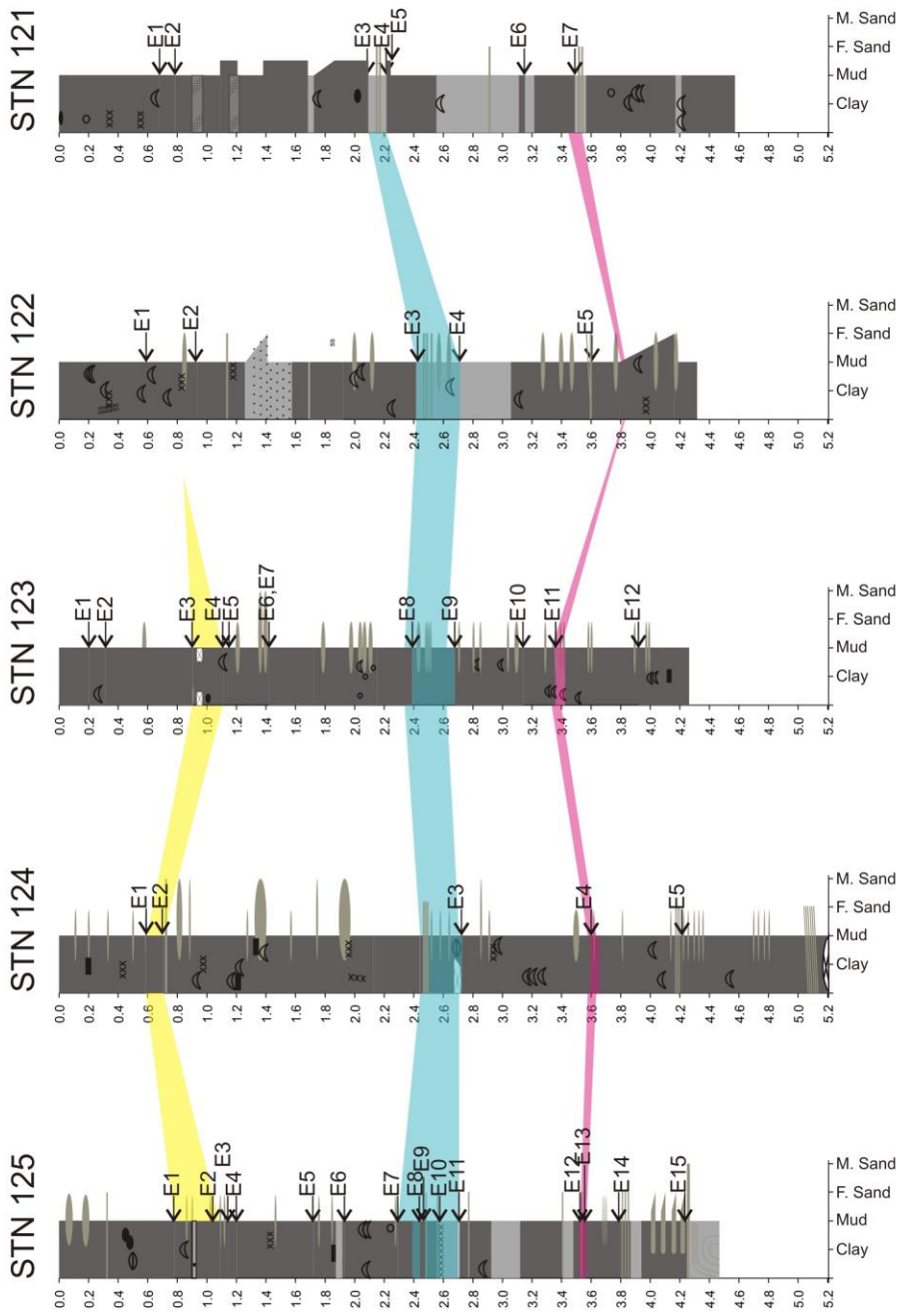

Fig. 4.4. Transect 1 - sand beds have been removed and replaced with and event marker (E number) to show mud thickness without the influence of sand beds. Yellow, blue and red colours correspond to depths of bed sets. Core event markers are in down-core sequences which apply to single cores only and do not im ply correlation of event numbers between cores (i.e., Core 125 E5 sand bed does not correlate to Core 124 E5 sand bed).

Based on thicknesses of mud intervals between sand bed sets (Fig. 4.4), core 125 appears to have a sediment accumulation rate which is very close to that of core 123. However, the ^{210}Pb calculations indicate a sediment accumulation rate less than that calculated for core 123. This is unlikely to be the result of eroded mud beds based on our ^{210}Pb model. The amount of material that would have been required to elevate the sediment accumulation rate to be consistent with core 123 would be greater than 20 cm under every F6 sand bed or greater than 60 cm under a single bed. This is an unrealistic amount of deposition relative to the adjacent cores.

A more likely explanation of the difference in calculated sediment accumulation rate is reworking by mechanisms of sediment transport. In order for variations in sediment accumulation rates to occur within a single transect there is likely a strong influence based on proximity to the levee crest. One explanation is that the proximity of core 125 to the levee crest, a high elevation feature, exposes it to higher amounts of tidal resuspension. Core 123, which is on the lee side of the levee with reference to flood tide, may be less susceptible to such tidal activity. In an attempt to moderate the effect of sediment reworking a higher number of subsamples were excluded from the sediment accumulation rate calculation for core 125.

Low r^2 values were calculated for sediment accumulation rates proximal to the river mouth and this supports the hypothesis of increased sediment transport (core 123 and 125). Resuspension activity from tidal currents have a greater effect on the seabed in shallower waters and likely account for a great deal of sediment transport and reworking which can attribute to the low r^2 values calculated in cores which are proximal to the river

mouth. Potential for mixing caused by bioturbation is expected to decrease with proximity to the river mouth due to environmental stresses including higher sedimentation rates and sandier substrate along with increased amounts of fresh water (Ayranci and Dashtgard, 2013), however bioturbation is present, as observed in x-radiography.

4.5 Correlation of Sand Beds to Documented Events and Frequency of Events

Approximate sand bed ages correlate well with documented slides at the lip of the delta (Table 4.1). The calculated ^{210}Pb age of the red bed set, consisting of two F6 sand beds, is consistent with a slide event in 1976. This event is predated by an event in 1972 and postdated by an event in 1977. The 1997 event could be related to the second sand bed in the red bed sets. The blue bed set contains the thickest sand beds, and its calculated ^{210}Pb age is consistent with the 1985 slide. The 1985 slide is the largest documented slide at the lip of the delta (McKenna et al., 1992). There are more sand beds in core 125 within the blue bed set than there are actual documented failure events, and this may reflect a retrogressive style of failure. This is consistent with the hypothesis of McKenna et al. (1992) that the volume of wasted material was large enough to be tsunamigenic, but no surface expression was observed. It is conceivable that the 1985 (largest) failure could have occurred as several slide events between the dates of bathymetric surveying and when the slide scar was discovered.

No single large failure event has been documented corresponding to the approximate timing of the yellow event. These sand beds may correspond to headwall erosion of tributary channels documented between surveys from 2002-2003, or may be related to an

earlier shift in activity where the north tributary experienced several meters of infill while the south tributary became more active (Hill, 2012).

Table 4.1 Ages of sand bed sets and documented failure events. Sand bed ages are approximate and are based on the exclusive sediment accumulation rates.

Sand bed Ages	Documented failure event (McKenna et al., 1992)
2000-2003 ± 1.0	n/a
1983-1991 ± 2.4	1984, 1985
1975-1984 ± 3.2	1972, 1976, 1977

Based on sand beds in the sediment record, the frequency of turbidity currents and inferred slide events is higher than previously reported from bathymetric surveys. Sand beds occur approximately once every 2 to 3 years. The sources of many of these deposits are likely not the same magnitude as observed slide events such as the 1985 event at the delta crest. Substantial events with multiple sand beds occur less often, with an approximate frequency of 10 to 15 years. This frequency is consistent with the frequency of slide events at the delta crest documented by McKenna et al. (1992) and suggests that some events occur without being detected. These frequencies are inferred from a fairly short period of time due to the relatively recent history of the Fraser River jetty construction; long term frequencies cannot be determined. According to the sediment record, the frequency of events does appear be somewhat stable since approximately the 1950s. If controlling factors that initiate turbidity currents remain the same, there is no reason to expect that they would become any more or less frequent.

Based on excess ^{210}Pb activities and the history we have observed from levee growth, the channel appears to be of a young age – approximately 100 years. If the channel is indeed

100 years old, its origins are likely related to the construction of the Steveston jetty which occurred over a period from 1912 to 1932.

4.6 Initiation Mechanisms

4.6.1 Peak Flood Events

During spring freshet, flow in the Fraser River increases dramatically from below the annual average of 3410 $m^3 s^{-1}$ to a flood average of 9790 $m^3 s^{-1}$. The highest measured flood on record was 15,200 $m^3 s^{-1}$ in 1948. The highest sediment transport volume was measured during the 1972 flood year (14,400 $m^3 s^{-1}$) at 29,061,000 t yr^{-1} (McLean et al., 1999). Rapid sedimentation occurs near the river mouth, and repeat multibeam surveys indicate that sediment accumulation rates are greater than 1 m y^{-1} at the delta slope (Hill et al., 2008). Rapid accumulation of unconsolidated sands and silt leads to over-steepening and destabilization resulting in slope failure at the delta crest (Chillarige et al., 1997).

Average frequencies of F5 and F6 sand beds, based on cores 125 and 94 (Tables 3.14A, 3.14B), are comparable to the average frequency of Fraser River flood years. Since the approximate age of 1956, 17 sand beds have been deposited with an average return interval of one sand bed every 3.2 years. Over the same time period, the annual spring flood maximum discharge of the Fraser River has been higher than average 19 times with an average return interval of 2.9 years.

Although sand beds occur in the approximate stratigraphic positions corresponding to the largest flood years of 1948 and 1972, they are not the thickest sand beds. The flood year of 1948 roughly corresponds to the top of the interbedded F6 sand bed unit. There is a F6

medium grained sand bed approximately 20 cm below the top of the interbedded unit in core 126. This is the coarsest sand bed of this interval, but is only 4 cm thick (Fig. 3.10C). A 3 cm F6 sand bed corresponds approximately to the 1972 flood year, but it is also possible that the red bed set which is dated to 1975 ± 3.2 years from core 125 with multiple F6 sand beds could correspond to this year. The thick F6 sand beds, as well as documented large failure events (McKinnon et al., 1993) of the blue bed sets correlate to flood years which were below the average in 1984 and 1985. Although these events, which are the thickest in the upper section of the sediment record, do not correspond to major flood years, they do occur after a stretch of nearly 10 years of flood activity below the average flood discharges.

Documented failure events occurred in 1976 and 1977 (McKenna et al., 1992), which are during the first two years of the period of low flood averages. The 1976 and 1977 slides do not correspond to sand beds in the sediment record.

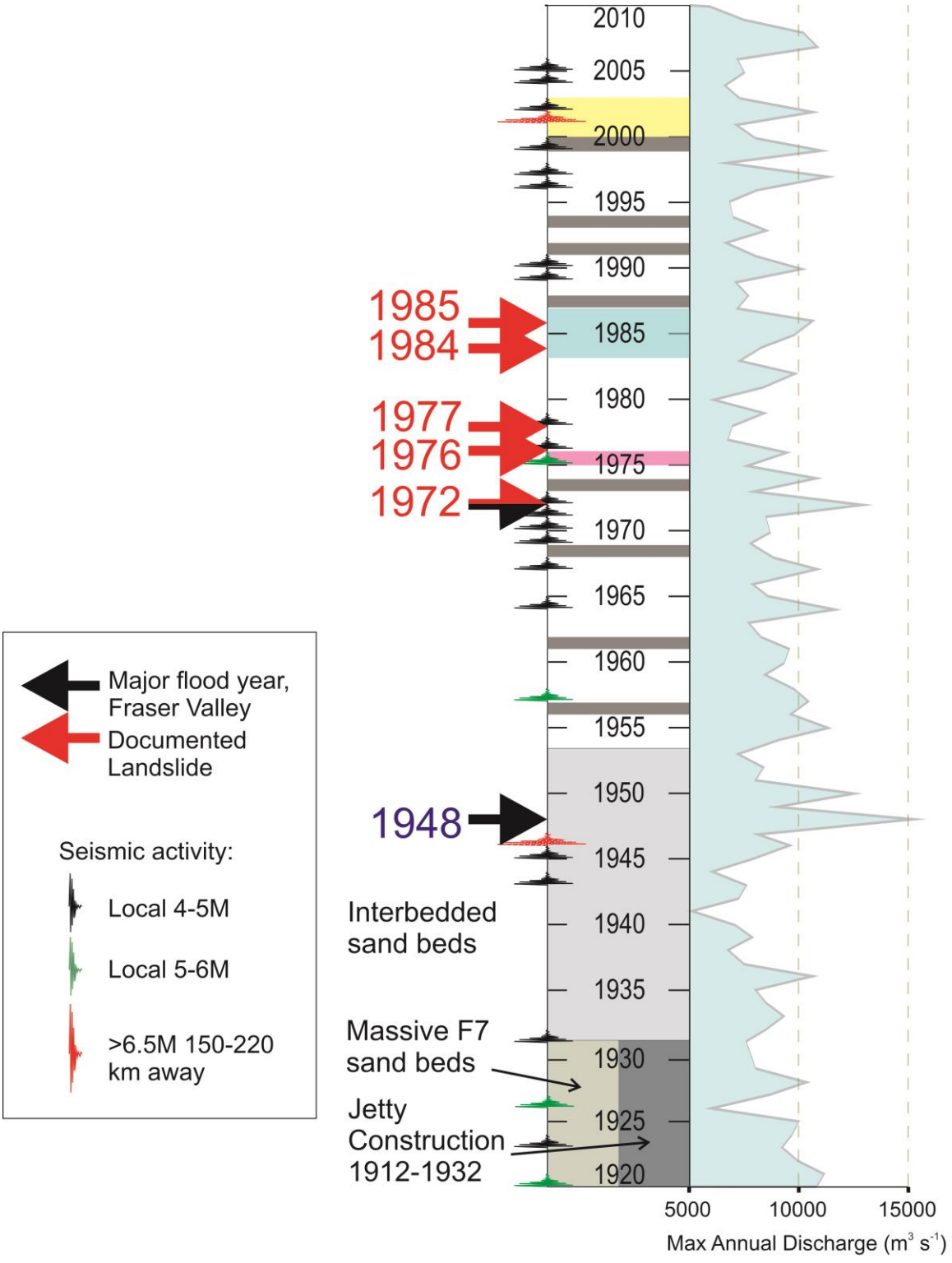
2010
2005
2000
1995
1990
1985
1980
1975
1970
1965
1960
1955
1950
1945
1940
1935
1930
1925
1920
1985
1984
1977
1976
1972
1948
Major flood year, Fraser Valley
Documented Landslide
Seismic activity:
Local 4-5M
Local 5-6M
>6.5M 150-220 km away
Interbedded sand beds
Massive F7 sand beds
Jetty Construction 1912-1932
5000
10000
15000
Max Annual Discharge (m3 s-1)

Fig. 4.5. Timeline of sand beds relative to large spring freshet years and earthquakes greater than 4 M. Older events are at the bottom of the timeline and younger at the top. The coloured bar represents the sediment record starting with the phase one basal phase shown in tan. Phase one is characterized by F7 sand beds. Construction of the Steveston jetty is shown at the bottom of the bar in dark grey. The phase two interbedded sand bed unit is shown in light grey and the phase three mud unit with less frequent overspill events is demarcated by white with colour bands: dark grey – single sand beds; red, blue and yellow – sand bed sets. All interpreted ages of bed sets are based on discrete dates from exclusive sediment accumulation rates from single cores. Sand beds younger than 1967 are based on sediment accumulation rate of 10 cm yr^{-1} from core 125. 1961 and 1956 sand beds are based on core 94. Sand beds older than 1955 are based on the large range sediment accumulation rate at cores 126 and 127.

4.6.2 Tidal Drawdown

The most likely slide trigger scenario is when the slope has been primed for failure by an increase in pore pressure. During falling and low tides lithostatic pressure is minimized resulting in excess pore pressures (Chillerige et al., 1997). Seepage pressure of groundwater from the delta may act to further increase pore pressure during low tide conditions (Terzaghi, 1956). Furthermore, at low tide, storm waves tend to break on the upper delta slope (Muele, 2005), from which the loading effect can serve to further decrease slope stability. Chillerige et al. (1997) calculated that at the time of the 1985 event, maximum tidal variations were about 5 m with a period of about 16 h; this would have substantially increased pore pressure at low tide. When multiple factors combine with over steepening from high sedimentation or other destabilizing factors, conditions become favourable for liquefaction induced slides.

4.6.3 Dredge Disposal

It is difficult to infer if failure events are related to dredging activity based on total amount of dredge disposal, because the amount of material dredged in a season is

calculated based on the predicted amount of snow pack (FREMP, 2005). During years of high snow pack there will be a corresponding high peak river flow so it is impossible to separate river discharge from dredging activity based on available data.

Sand beds in sediment cores are unlikely to be related to any discrete dredge disposal activity. The disposal barge carries a maximum capacity of 2600 m^3 of sediment. This volume of sediment is unlikely to ignite a turbidity current that could entraining new sediment and flow downslope far enough to reach the coring site with a concentrated sand load thick enough to generate levee overspill deposits. Sediment loads are more likely to settle out in the vicinity of the area where they leave the ship and remain on the upper slope of the delta front (Hill, 2012; Lintern et al., 2009). Sedimentation from dredge disposal is also distributed over a broader area and would be more likely to result in rapid deposition at the lip of the delta rather than over steepening (Hill, 2012). Although it is unlikely that a single dredge disposal event contributed to any substantial far reaching turbidity current, it is possible that repeated discharge of dredge loads on the same position could contribute to local over steepening and increasing the risk of slope failure.

4.6.4 Seismic Activity

There are many documented cases of submarine slides generated by large magnitude seismic events (Piper et al., 1999, Inouchi et al., 1996). Liquefaction becomes a concern with seismic activity, especially in deltaic environments composed of unconsolidated fine sand and silt. Shear induced excess pore water pressure may transform granular deposits from solid state to liquid state resulting in slope failure. Scientific literature on small to

moderate earthquakes is sparse, likely because low magnitude earthquakes have not been known to trigger substantial slides. As such, low magnitude earthquakes are not as well represented in the sediment record as are large magnitude earthquakes.

Two west coast earthquakes are notable due to their high magnitude and local impact, although they both occurred at a distances from Sand Heads. A 1946 earthquake on central Vancouver Island, 161 km away, had a magnitude of 7.3 and was felt in Victoria and Vancouver. Another earthquake occurred in 2001 in southern Puget Sound, 220 km away, with a magnitude of 6.8 and was felt in Vancouver.

Since the 1920's, no major earthquakes have occurred within a radius of 100 km of the Sand Heads area. However, earthquakes above a magnitude of 3 have occurred almost every year on an irregular basis within 100 km from Sand Heads. Events greater than 4M are more rare, with 36 on record since 1864 (Fig. 4.5). Earthquakes between 4 and 5.9M are classified as light to moderate. The largest recorded earthquake in this region was 6M and occurred in 1909. No direct correlation can be made between seismic activity and event beds (Fig. 4.5). The largest earthquake to occur in the Strait of Georgia during the time frame of the cored sediment record occurred in 1976. It had a magnitude of 5.97 and an epicentre located 34 km to the south of the Sand Heads area. There were small slides at the lip of the delta in both 1976 and 1977, but the 1976 event also corresponds to a larger than average flood year. Another moderate earthquake occurred in 1957 (5M) which could potentially correspond to the top of the thick interbedded sand bed unit. Other moderate earthquakes occurred before the 1930s during jetty construction, when the sediment record was dominated by massive F7 sand beds or frequent interbedded

sand beds. It is impossible to discern any discrete event in this sand-dominated interval. There were no earthquakes with a magnitude greater than 4 in 1985, corresponding to the largest event, both in terms of displacement of the delta crest and with the thickest sand beds since approximately 1950.

It is worth noting that the timing of the 1946 7.3M earthquake does occur at roughly the same time as the first phase of levee development. If inception of the Main Submarine Channel required a large slide to generate a powerfully ignitive turbidity current, this large earthquake is a candidate for its initiation. It is possible that with jetty construction being completed in the 1930s, rapid sedimentation at the river mouth began soon after and an unstable slope began to develop until being shaken loose by the 1946 earthquake.

4.7 Channel Confinement vs. Unconfined Turbidity Currents

Thick sand beds are found on the levees of the channel and result from overspill from channelized turbidity currents. High-density turbidity currents transport large volumes of sandy material and are sourced from slides at the head of the channel system. On the delta slope, these thick sand beds are only observed in association with the active Main Submarine Channel and with relict channels that once acted to confine older turbidity currents (Evoy, 1994; this study). High backscatter intensities, interpreted to represent coarser surface material, are found in association with channel overspill and fan deposit areas (Fig. 3.7) and are lacking in unchannelized margins of the delta front. Mid-slope, interchannel cores have thicker intervals of sandy mud and only thin beds or laminations of sand are interpreted to represent unconfined turbidity currents (Evoy, 1994; Hart et al., 1992).

Cores collected from positions between channels lack the thick sand beds of those collected from channelized margins. This is because they do not originate from large slide events and are sand rich enough to create a high-density turbidity current. The unconfined turbidity currents are interpreted to result from river flood events and are lower density, transporting lower volumes of sand than a slide generated turbidity current. F5 sand beds, which have a distinct contrast in depositional style from F6 sand beds are dated to corresponding river flood events and likely represent unconfined turbidity currents.

Instead of carrying high density sediment from a focused source, they carry sediment from a source which is laterally more extensive than the submarine channel and may be as wide as the river mouth. The turbidity currents flow down the delta front fanning out as sheet flows over the sea bed. Frequent sheet flow events are likely responsible for the formation of a field of sediment waves which were described by Hill (2012) as strike parallel upslope migrating bedforms in an environment where tidal currents are creating traction along slope. These strike parallel sediment waves are interpreted to be the result of unchannelized turbidity currents (Hill, 2012).

4.8 Evaluation of Model

The dating of levee turbidite deposits to infer a chronology of slide events at the lip of the delta is a well suited approach to the conditions on the Fraser Delta. Although sediment cores show signs of reworking in places, levee deposits have been shown to have overall well preserved sand and mud beds which have retained many aspects of their primary depositional structure. Multiple transects at different distances from the river mouth

demonstrate how the sediment accumulation rate decreases with distance from the river mouth. Multiple cores from each transect show similar patterns of sedimentation with little variation are easy to correlate, and show the lateral extent of sandy event beds. Dating mud intervals by using excess ^{210}Pb activity has not been performed with long cores such as the ones used in this study, but with the high sediment accumulation rate and the young (approximately 100 years) history of the channel confinement this technique is suitable. The alternative dating method would be ^{137}Cs analysis, but in bioturbated sediment the signal is often smeared, making it difficult or impossible to determine where the signal begins. In cores with thick mud intervals and especially in transect 3 where there are few sand beds in the upper sediment record, the potential to distort the ^{137}Cs signal is maximized.

5 Conclusions

- Levee deposition on the Main Submarine Channel is characterized by a general fining up through three phases of levee growth. In phase one, the newly formed channel has low relief and continuous overspill occurs when turbidity currents are active. In phase two, levees begin to accumulate and overspill is still common, but the medium sand from the base of the high density flows is lacking and is presumably being channelized and transported further down slope. The third phase occurs as levees are well established, resulting in increasing channel relief. This phase is characterized by thick mud intervals, which represent long periods of no turbidity current deposition on the levees. Sand deposits from events in phase 3 which are large enough to overspill the channel. The entire channel-levee system appears to have evolved over the past 100 years approximately.

- Two distinct types of sand beds are recognized and have different origins. Facies 6 sand beds are linked to high-density turbidity currents generated by slide events and Facies 5 sand beds are interpreted to represent lower density turbidity currents initiated by sediment laden river flow during spring freshet. The presence of a river source for density flows supports the existence of unconfined turbidity currents on the delta front, which has been proposed by other researchers.

- ^{210}Pb dating of sediment cores shows that sand beds from levee deposits can be used to represent slide events. This is confirmed by the clear correlation of ages of bed sets to historical events. All known slide events are accounted for in the sediments cored

from the channel levees. There are more sand beds than have been accounted for by known slides, indicating that smaller slide events have gone undetected.

- The dating of sand beds has revealed a return interval of 10 to 15 years for large, high density events, and 4 to 5 years for smaller, low density events. Regular occurrence likely reduces the risk of a large failure.

- The timing of submarine slide events does appear to have a relationship to river flood years, although there is no relationship between magnitude of the deposit and magnitude of river event. The largest sand beds correspond to flood years which, although above average, are nowhere near the largest flood years. There is likely a combination of preconditioning factors which destabilize the delta slope including increased pore pressure and over steepening.

Bibliography

Ages, A., Woollard, A., 1976. The tides of the Fraser River estuary. Pacific Marine Science Report. Institute of Ocean Sciences, Sidney, BC. p. 76–85.

Arnott, R.W.C, 2010. Deep marine sediments and sedimentary systems, Facies models 4 eds. James, N.P., Dalrymple, R.W., Geological Association of Canada, Geotext Special publication, p. 295-322.

Atkins, R.J., Sayao, O., and Hay, D., 1998. Evaluation of erosion at Roberts Bank, Fraser River, British Columbia, Canada. In: Moore, D.P. and Hungr, O., (eds.), Engineering Geology; A Global View from the Pacific Rim. Proceedings, 8th Congress of the International Association for Engineering Geology and the Environment, Vancouver, B.C., 21–25 September 1998. Rotterdam: A.A. Balkema, p. 3833–3837.

Ayranci, K., Lintern, D.G., Hill, P.R., Dashtgard, S.E., 2012. Tide-supported gravity flows on the upper delta front, Fraser Delta, Canada. Marine Geology, vol. 326-328, p. 166-170.

Ayranci, K., Dashtgard, S.E., 2013. Infaunal holothurians distributions and their traces in the Fraser River delta front and prodelta, British Columbia, Canada. Palaeogeography, Palaeoclimatology, Palaeoecology, vol. 392, p. 232-246.

Bouma, A.H., 1962. Sedimentology of some Flysch deposits. A graphic approach to facies interpretation. Amsterdam: Elsevier, 168 p.

Carle, L, Hill, P.R., 2009. Subaqueous dunes of the upper slope of the Fraser River Delta (British Columbia, Canada). Journal of Coastal Research, vol. 25, p. 448-458.

Chillarige, A.V., Morgenstern, N.R., Robertson, P.K. and Christian, H.A., 1997. Seabed instability due to flow liquefaction in the Fraser River delta. Can. Geotech. J., vol. 34, p. 520–533.

Clague, J.J, Luternauer, J.L, Hebda, R.J., 1983. Sedimentary environments and postglacial history of the Fraser Delta and lower Fraser Valley, British Columbia. Canadian Journal of Earth Science, vol. 20, p. 1314-1326.

Christian, H.A., Mosher, D.C., Mulder, T., Barrie, J.V., Courtney, R.C., 1997. Geomorphology and potential slope instability on the Fraser River delta foreslope, Vancouver, British Columbia. Canadian Geotechnical Journal, vol. 34, p. 432-446.

Conway, K.W., Barrie, J.V., Picard, K., 2012. Submarine channel evolution: active channels in fjords, British Columbia. Geo. Marine Letters, vol. 32, p. 301-312.

Ercilla, G., Wynn, R.B., Alonso, B., and Baraza, J., 2002. Initiation and evolution of turbidity current sediment waves in the Magdalena turbidite system. Marine Geology, vol. 192, p. 153–169

Evoy, R.W., Moslow, T.F., Kostaschuk, R.A., Luternauer, J.L., 1994. Origin and variability of sedimentary facies of the Fraser River delta foreslope, British Columbia, Marine Geology, vol. 118, p. 49-60.

Evoy, R. W. Moslow, T. F. and Luternauer. J.L., 1997. Grain Size Distribution Patterns Supporting Sediment Bypassing on the Fraser River Delta Foreslope, British Columbia, Canada Journal of Coastal Research, vol. 13, p. 842-853.

Fraser River Estuary Management Plan (FREMP) Sediment Budget & Dredging Activities Annual Report. April 1, 2005 – March 31, 2006.

Hart, B.S., Hamilton, T.S. and Barrie, J.V., 1998. Sedimentation on the Fraser Delta slope and prodelta, Canada, based on high-resolution seismic stratigraphy, lithofacies and 137Cs fallout stratigraphy. Journal of Sedimentary Research, vol. 68, p. 556-568.

Hart, B.S., Prior, D.B., Barrie, J.V., Currie, R.G., and Luternauer, J.L. (1992). A river mouth submarine channel and failure complex, Fraser Delta, Canada: Sedimentary Geology, vol. 81, p. 73-87.

Hay, A.E., 1987. Turbidity currents and submarine channel formation in Rupert Inlet, British Columbia. The roles of continuous surge-type flow. Journal of geophysical research, vol. 92, No. C3, p. 2883-2900.

Hickson, T.A., and Lowe, D.R., 2002. Facies architecture of a submarine fan channel–levee complex: the Juniper Ridge Conglomerate, Coalinga, California. Sedimentology, vol. 49, p. 335–362.

Hill, P.R., Conway, K., Lintern, D.G., Meule, S., Picard, K., Barrie, J.V., 2008. Sedimentary processes and sediment dispersal in the southern Strait of Georgia, BC, Canada. Marine Environmental Research, Vol. 66, Suppliment, p. 39-48.

Hill, P.R., 2012. Changes in submarine channel morphology and slope sedimentation patterns from repeat multibeam surveys in the Fraser River Delta, western Canada. International Association of Sedimentologists Special Publication, vol. 44, p. 47-70.

Hughes Clarke, J., Brucker, S., Muggah, J., Church, I., Cartwright, D., Kuus, P., Hamilton, T., Pratomo, D., Eisan, B., 2012. The Squamish prodelta: Monitoring active landslides and turbidity currents. CHC 2012, the arctic, old challenges new, Canada 15-17 May.

Inouchi, Y. et al. 1996. Turbidites as records of intense paleoearthquakes in Lake Biwa, Japan. Sedimentary Geology, vol. 104, p. 117-125.

Irman, J., Parker, G., 1998. A numerical model of channel inception on submarine fans, Journal of geophysical research, vol. 103, no. C1, p. 1219-1238.

Johannessen, S.C., Macdonald, R.W., Paton, D.W., 2003. A sediment and organic carbon budget for the greater Strait of Georgia. Estuarine, Coastal and shelf science, vol. 56, p. 845-860.

Johannessen, S.C., Macdonald, R.W., 2012. There is no 1954 in that core! Interpreting sedimentation rates and contaminant trends in marine sediment cores. Marine pollution bulletin, vol. 64(4), p. 675-678.

Johnston, W.A., 1921. Sedimentation of the Fraser River delta. Geological Survey of Canada, Memoir 125. The character of stratification of the sediment in the recent delta of the Fraser River, British Columbia, Canada. Journal of Geology, vol. 30, p. 115-129.

Kane, I.A., Kneller, B.C., Dykstra, M., Kassem, A., and McCaffrey, W.D., 2007. Anatomy of a submarine channel–levee: An example from Upper Cretaceous slope sediments, Rosario Formation, Baja California, Mexico. Marine and Petroleum Geology vol. 24, p. 540–563.

Kostaschuk, R.A., Stephan, B. A., and Luternauer, J.L. 1993. Suspended sediment concentration in a buoyant plume: Fraser River, Canada. Geo-Marine Letters, vol. 13, p. 165-171.

Kostaschuk, R.A., Luternauer, J.L., Barrie, J.V., LeBlond, P.H., Werth von Deichmann, L., 1995. Sediment transport by tidal currents and implications for slope stability: Fraser River delta, British Columbia. Canadian Journal of Earth Sciences vol. 32, p. 852–859.

Lintern, D.G., Bostrom, C., Hill, P., Conway, K., 2009. Stability of Sand Heads Disposal site: Work conducted to date on behalf of Environment Canada to develop tools and methods to assess the sediment stability of the Sand Heads Disposal Site (Internal file report).

Lintern, D.G., Hill, P.R., 2010. An underwater laboratory at the Fraser River Delta. Eos, Transactions American Geophysical Union, 91(38), p. 333-334.

Lintern D.G., Hill, P.R., Stacey, C.D., 2013. First cabled delta-observatory documents new type of remarkably powerful unconfined turbidity current. Manuscript submitted for publication.

Lowe, D., 1976. Subaqueous liquefied and fluidized sediment flows and their deposits. Sedimentology, vol. 23, p. 285-308.

Lowe, D., 1982. Sedmient gravity flows; II, Depositional models with special reference to the deposits of high-density turbidity currents. Journal of Sedimentary Research, vol. 52, no 1, p. 279-297.

Manley, P.L., Pirmez, C., Busch, W., Cramp, A., 1997. Grain size characterisation of Amazon Fan deposits and comparison to seismic facies units. Proceedings of the Ocean Drilling Program, Scientific results. (eds.) Flood, R.D., Piper, D.J.W., Klaus, A., Peterson, L.C., vol. 155, p. 35-52.

Mathews, W. H., and Shepard, F.P., 1962. Sedimentation of Fraser River delta, British Columbia. American Association of Petroleum Geologists Bulletin, 46, p. 1416-1443.

McKenna, G.T., Luternauer, J.L., Kostaschuk, R.A., 1992. Large scale mass-wasting events on the Fraser Delta near Sand Heads, British Columbia. Canadian Geotechnical Journal, vol. 29, p. 151-156.

McLean, D.G., Church, M., Tassone, B., 1999. Sediment transport along lower Fraser River. Measurements and hydraulic computations. Water Resources Research, vol. 35, No. 8, p. 2533-2548.

Meulé, S., 2005. Processus mis en jeu dans l'évolution morpho-dynamique de Roberts Bank (Delta du Fraser): observation et modélisation hydrodynamiques et sédimentaires. Ph.D. Thesis, Rimouski, Quebec, Université du Québec à Rimouski. p. 224.

Migeon, S., Savoye, B., Babonneau, N., Anderson, F.S., 2004. Processes of sediment wave construction along the present zaire deep sea meandering channel: role of meanders and flow stripping. Journal of Sedimentary Research, vol. 74, no. 4, p. 580-598.

Mulder, T., Alexander, J., 2001. The physical characteristics of subaqueous sedimentary flows and their deposits. Sedimentology, vol. 48, p. 269-299.

Mulder, T., Savoye, B., Syvitsky, J.P.M 1997. Numerical modelling of a mid-size gravity flow: The 1979 Nice turbidity current (dynamics, processes, sediment budget and seafloor impact). Sedimentology, vol. 44, p. 305–326

Mulder, T., Syvitski, J.P.M., 1995. Turbidity currents generated at river mouths during exceptional discharges to the world oceans. Journal of Geology, vol. 103, p. 285–299.

Mulder, T. Syvitski, J.P.M., Migeon, S., Faugeres, J.C., Savoye, B., 2003. Marine hyperpycnal flows: initiation, behavior and related deposits. A review. Marine and Petroleum Geology, vol. 20, p. 861-882.

Nemec, W., 1995. The dynamics of deltaic suspension plumes. In Oti, M.N., Postma, G., (eds.), Geology of Deltas, Rotterdam, À.A. Balkema, p. 31-93.

Parker, G., 1982. Conditions for the ignition of catastrophically erosive turbidity currents. Marine Geology, vol. 46, p. 307-327.

Piper, D.J.W., Normark, W.R., 1983. Turbidite depositional patterns and flow characteristics, Navy submarine fan, California Borderland. Sedimentology, vol.30, p. 681-694.

Piper D.J.W., Cochonat, P., Morrison, M., 1999. The sequence of events around the epicentre of the 1929 Grand Banks earthquake: initiation of debris flows and turbidity currents inferred from sidescan sonar. Sedimentology, vol. 46, p. 79-97.

Pirmez, C., Hiscott, R.N., Kronen, J.D., 1997. Sandy turbidite successions at the base of channel-levee systems of the Amazon fan revealed by FMS logs and cores: Unraveling the facies architecture of large submarine fans. Proc. Ocean Drill. Program Sci. Results, 155, p. 7–33.

Robbins, J.A, 1997. Geochemical and geophysical applications of radioactive lead, the biogeochemistry of lead in the environment, vol. 1, p. 285-337.

Shepard, F.P., Marshall, N.F., 1973. Storm-generated current in La Jolla Submarine Canyon, California, Marine Geology, vol. 15, p. 19–24.

Skene, K. I., Piper, D.J.W., Hill, P.S., 2002. Quantitative analysis of variations in depositional sequence thickness from submarine channel levees. Sedimentology, vol. 49, p. 1411–1430.

St-Onge, G., Chapron, E., Guyard, H., Rochon, A., Lajeunesse, P., Locat, J., Scott, D., Stoner, J.S., Hillaire-Marcel, C., 2008. High-resolution physical and magnetic properties of rapidly deposited layers associated with landslides, earthquakes, and floods. In: J. Locat, D. Perret, D. Turmel, D. Demers and S. Leroueil (eds.), Proceedings of the 4th Canadian Conference on Geohazards: from Causes to Management, Presses de l'Université Laval, pp. 219–228.

Straub, K. M., Mohrig, D., 2008. Quantifying the morphology and growth of levees in aggrading submarine channels. Journal of Geophysical Research – Earth Surface, v. 113,

Terzaghi, K. 1956. Varieties of submarine slope failures. Proceedings, 8th Texas Conference on Soils and Foundation Engineering, University of Texas, Austin, p. 1–41.

Thomson, R.E., 1981. Oceanography of the British Columbia coast. Department of Fisheries and Oceans, Ottawa. Vol. 56, p. 291.

Appendix A

^{210}Pb Subsamples - Intervals and Activities

Subsample information is presented where two depths are provided. The depth with sand beds includes all sand beds and voids, while the corrected depth includes intervals where voids and cracks have been subtracted from depth measurements. Excess ^{210}Pb is calculated by subtracting the average background ^{226}Ra activity from each core from the total ^{210}Pb activity of each subsample. The total average background ^{226}Ra activity is 0.50 DPM g^{-1} and the maximum value was found in core 127 with a value of 0.60 DPM g^{-1}. No total ^{210}Pb activities are lower than ^{226}Ra activities indicating that the ^{210}Pb isotopes have not fully decayed.

Core 123

Subsample number	Depth w sand beds (cm)	Corrected Depth (cm)	Total ^{210}Pb (DPM g^{-1})	Excess ^{210}Pb (DPM g^{-1})	ln(excess ^{210}Pb)
1	52	46	2.44063	2.02730	0.70670
2	87	81	2.04962	1.63628	0.49243
3	138	102	1.19237	0.77903	-0.24970
4	180	133	2.48109	2.06776	0.72647
5	215	168	1.51357	1.10023	0.09552
6	255	203	2.15407	1.74074	0.55431
7	304	238	0.87392	0.46058	-0.77526
8	352	273	2.02854	1.61520	0.47946
9	387	306	1.61613	1.20280	0.18465
10	426	341	1.13112	0.71778	-0.33159
11	462	376	1.32967	0.91634	-0.08737
12	497	406	1.09616	0.68283	-0.38151

Subsample number	Mid-depth (cm)	^{226}Ra Activity (DPM g^{-1} Dry wt.)
1	46	0.38
7	238	0.57
12	406	0.29
	avg	0.413333333

Core 125

Subsample number	Depth w sand beds (cm)	Corrected Depth (cm)	Total ^{210}Pb (DPM g^{-1})	Excess ^{210}Pb (DPM g^{-1})	ln(excess ^{210}Pb)
1	47	47	2.34674	1.87341	0.62776
2	93	84	1.58876	1.11543	0.10924
3	143	116	1.42087	0.94754	-0.05389
4	179	152	2.04727	1.57393	0.45358
5	223	189	1.30480	0.83147	-0.18456
6	268	226	1.82197	1.34863	0.29909
7	339	271	1.72274	1.24940	0.22267
8	391	308	2.30856	1.83523	0.60717
9	427	346	1.14448	0.67115	-0.39876
10	471	385	1.62581	1.15248	0.14191
11	508	418	0.84312	0.36979	-0.99483
12	551	453	0.92228	0.44895	-0.80084

Subsample number	Mid-depth (cm)	^{226}Ra Activity (DPM g^{-1} Dry wt.)
1	47	0.55
7	271	0.54
12	453	0.33
	avg	0.473333333

Core 126

Subsample number	Depth w sand beds (cm)	Corrected Depth (cm)	Total ^{210}Pb (DPM g^{-1})	Excess ^{210}Pb (DPM g^{-1})	ln(excess ^{210}Pb)
1	34	31	4.21838	3.69838	1.30790
2	53	50	2.39667	1.87667	0.62950
3	76	76	1.71768	1.19768	0.18039
4	96	90	1.46190	0.94190	-0.05986
5	116	110	1.14990	0.62990	-0.46220
6	135	129	1.47032	0.95032	-0.05095
7	155	149	1.32901	0.80901	-0.21194
8	175	169	1.50024	0.98024	-0.01995
9	195	189	1.41269	0.89269	-0.11352
10	214	208	0.70848	0.18848	-1.66878
11	234	228	1.03206	0.51206	-0.66930
12	254	248	1.13295	0.61295	-0.48947

Subsample number	Mid-depth (cm)	^{226}Ra Activity (DPM g^{-1} Dry wt.)
1	31	0.53
8	169	0.56
15	333	0.47
	avg	0.52

Core 127

Subsample number	Depth w sand beds (cm)	Corrected depth (cm)	Total ^{210}Pb (DPM g^{-1})	Excess ^{210}Pb (DPM g^{-1})	ln(excess ^{210}Pb)
1	39	29	3.20452	2.61118	0.95980
2	66	46	1.90938	1.31605	0.27464
3	84	64	1.43968	0.84634	-0.16683
4	102	82	1.69444	1.10111	0.09632
5	119	99	1.44322	0.84988	-0.16266
6	146	117	1.19229	0.59896	-0.51256
7	164	135	1.12186	0.52853	-0.63766
8	182	152	0.95499	0.36166	-1.01706
9	199	170	0.92917	0.33584	-1.09113
10	225	186	0.78739	0.19405	-1.63962
11	252	204	1.04214	0.44881	-0.80115
12	295	214	0.73686	0.14353	-1.94123

Subsample number	Mid-depth (cm)	^{226}Ra Activity (DPM g^{-1} Dry wt.)
1	29	0.59
6	117	0.59
10	204	0.6
	avg	0.593333333

Appendix B

Density and Porosity

Density values were calculated for subsamples taken from mud intervals which were to be analyzed for ^{210}Pb activity using the following equations (Fig. B.1):

Density = D = M/V

M = mass = (dry mass-(salt correction * wet mass))/(1-salt correction)
V = volume
Salt correction = 0.031 (Johannessen et al., 2003).

Porosity = 1- (D/2.65)

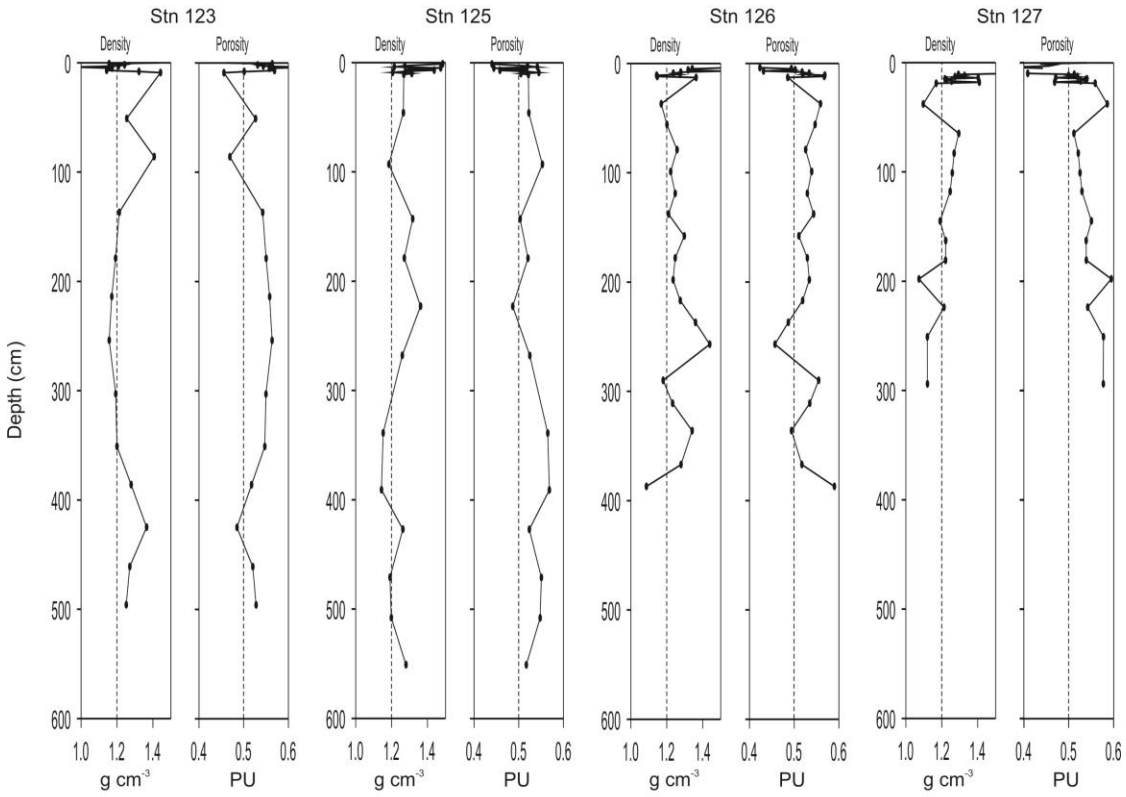

Fig. B.1. Density and porosity of subsampled mud intervals.